Republic of Iraq
Ministry of Higher Education
and Scientific Research

A NUMERICAL STUDY OF COMBUSTION CHARACTERISTICS VARIATION FOR A FOUR STROKE SPARK IGNITION ENGINE

A Thesis

Submitted to the College of Engineering of the University of Babylon in Partial Fulfillment of the Requirements for award of the Degree of Master of Science in Mechanical Engineering / Power

By

INTESAR FADHIL HACHIM

(B.Sc., 2002)

2007 A.D **1428 A.H**

جمهورية العراق
وزارة التعليم العالي
والبحث العلمي

دراسة عددية لتغير خصائص الاحتراق لمحرك احتراق داخلي يعمل بالشرارة

رسالة
مقدمة إلى كلية الهندسة في جامعة بابل
كجزء من متطلبات نيل درجة ماجستير علوم
في الهندسة الميكانيكية

أعدت من قبل
المهند سة

انتصار فاضل حاجم الحسناوي
بكالوريوس هندسة ميكانيك
٢٠٠٢م

١٤٢٨هـ 2007م

بسم الله الرحمن الرحيم

اقرأ باسم ربك الذي خلق *

خلق الإنسان من علق * اقرأ

وربك الأكرم * الذي علم

بالقلم * علم الإنسان ما لم يعلم

صدق الله العلي العظيم *

العلق (الاية 1– 5)

الأهـداء

الــى من أحبهم قلبي.. رمز المثابرة وعنوان التضحية

والديّ العزيزين .. بـراً واحساناً

الــى من شدوا أزري وساندوني.. رمز الايثار

زوجي الغالي و أخواني .. محبةً وعرفاناً

والــى كل من يسره نجاحي

..امتناناً واعتزازاً

أهـدي هـذا الجــهد

انتصار فاضل حاجم
2007/12/4

الخلاصة

في السنوات الاخيرة، التاثيرات المشتركة للتشريع البيئي ومتطلبات توفير الطاقة ادت الى توسع هائل في البحوث و تطوير محركات الاحتراق الداخلي لضمان حرق جميع الوقود الداخل إلى حجرة الاحتراق للاستفادة من جميع طاقته وتقليل الملوثات. في ظل هذه المعطيات تم عمل برنامج لتمثيل العمليات التي تحدث داخل المحرك وذلك بتطوير نموذج رياضي شبه بعدي لمحرك احتراق داخلي رباعي الشوط يعمل بالشرارة، آخذا بنظر الاعتبار تطبيق قانوني حفظ الطاقة و حفظ الكتلة. و قد تم دراسة التغيرات اللحظية في الخواص الثرموديناميكية للغازات، درجة الحرارة، الضغط ، سرعة تقدم أللهب والملوثات.

تم حساب الضغط وتراكيز الملوثات عند كل زاوية، في حين تم حساب درجة الحرارة و سرعة تقدم اللهب عند كل نصف قطر لهبة. وقد وجد إن الارتفاع في درجة الحرارة والضغط يتأثر بشكل كبير بالزمن الذي تستغرقه أللهبة للوصول إلى الجدار، كما إن أعظم درجة حرارة وضغط تحدث بالقرب من الجدار و ان قيمة درجة الحرارة والضغط وسرعة تقدم اللهب وتراكيز الملوثات تعتمد على عدة متغيرات مثل نسبة الانضغاط ، النسبة المكافئة لنسبة الوقود إلى الهواء، وقت الشرارة، موقع شمعة القدح. هذه المتغيرات تؤثر كالأتي:

- نسبة الانضغاط عندما تزداد بنسبة 12.5% فان سرعة اللهب تزداد بنسبة 10.5 % . أعظم ضغط يزداد بنسبة 8.5% و أعظم درجة حرارة تزداد بنسبة 0.18% مما يؤدي الى زيادة تراكيز الملوثات.
- النسبة المكافئة لنسبة الوقود إلى الهواء عندما تزداد بنسبة 10% فان سرعة اللهب تزداد بنسبة 5 % لكنها تبدأ بالنقصان عندما تكون النسبة المكافئة لنسبة الوقود إلى الهواء مساوية إلى 1.2. أعظم درجة حرارة تحدث عندما تكون النسبة المكافئة لنسبة الوقود إلى الهواء مساوية إلى 1.1 .
- وقت الشرارة يحدد قيمة و موقع أعظم ضغط و درجة حرارة، إن زيادة النقصان في وقت الشرارة يؤدي الى نقصان جميع المتغيرات المدروسة .
- ان تغير موقع شمعة القدح من المركز باتجاه الجدار يؤدي إلى تناقص جميع المتغيرات المدروسة .

ABSTRACT

In recent years the combined effects of environmental legislation and the energy saving demands have led to a major expansion of research and development work in order to make better fuel combustion, and reduce pollutants emission. Keeping this in mind a two zone quasi-dimensional model that analyze the compression, combustion, expansion processes has been developed for a single-cylinder four stroke spark ignition engine. The model takes in to consideration mass and energy conservation in the engine cylinder.

The model calculates instantaneous variation in gas thermodynamic states, gases concentrations, cylinder pressure, burn temperature, turbulent flame speed, and pollutants formation.

The pressure and the pollutants concentration are calculated at each crank angle. Burnt gas temperature and flame speed are calculated at each flame radius. It is found that the burnt gas temperature rises as well as the cylinder pressure due to combustion. The maximum temperature and pressure occur close to the time that the flame makes contact with the cylinder wall. The value of this maximum pressure, temperature, flame speed, and pollutants concentration affected by engine variables such as compression ratio, equivalence ratio, spark timing, engine speed and spark plug location.

- When the compression ratio is increased by 12.5%, the flame speed increases by about 10.25%. The maximum pressure increases by about 8.5%, the maximum temperature increases by about 0.18% this causes that the NOx and CO emission increased.

- When the equivalence ratio is increased by 10%, the flame speed increases by about 5%, and flame speed reduces after Φ =1.2. Maximum burned gas temperature occurs at Φ =1.1. CO emission also increased. NOx emission is maximum at Φ =1 and then decreased.

- Spark timing affects the value and the location of the maximum pressure. It is found that the cylinder maximum pressure, temperature, NOx and CO emission decrease with the retarding the spark timing than 30º BTDC.

- The position of the spark plug has a strong effect on the pressure, temperature field, flame speed, NOx and CO concentrations. Shifting the spark plug from central position toward the wall reduces all studied parameters.

EXAMINING COMMITTEE'S CERTIFICATE

We certify that we have read this thesis entitled "***A NUMERICAL STUDY OF COMBUSTION CHARACTERISTICS VARIATION FOR A FOUR STROKE SPARK IGNITION ENGINE"*** and as an examining committee, examined the student, "***INTESAR FADHIL HACHIM***", in its contents and that in our opinion it meets standard of a thesis for the degree of Master of Science in Mechanical Engineering.

Signature:
Name: Asst. Prof.
Dr. Haroun A. K. Shahad
(Supervisor)
Date: / / 2007

Signature:
Name: Asst. Prof.
Dr. Tahssen AL-Hattab
(Supervisor)
Date: / / 2007

Signature:
Name: Asst Prof.
Dr. Emad S. Ali
(Member)
Date: / / 2007

Signature:
Name: Asst Prof.
Dr. Khathair S. Mashatat
(Member)
Date: / / 2007

Signature:
Name: Asst. Prof.
Dr. Adil AL-Moosawy
(Chairman)
Date: / / 2007

Approval of the Mechanical Engineering Department.
Head of the Mecanical Engineering Department.

Signature:
Name: Asst. Prof.
Dr. Adil AL-Moosawy
Date: / / 2007

Approval of College of Engineering.
Dean of the College of Engineering.

Signature:
Name: Prof.
Abd-Al-Wahid K. Rajih
Date: / / 2007

CERTIFICATE

We certify that this thesis titled **''A NUMERICAL STUDY OF COMBUSTION CHARACTERISTICS VARIATION FOR A FOUR STROKE SPARK IGNITION ENGINE''** was prepared by **INTESAR FADHIL HACHIM** under our supervision at **BABYLON UNIVERSITY** in partial fulfillment of the requirements for the degree of Master of Science in Mechanical Engineering (Power Engineering).

Signature:
Name: Asst. Prof.
Dr. Haroun A.K. Shahad
Date: / /2007

Signature:
Name: Asst. Prof.
Dr. Tahssen AL-Hattab
Date: / /2007

CHAPTER 1

INTRODUCTION

1.1 General

About 90% of the world's energy comes from the combustion of fossil fuels. Energy is needed for transport (land, sea, air), electricity generation, heating, and industrial processes. For the foreseeable future combustion will be the major source for the production of mechanical and electrical energy. According to the world energy concile the energy demand will increase by 65% until 2020 [1]. Against this back ground it is of primordial interest to make economic use of the available resources while at the same time minimizing the impact of pollution.

Combustion can be defined as a chemical reaction between a fuel and an oxidizer involving significant release of energy as heat. Fuel is any substance that release energy (e.g. C_8H_{18}). Oxidizer is any oxygen containing substance (e.g. air) that reacts with fuel. The reaction occurs usually in a small fraction of the available volume in the reaction zone. This is known as the rapid mode of combustion. Reaction may produce intermediates that chemiluminesce or particales that glow and give the color of the flames. Combustion may also be occuring close to a catalytic surface at low temperature; this is the slow mode of combustion. The most common type is the rapid form of combustion, i.e rapid oxidation at high temperature (>1500 K), and this is the type of combustion that occurs in the internal combustion engine. In this type of engine the chemical energy

of the fuel is first converted to thermal energy by means of combustion or oxidation. This thermal energy raises the temperature and pressure of the gases within the engine, and the high-pressure gas then expands against the mechanical mechanisms of the engine and produces work [2].

Combustion is important for its impact on several other engine characteristics or requirements. The process by which the engine's emissions within the cylinder are closely linked with the details of the combustion process. The anti-knock and volatility requirements of the fuel are dictated by the engine combustion process. Even the breathing of the engine, and hence its power, are affected by what the designer must do to achieve a good combustion process. It is not surprising, therefore, that understanding the engine combustion process, and modeling that process from a fundamental perspective, are such important topics for the engine research. So analysis of in-cylinder temperature and pressure characteristics during combustion has become an important research field so far, because it must proceed to analyze combustion characteristics accurately [3].

1.2 Physics of The Spark-Ignition Engine Combustion Process

The spark discharge generates, on a sub-microsecond time scale, a high temperature kernel of order one millimeter in diameter between the spark plug electrodes. The size of the spark-generated kernal depends on the breakdown energy that the ignition system delivers to the gas. The extremely high discharge generated temperatures of order (60,000 K) result in rapid heat conduction to the surrounding gas and the electrodes. The chemical energy of the fuel-air mixture heated by the discharge is released. An outward propagation flame kernel results, as shown in the schlieren photographs of an engine ignition process in Figure(1.1), during the first 300 μsec after spark onset.

This flame kernal growth is initially laminar like, at least at low to mid-speed engine operating conditions. However, the electrical energy released in the kernel and heat losses from the kernel to the spark plug make this early flame development process non adiabatic. Also, when the flame radius is less than or of order 1 mm, flame curvature effects on the growth rate are significant.

The flame propagates outward in an approximately spherical manner from its center under normal in cylinder flow conditions. As the flame grows, the flame front contacts the combustion chamber walls and then, locally, quenches. The walls obviously prevent continuing flame growth where the enflamed region is in contact with the combustion chamber walls[3].

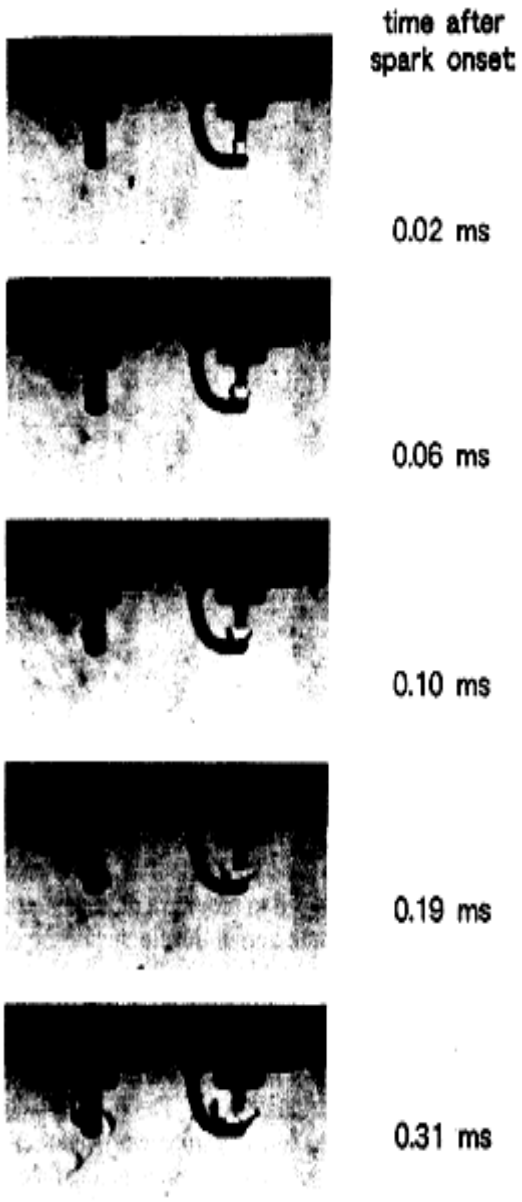

Figure(1.1): Schlieren photographs of the spark discharge to flame kernel transitions [3].

The operating cycle of an internal combustion engine consists of intake, compression, combustion, expansion, and exhaust process.

The processes of the engine cycle are illustrated in Figure (1.2).

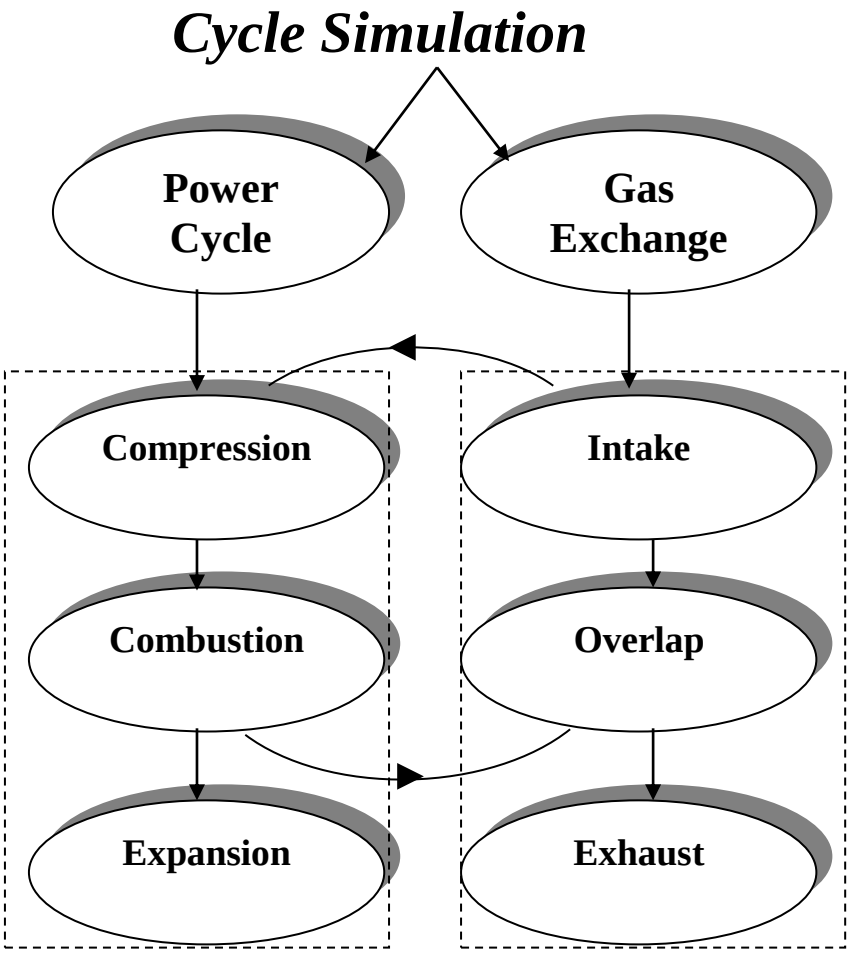

Figure (1.2): Thermodynamic cycle processes.

This work focuses on the engine combustion process itself, which starts with ignition by the spark discharge, followed by the development of a small flame kernel which then grows into a turbulent flame and propagates across the engine combustion chamber, finally extinguishing close to the chamber walls. For much of its existence, this flame is growing as unsteady turbulent flame, confined by the specific geometry of the combustion chamber walls and piston crown, with the reactants (the fuel vapor, air, and residual burned gases) essentially pre-mixed.

The combustion process is an especially important part of the engine's operating cycle. Combustion releases the chemical energy of the fuel (the primary source of energy for the engine) in a relatively short time period between the compression and expansion process, thereby producing the high pressure, high temperature, and burned gases which expand within the cylinder transferring work to the piston. A robust combustion process is important for high quality engine operation. The combustion process must be fast, that is occupy a small fraction of the total cycle time so that the engine's energy conversion process is efficient, and highly repeatable so that variations from one cycle to the next are small enough to be barely noticeable. Therefore, the mathematical models is very signification to study the in-cylinder temperature, pressure, pollutants and the flame speed as functions of engine variables.

A computer program has been constructed and developed using a Quasi-Dimensional Model with a set of semi-empirical equations to simulate the combustion process in a reciprocating spark ignition engine which is fueled with iso-octane fuel. Runge-Kutta methods are used to solve the differential equations.

1.3 Objective of the Present Work

The aim of the present work is:

1- Define more explicitly the effect of engine variables on predicted pressure, temperature contours, flame speed contours, NOx and CO concentrations in spark ignition engines.

2- Present a numerical method to analyze the combustion process in premixed spark ignition engine.

The model is used to predict the following parameters;

- Cylinder pressure.
- Temperature contours.
- Flame speed contours.
- NOx and CO concentrations.

1.4 Layout of the Thesis

This thesis falls into six chapters. Chapter one is an introduction. Chapter two is concerned with a brief literature review. Chapter three is devoted to the theoretical analysis that leads with the estimation of power cycle parameters. Chapter four deals with the computational procedure and computer program which is developed to perform all the calculations based on the theoretical analysis. Chapter five gives the presentation and discussion of the results. Chapter six presents the conclusions drawn from this work and introduces suggestions to develop this work in the future.

CHAPTER 2

LITERATURE REVIEW

2.1 Literature Review Related to Combustion Process, In-cylinder Pressure and Temperature

Since the internal combustion engine is introduced, many researches concerned with an accurate analysis of combustion phenomenon in-cylinder have been conducted. Among these researches, a numerical study of combustion characteristics variation and the effect of engine variables and operating condition on the predicted pressure, temperature, and flame speed are studied.

Alkidas A. C. [1980] studied the heat transfer characteristics of a spark ignition engine. Transient heat flux measurements were obtained at four position on the cylinder head of a four stroke single cylinder spark ignition engine. Tests were performed for both fired and motored operation of the engine. The primary engine operational variable was engine speed. The results showed that the heat flux varies considerably with position of measurement. At fired conditions, the initial high rate of the increase of heat flux at each position of measurement correlated with calculated arrival time of the flame at that position. The peak heat flux was found to increase with the increased engine speed.

Mohammed M. [1980] studied experimentally the laminar burning velocity of propane air mixtures. The laminar burning velocity has been measured in the pressure range (0.4 - 40 atm) and temperature range (298 – 750 K) for equivalence ratios (0.8 - 1.5). The measurements were made in a constant volume spherical combustion bomb, which could be heated, to 500 K. A thermodynamic analysis was used to calculate the laminar burning velocity from a pressure time history of the combustion process. The measured values were correlated using both power law and experimental expressions.

Mohammed M. and Keck J.C. [1982] studied the burning velocities of mixtures of air with methanol, iso-octane, and indolene at high pressure and temperature using the constant volume bomb method for fuel air equivalence ratios (0.8 - 1.5) over the pressure and temperature ranges (0.4-50 atm) and (298 – 700 K). The effect of adding combustion products to stoichiometric iso-octane air mixture was also studied for diluents mass fractions(0 - 0.2). Over the range studied, the results fit within $\pm 10\%$ accuracy compared with the result predicted by the following equation;

$$S_u = S_{u\circ}(\frac{T_u}{T_\circ})^{\mu}.(\frac{P}{P_\circ})^{\beta}(1-2.1\beta) \qquad (2.1)$$

Where; $S_{u\circ}$ flame speed at reference condition depends on fuel type and equivalence ratio.

μ and β constants depend only on equivalence ratio.

The results agree well with those previously reported.

Stephan G. Poulos and Johan B. Heywood [1983] examined the way in which combustion chamber geometry affects combustion in SI engines using a one dimensional cycle simulation. Calculation were performed to investigate the followings:

1. The sensitivity of geometric effects on combustion to engine operating conditions.
2. The differences in burn duration between ten chamber geometries and spark plug locations.
3. The relative merits of improved chamber design and amplified turbulence as means to reduce burn duration.

Two methods are commonly used to increase the burning rate. The first involves generation of more turbulent charge motion via the use of intake flow restrictions or combustion chambers with large squish regions. The second approach to increasing burn rate is to increase the frontal area of the flame as it propagates in to the unburned charge. To achieve faster burning by this method requires a combustion chamber designed to minimize contact between the flame and the chamber walls.

Elia C. Bedran and Gian P. Beretta [1986] presented a general analytical treatment of the energy and entropy balance equations in an open control volume by a method that can be applied to any level of modeling (zero-dimensional, quasi-dimensional, and multi-dimensional) of any internal combustion engine (homogeneous-charge, stratified charge, direct-injection, diesel, …). The method involves no major assumptions and is, therefore, compatible with any detailed model for physical effects such as (liquid fuel atomization and vaporization, heat transfer within the combustion chamber and through its walls, mass transfer (convective and diffusive) within the combustion chamber, …). The result is in the form of differential equations for the instantaneous mass fraction of burnt gas mixture and for the entropy generation by irreversibility within the chosen control volume, in terms of the pressure and volume histories and appropriately define mean variables.

Naitoh K. [1990] performed three-dimensional computation to describe the details of the intake, compression, and expansion processes in a homogeneous-charge, spark-ignition engine. Emphasis is placed on the behavior of small vortices crushed by the piston during the compression process and the flame propagation influenced by these vortices. The Navier-stokes equations are solved without using any explicit turbulence models. As to the chemical reaction, a one step reaction model of octane, which obeys the Arrhenius Kinetics Law, is incorporated in the computations. The numerical results display that, after ignition sets in, the propagating flame is wrinkled with the curvatures over the grid size. It is qualitatively demonstrated that the propagation speed of this wrinkled flame is higher than that of the smooth flame which would be seen in the flow field when the intake and compression strokes are not taken into account.

Ishii K. and Kono M. [1990] simulated numerically the formation process of flame kernels produced by short duration sparks in a stoichiometric propane-air mixture by using the model which considers heat release by chemical reaction.

Simulation is done with emphasis on physical effects such as gas movement near spark gaps and heat transfer from the flame kernel to spark electrode surfaces. To estimate the effect of heat release, formation process of hot gas kernels in air is also simulated. Simulation is made with the partial differential equations for two dimensional cylindrical coordinates.

To simplify the model, several assumptions are made:

1. The flame kernel is symmetric with respect to the z and r axes.
2. Natural convection and heat transfer by radiation are neglected.
3. Chemical species are assumed to be propane, oxygen, nitrogen, and combustion product, and an irreversible overall reaction.

4. Heat transfer from the flame kernel to the spark electrode surface, whose temperature is 300 K, is considered.
5. Prandtl number and Lewis number are unity.

The calculated minimum ignition energy agrees qualitatively with the experimental one for various spark gap width, spark electrode diameter and spark duration. The calculated results show that the flame kernel configuration is governed by the gas flow pattern is affected by the spark electrodes diameter, spark gap width and spark duration.

Connolly F.T. and Yagle A.E. [1993] investigated a new model relating cylinder combustion pressure to crank shaft angular velocity in an internal combustion engine. Primarily the fluctuations in velocity were near the cylinder firing frequency. There are three aspects to this model. First by changing the independent variable from time to crank shaft angle, a nonlinear differential equation becomes a linear first-order equation. Second, a new stochastic model for combustion pressure uses the sum of a deterministic wave from and a raised-cosine window amplitude modulated by a Bernoulli – Gaussian random sequence, parametrizing the pressure by the sample modulating sequence. This results in a state equation for the square of angular velocity sample every combustion, with the modulating sequence as input. Third, the inverse problem of reconstructing pressure from noisy angular velocity measurement was formulated as state-space deconvolution problem, and solved by using a Kalman-filter-based deconvolution algorithm. Results show that the parameterized pressure can be deconvolved at low to moderate noise level, and combustion misfires detected all in a real time.

Yacoub Y.M. and Bata R.M. [1998] developed a multi zone quasi-dimensional model that illustrates the intake, compression, combustion, expansion, and exhaust processes for a single cylinder four-stroke spark

ignition engine. The model takes into consideration mass and energy conservation in the engine cylinder, intake and exhaust plenums, crank case plenum. The model calculates instantaneous variations in gas thermodynamic states, gas properties, heat release rates, in cylinder turbulence, piston ring motion, nitric oxide, and carbon monoxide formation. The cycle simulation accounts for the induced gas velocities due to flame propagation in the turbulence model, which is applied separately to each gas zone. This allows for the natural evolution of the averaged mean and turbulent velocities in burned and unburned gas regions. The present model predictions of thermal efficiency, indicated mean effective pressure, peak values of gas pressure, ignition delay, concentration of nitric oxide, carbon monoxide, and carbon dioxide are proven to be in a agreement with experimental data.

Jaekeun P., and Jaewon H. [2000] introduced a new experimental method to predict the temperature of the combustion chamber during the combustion period

by measuring the breakdown voltage between spark plug electrodes.

This research is based on the principle that breakdown voltage is mainly effected by temperature and pressure at the same material and width of electrode. A constant volume bomb is used in order to confirm the theory and correlate the breakdown voltage measurement system.

The major factors that effects the breakdown voltage are:

1. gap width.
2. gas nature.
3. gas pressure.
4. gas temperature.

In order to extract the temperature profile from breakdown voltage; Pashen's equation is used;

$$Vo_b = A.\rho.d + B\sqrt{\rho.d} \quad (2.2)$$

$$\rho = (\frac{P}{1013}).(\frac{293}{T+273}) \quad (2.3)$$

Where; Vo_b breakdown voltage.

ρ density which is depend on pressure and temperature.

d width between electrode.

A and B coefficients depend on electrode material and shape and they decided experimentally.

The temperature profile can be done by measuring the pressure and breakdown voltage in the following equation;

$$T = \frac{0.334.A^2.d^2.P}{(-0.538.B\sqrt{d} + \sqrt{0.289B^2d + 1.156AdVo_b})^2} \quad (2.4)$$

The result was compared with the two-zone model of heat release rate. The result show that, the maximum temperature increase as the load increase and the results from breakdown voltage method coincide with the results from two-zone model.

Catania A. E. [2001] developed a refined two zone heat release model to use combustion diagnostic for determining the actual burning rate in spark-ignition engines. The convective surface-averaged heat flux is determined by a quasi-steady application of Newton's law, regarding the heat transfer coefficient as a function of the instantaneous flow properties as well as of geometric and operating engine variables. The thermodynamic properties of both reactants and products were evaluated from JANAF tables with a multiple species equilibrium composition calculation performed for the burned zone.

A CAD procedure was introduced in order to estimate the burned and unburned zone heat transfer wall areas for assigned geometric features of the flame front, whereas the burned and unburned gas volumes are often

used as weighting factors of their related heat fluxes in the global heat transfer calculation. Furthermore, the energy conservation equation was applied to the unburned gas zone instead of the isentropic relation that is commonly used for evaluating the temperature of the unburned gas. A refinement was also included for the calibration procedure of the cumulative mass fraction burned or of the fuel energy released, at the flame propagation process. This model appeared to be an accurate tool of combustion diagnostic for spark ignition engine.

Holger P., and Ralph W. [2001] investigated numerical calculations performed in a 6-cylinder 2.81 SI-engine running at wide open throttle. The numerical calculations were performed using the finite volume CFD code. The mesh generation process, including the description of the piston and the valve motion, was automated using ICE. Combustion in the present study was treated with the one-equation Weller flamelet model. The mass fractions of the combustion products were assumed to follow the local and instantaneous thermodynamic equilibrium values. Eleven species were considered: O_2, CO_2, H_2O, N_2, H, O, N, H_2, OH, CO, and NO. Isooctane was used as fuel. The calculated cylinder pressure and mass fraction burned are compared with the experimental results, and indicated a good agreement for equivalence ratios between 0.9 and 1.3 and engine speeds up to 3000 rpm.

Inyong C. [2001] studied experimentally the unburned end-gas tempera- tures in a combustion chamber of a conventional 4-cylinder spark-ignition engine by using the broadband CARS temperature measurement technique. The measured CARS temperatures were compared with adiabatic core temperatures calculated from measured pressures. CARS temperatures measured at the cylinder pressure of 1400 kPa and above were higher than adiabatic core temperatures. The temperature

elevation due to the pre-flame reaction correlated better with the CARS temperature than with the cylinder pressure. The temperature elevation showed a very good correlation with the unburned gas temperature without regard to the research octane number of fuel.

Razavi M. R. [2002] studied the effect of spark plug position on the combustion process in spark ignition engine by using the developed quasi-dimensional cycle simulation (using two-zone burning model). The purpose of this work is to model the geometric interaction between the propagation flame and the general cylindrical combustion chamber. Eight different cases were recognized. Appropriate equations to calculate the flame area(A_f), the burned and the unburned volume (V_b and V_u) and the heat transfer areas related to the burned and unburned regions were derived and presented for each case. The result show that the combustion chamber geometry and the position of spark plug have a strong effect on the burning time duration.

Zhichao T. ,and Rolf D. [2003] developed a multi-dimensional model to predict the combustion process in a direct injection spark ignition engine. An equation to calculate ignition kernel growth rate is derived in this study. The kernel growth rate is highly influenced by the spark discharge energy in the early stage of the ignition process. After the kernel becomes bigger, the effects of flow turbulence on the kernel growth rate become apparent. The kernel flame surface positions are marked by Lagrangian Maker particles to make the model suitable to 3-D engine simulations. Even when the ignition kernel size is smaller than the computational grid size, the kernel growth can still be tracked well. Thus, the use of fine numerical mesh to predict the ignition process is not needed. The diffusion combustion behind the premixed flame branches is modeled

by using a modified characteristic time scale model. In practical engine calculations, the size of the computational cells is of the same order as the thickness of the turbulent flame brush. So in this study the detailed turbulent flame brush structure can be ignored. The results agree well with available experimental cylinder pressure data.

Tastschl R., and Bogensperger M. [2005] presented a CFD analysis of spark ignition engine combustion. Flame initiation is modeled based upon a spark-ignition model accounting for the local thermochemistry, velocity and turbulence conditions at the spark location. The flame propagation characteristics in terms of turbulent flame speed was governed by the local thermodynamic conditions and mixture composition as well as the local turbulence intensity. The spatial evolution of the flame, however, is a result of the superimposed effects of turbulent flame propagation, the volumetric expansion of the hot combustion products behind the flame front and the convective effects of the in-cylinder flow field. In addition, the in-cylinder flow field during combustion is altered by the combustion process itself, but also by its interaction with the combustion chamber and piston bowl geometry. In the flame contour plot, each contour presented the flame front position at a certain crank angle. The result shows how the spark location and the spark timing influence the flame contours and knock-onset characteristics. The initial and boundary condition of this model were taken from 1D cycle simulation results.

2.2 Literature Review Related to Automotive Engine Pollutants Emission

During the course of the past six decades, the internal combustion engine has been under ever tighter scrutiny, regarding its role as a major source of air pollution. The emissions for spark ignition engine can be approached either by exploratory testing or indirectly by using a mathematical model to predict low-emission modifications. Experimental investigations, however valuable in themselves, yield only qualitative conclusions about pollutant formation mechanisms. It is cost effective in the long term to generate a mathematical model which embodies the key combustion mechanisms well enough to guide the development and the design of engines.

Benson R.S. [1975] presented a model including intake and exhaust systems for a single cylinder four-stroke cycle spark ignition engine. The power cycle simulation requires only one empirical factor to correct for turbulent speed of the flame front in order to complete the cycle calculation including NO. Calculations are presented and compared well with the previous work.

The model combines a full power cycle simulation with the prediction of NO emission with a comprehensive gas dynamic model for the cylinder and ducts allowing for chemical reactions in the exhaust pipe. Calculations are presented comparing the predicted NO with test results from a single cylinder engine. It is shown that good agreement is obtained between the predicted and measured NO over an equivalence range (0.8-1.1) when the flame speed is corrected at the equivalence (0.9) corresponding to the peak NO.

Mayo J. [1975] studied the effect of engine design parameters on combustion rate in spark ignition engines, by calculation, showed that the

fast combustion rates tend to produce low NO_X levels. Their analysis has been partially confirmed by actual engine data on a highly turbulent fast burn engine. Thus, an experimental program was conducted to develop quantitative data on the effect of some of the engine design features that are known to have a significant influence on combustion rate. The effect of five engine design factors on combustion rate was determined. Burn time measured on 17 different engine configurations, each configuration containing different design levels of the five design factors. Burn time measurement was made on a carbureted highly turbulent bowl-in piston fast burn engine with a centrally located spark plug. Significant reduction in burn time was achieved by application of the design factors. The effect of emissions was also examined.

Way R.J.B [1977] studied two alternative methods for the calculation of gas composition. These are:

1. Complete chemical equilibrium.
2. Combination of chemical rate equations for some slower reactions with partial equilibrium for faster reaction. Some calculated results are given in the form of comparisons between the two methods, showing the changes in gas composition caused by a temperature rise and fall with a constant rate of change of temperature. Equations are also given for thermodynamic properties of individual species, which may be used together with the appropriate gas composition to obtain properties of the gas mixture. Methods of gas composition in engines are presented as means to the calculation of both thermodynamic properties and exhaust emissions. The equilibrium calculation based on empirical equations is given for thermodynamic properties of individual

gases, overall gas properties may be obtained which are sufficiently accurate over a wide temperature range.

The result presented shows that the deviations from equilibrium for the C-H-O and N-O systems occur at sharply different temperatures so that under all conditions that lead to significant changes in Nitric Oxide concentrations the C-H-O reactions are so fast as to approach equilibrium.

Westbrook C. K. and Pitz W. J. [1988] studied experimentally the inevitability of engine-out NOx emissions from spark ignition and diesel engines. Combustion experiments were carried out for fuels including natural gas, propane and indolne. This study clearly indicates that a limiting temperature exists for sustaining viable combustion for both lean-burn spark and diesel engine configurations presently used in heavy-duty applications. At the pressures typical of both spark ignition and diesel engines(50 – 100 bars), the limiting temperature is of the order of 1900K. Above this temperature, NOx production is significant, while below this limit, significant emissions of unburned hydrocarbons are the result. This limiting temperature for combustion viability leads directly to a limit in the potential for NOx reductions in-cylinder.

Ivan A., and Antonio B. [1998] presented a simulation of steady state engine performance and emissions in spark ignition engines.
The modeling approach is based on a one dimension simulation of the unsteady gas flow in intake and exhaust ducts and a turbulent combustion model. In order to accurately predict exhaust emissions, these models were coupled with a quasi-dimensional, multi-zone model developed for the estimation of the in cylinder thermal distribution, and a NO model based on the zeldovich mechanism. The accuracy of the developed model structure

has been tested on a reference set of 88 engine measurements at different operating conditions.

The results were extremely satisfactory and a good agreement between measured and predicted indicated torque and NO emissions in a wide engine operating range has been found.

Gupta H. N., and Jehad Y. [2003] developed analytical model to study the effect of various operating parameters on the combustion duration as well as the effect of combustion duration on the engine performance and emission characteristics to get a better understanding of the interaction between these parameters.

This model was verified for gasoline-fueled engines and then verified it for the case of propane fueled engines. This was the first part of this study. For this part certain thermodynamic properties and coefficients of internal energies of the reaction for propane fuel were introduced

The second part of the study was carried out by first finding the Maximum Brake Torque angle for each engine speed. This is done to eliminate the effect of ignition angle. Furthermore, the compression ratio was chosen to be equal to 9. The combustion duration was then varied by varying the equivalence ratio of the mixture and the effect of some engine design parameters on combustion duration (in milliseconds) was studied. The model was tested and verified against experimental data of several engines.

2.3 Summary

The spark ignition engine combustion process is an extremely complicated combination phenomena. There is an extensive experimental and modeling literature on engine combustion as shown in the previous literature. But due to the complexity of the combustion process, such researches are always in complete to a significant extent. These models often must incorporate correlations of experimental data, and that the field of combustion modeling is continually developing. In the present work a mathematical model to analyze the combustion process which predict the cylinder pressure, temperature field, flame speed, and pollutants concentration as function of engine variables. This work increases the understanding of the interactions between the processes and/or the variables involved.

CHAPTER 3

THEORETICAL ANALYSIS

3.1 Introduction

The spark-ignition engine combustion process is extremely complicated combination phenomena. It involves an arc discharge, the fuel oxidation chemistry, heat losses in a complex geometry, and the role of turbulence over a wide range of length and time scale.

A mathematical model has been developed in the present work, to study the engine combustion process which predicts the in-cylinder pressure, temperature, flame speed, NOx, and CO concentrations as function of engine variables.

3.2 The Mathematical Model

Mathematical models of spark ignition engine cycle calculation can be classified as zero-dimensional, quasi-dimensional, or multi-dimensional, depending on how critical processes such as combustion are related to the in cylinder flow field [26].

Zero dimensional models are based on the equations of thermodynamics, which do not involve any flow-field details, and are primarily of value in analyzing the energy conservation aspects of internal combustion engines. The cylinder charge is assumed to be homogenous in both temperature and composition. This model can be used as a predictive or a diagnostic tool depending on whether the pressure or the mass burning rate is specified as

a function of the crank shaft angle. Frequently a Wiebes function is used to specify the mass fraction of burnt gases as a function of the crank angle [27].

$$X_b = 1 - exp[-I_1(\frac{\theta - \theta_{ign}}{\Delta\theta_b})^{I_2+1}] \quad (3.1)$$

Where; X_b mass fraction of the burned mixture.

θ crank angle[degree].

θ_{ign} start of combustion angle.

$\Delta\theta_b$ crank angle interval from start to completion of combustion [degree].

I_1 and I_2 adjustable parameters.

Multi-dimensional models are based on the solution of the Navier-Stokes equation, and directly related in cylinder processes to the details of the in-cylinder flow.

These models have been used more to develop critical engine processes rather than to predict the engine's operating characteristics.

Quasi-dimensional models Figure(3.1) were developed to bridge the gap between the zero and multi-dimensional models. Quasi-dimensional models are fast execution models, which can be used extensively by automotive industry in order to develop engine design and filling and emptying operation very fast [3]. It introduces a spatial dependence into processes such as combustion and heat transfer in an explicit phenomological manner, rather than deriving that spatial dependence from the solution of the full set of conservation equations.

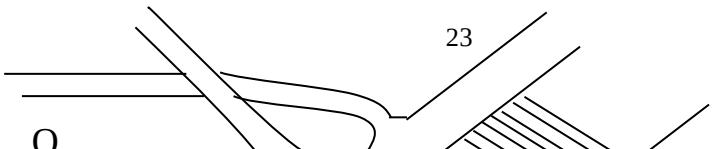

Figure(3.1): Schematic diagram of the combustion chamber
u.. unburned zone, b.. burned zone, W.. work, and Q.. heat.

In this work the spark ignition cycle is treated as a sequence of four continues process: intake, compression, combustion, expansion. The combustion process is simulated as a two zone quasi-dimensional model. The combustion chamber is divided into two volumes: the unburned zone(sub index u) composed by air, fuel and residuals and burnt zone(sub index b) composed by combustion products. The energy equation for each zone is applied to an open system. The Woshni correlation[28] is used to calculate the rate of heat transfer from the engine. The numerical method for solving the differential equations in this work is Runge-Kutta of fourth order.

3.3 The State of the Cylinder Content

Mixture requirements and preparation are usually discussed in terms of equivalence ratio Φ (actual fuel-air ratio / stoichiometric fuel-air ratio), which is calculated as follows [2];

$$\Phi = \frac{\left(\frac{[Fuel]}{[Air]}\right) Act.}{\left(\frac{[Fuel]}{[Air]}\right) St.} \tag{3.2}$$

The composition of the working fluid for spark ignition engine during intake and compression strokes consists of air, fuel, and residual gases (see Appendix A).

3.4 Geometrical Properties of Reciprocating Engine

The basic geometry of a reciprocating internal-combustion engine is shown in Figure (3.2). The Figure includes cylinder, piston, crank shaft, and connecting rod, and most geometric and kinematics' properties of the engine can be derived from this simple schematics.

Compression ratio CR;

$$CR = \frac{maximum\,cylinder\,volume}{minimum\,cylinder\,volume} = \frac{V_{dic} + V_c}{V_c} \tag{3.3}$$

Where; V_{dic} is the displaced or swept volume and V_c is the clearance volume.

The angle θ, defined as shown in Figure (3.2), is called the crank angle.

The total cylinder volume at any crank angle position θ is given by Ferguson [29] as;

$$V(\theta) = V_C + \left[\frac{V_{cyl} - V_C}{2}\right]\left[\frac{\ell}{r} + 1 + \cos(\theta) - \sqrt{\left(\left(\frac{\ell}{r}\right)^2 - \sin^2(\theta)\right)}\right] \tag{3.4}$$

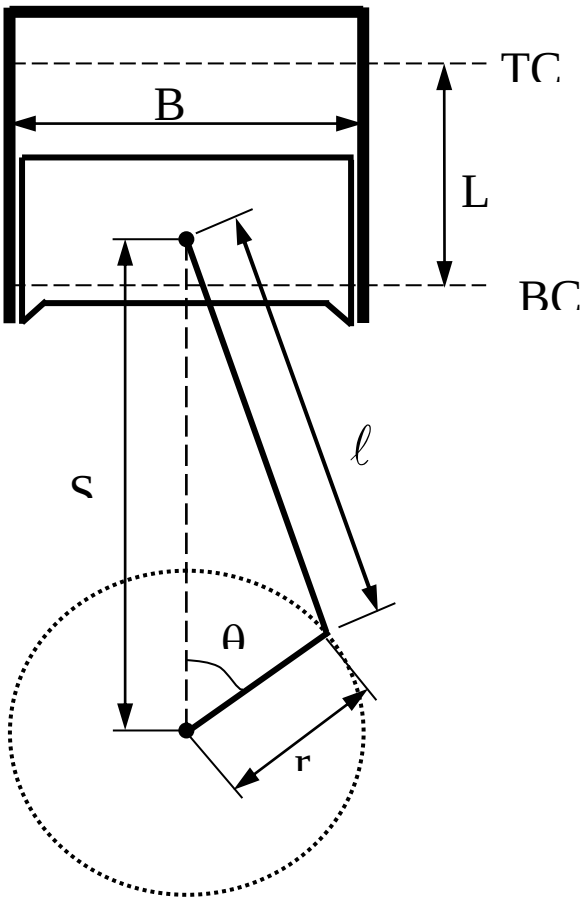

Figure (3.2): Geometry of cylinder, piston, connecting rod, and crankshaft [29].

The area must be known as a function of time. The formula suggested by J.B. Heywood [2] is used in the present work;

$$A = A_{Piston} + A_{Head} + \pi.B.P_{disp} + \frac{4V_C}{B} \tag{3.5}$$

And

$$P_{disp} = \ell + \frac{L}{2}.(1 - cos(\theta)) - \sqrt{\left(\ell^2 + \frac{L^2}{4}.(cos^2(\theta - 1))\right)} \tag{3.6}$$

Where; A total area of the combustion chamber [m^2].

A_{Piston} piston surface area [m^2].

A_{Head} cylinder head surface area [m^2].

V_C clearance volume [m^3].

Detailed specification of engine test are given in the Appendix (B).

An important characteristic speed is the mean piston speed u_p

$$u_P = 2L.rps \tag{3.7}$$

Where rps is the rotational speed of the crankshaft (rev/sec).

3.5 Thermodynamic Properties of Mixtures

When large numbers of computations are being made or high accuracy is required, engine process calculations are carried out on a computer. Relationships which model the composition and thermodynamic properties of gas mixtures have been developed for computer use. The most complete models are based on polynomial curve fitting to the thermodynamic data for each species in the mixture and the assumptions that the unburned mixture is frozen in composition and the burned mixture is in equilibrium. The different thermodynamic properties of gas mixture are calculated as follows;

3.5.1 Enthalpy, Internal Energy and Specific Heats

The specific enthalpy is [30];

$$h = h_\circ + h(T) \quad \text{[kJ/Kmol]} \tag{3.8}$$

The internal energy is;

$$e = e_\circ + e(T) \quad \text{[kJ/Kmol]} \tag{3.9}$$

$$e(T) = h(T) - R_{mol}.T \quad \text{[kJ/Kmol]} \tag{3.10}$$

$$h_\circ = e_\circ \tag{3.11}$$

Where; $e_\circ$ and $h_\circ$ are the specific internal energy and specific enthalpy at the absolute zero, respectively. Hence: -

The specific enthalpy $h(T)$ and the internal energy $e(T)$ for gas i is given by Benson [30] as;

$$h_i(T) = R_{mol}.\left(\sum_{i=1}^{5} U_{i,j} T^j\right) \quad \text{[kJ/Kmol]} \tag{3.12}$$

$$e_i(T) = R_{mol} \cdot \left[\left(\sum_{J=1}^{J=5} U_{i,j} . T^{j} \right) - T \right] \qquad \text{[kJ/Kmol]} \qquad (3.13)$$

The coefficients $U_{i,j}$ are given in Appendix(C) with the following subscripts for the species.

species : H_2O H_2 OH H N_2 NO N CO_2 CO O_2 O ARGON C_nH_m

subscript (i) : 1 2 3 4 5 6 7 8 9 10 11 12 13

The total internal energy E is given by the following equation;

$$E = E(T) + E_\circ \qquad [\text{kJ}] \qquad (3.14)$$

Where;

$$E(T) = \sum_{i=1}^{i=n} N_i . e_i(T) \qquad (3.15)$$

$$E_\circ(T) = \sum_{i=1}^{i=n} N_i . (e_\circ)_i \qquad (3.16)$$

N_i is the total number of moles of gases i.

Hence, the total internal energy for a gas mixture of n species is;

$$E = R_{mol} \cdot \sum_{i=1}^{i=n} N_i \cdot \left[\left(\sum_{J=1}^{J=5} U_{i,j} . T^{j} \right) + \frac{(e_\circ)_i}{R_{mol}} - T \right] \qquad \text{[kJ]} \qquad (3.17)$$

The other important properties are the specific heats, and are calculated as follows;

$$C_V(T) = \frac{de(T)}{dT} \qquad \text{[kJ/Kmol.K]} \qquad (3.18)$$

Thus

$$C_V(T) = \frac{1}{Wm} . \frac{dE}{dT} \qquad \text{[kJ/Kmol.K]} \qquad (3.19)$$

Where; $\{Wm = \sum N_i\}$ total number of moles of the mixture.

By differentiating equation (3.17) with respect to temperature T at constant volume and combining with equation (3.19), the following equation obtained;

$$c_V(T) = R_{mol} \cdot \sum_{i=1}^{i=n} \frac{(N_i)}{Wm} \left[\left(\sum_{j=1}^{j=5} j . U_{i,j} . T^{j-1} \right) - 1 \right] \qquad (3.20)$$

The specific heat at constant pressure is defined as;

$$c_P(T) = C_V(T) + R_{mol} \quad \text{[kJ/Kmol.K]} \quad (3.21)$$

3.5.2 Equilibrium Constant

The Equilibrium Constant K_P for any chemical reaction is given by Benson and White house [31]

$$\ln K_P = \frac{-\Delta GT}{Rmol.T} \quad (3.22)$$

Where; GT gibbs free energy of formation at temperature T and a unit pressure p [kJ] hence;

$$\ln K_P = \left[\sum \left(\frac{v_i . g_i(T)}{R_{mol}.T} + \frac{v_i . g_\circ}{R_{mol}.T} \right)_R - \sum \left(\frac{v_i . g_i(T)}{R_{mol}.T} + \frac{v_i . g_\circ}{R_{mol}.T} \right)_P \right] \quad (3.23)$$

Where; vi stoichiometric coefficient of gas i [Kmol].

$g_i(T)$ specific gibbs free energy function at temperature T[kJ/Kmol].

$g_\circ(T)$ specific gibbs free energy function at absolute zero[kJ/Kmol].

The term $\left(\frac{g_i(T)}{R_{mol}.T} \right)$ is given by Benson [31] as;

$$\frac{g_i(T)}{R_{mol}.T} = U_{i,j} - (\ln T) - \sum_{j=2}^{j=5} \frac{U_{i,j}}{j-1} . T^{j-1} - U_{i,j} \quad (3.24)$$

The coefficients $U_{i,j}$ are given in the Appendix (C) with the following subscripts for the species;

Species:	H_2O	H_2	OH	H	N_2	NO	N	CO_2	CO	O_2	O	Argon
Subscript (i):	1	2	3	4	5	6	7	8	9	10	11	12

The equilibrium constant Kp for the following stoichiometric reaction;

$$v_a . A + v_b . B \leftrightarrow v_c . C + v_d . D \quad (3.25)$$

is expressed as;

$$K_P = \left(\frac{X_c^{vc} . X_d^{vd}}{X_a^{va} . X_b^{vb}} \right) . P^{vc+vd-va-vb} \quad (3.26)$$

Where; v stoichiometric coefficient [Kmol].

X_i molar fraction.

P total pressure in atmospheres divided by reference pressure.

Equations (3.23) and (3.26) are used to determine the mole fraction X_i for each species.

3.6 Heat Transfer Model

Heat transfer term represents heat transfer across the system boundary. Heat transfer between the cylinder gases and the cylinder walls takes place during the whole engine cycle. During intake and early compression, heat is transferred from the cylinder walls to the gases, and during combustion and expansion, heat is transferred from the gases to the cylinder walls.

In internal combustion engines, throughout each cycle, the heat transfer takes place under conditions of varying cylinder pressure, unburnt and burnt gas temperature, and local gas velocities. The local gas velocities vary more or less rapidly depending on intake passage design, mean piston speed and combustion chamber configuration. In addition, the surface area of the combustion chamber varies through out the cycle.

Heat transfer affects engine performance, efficiency, and emissions. For a given mass of fuel within the cylinder, higher heat transfer to the combustion chamber walls will reduce the average combustion gas temperature and pressure, and reduce the work transfer to the piston. Changes in gas temperature due to the heat transfer impact on pollutants formation processes, both within the engine cylinders and in the exhaust system. So the balance is very necessary between heat transfer rate and limitation of the combustion chamber wall material. Therefore, the engine heat transfer is of an obvious importance to the engine designer[2].

The heat transfer rate is expressed as;

$$\frac{dQ_{ht}}{dt} = \frac{dQ_{Convection}}{dt} + \frac{dQ_{Radiation}}{dt} \qquad (3.27)$$

The magnitude of the rate of energy transfer by convection, which occurs in a direction perpendicular to the surface fluid interface, is obtained from Newton's law of cooling;

$$\frac{dQ_{Convection}}{dt} = h_C.A.(T_g - T_w) \qquad (3.28)$$

Where; T_g average gas temperature [K].

T_w average wall temperature [K].

A surface area for heat transfer equation (3.5) [m^2].

h_C heat transfer coefficient [$W/m^2.K$].

The most important task is to accurately predict the magnitude of the convection heat transfer coefficient (h_c). Since this quantity is a composite of both microscopic and macroscopic phenomena, many factors must be taken into consideration. For many flow geometries, Nu, is given by the relation;

$$Nu = C.(Re)^m.(Pr)^n \qquad (3.29)$$

The correlation used to calculate the instantaneous spatially averaged heat transfer is based on the form proposed by Woshni [28], which essentially is a Nusselt-Reynolds number of the form;

$$Nu = 0.035\,Re^{0.8} \qquad (3.30)$$

Where; $Nu = \frac{h_C.B}{k}$ is the Nusselt number. (3.31)

$Re = \frac{\rho.w.B}{\mu}$ is the Reynolds number. (3.32)

Assuming $k \propto T, \mu \propto T, and P = \rho RT$, the above correlation can be rewritten;

$$h_C = 3.26\,B^{-0.2}.P^{-0.55}.w^{0.8} \qquad [W/m^2.K] \qquad (3.33)$$

During the compression stroke, Woschni [28] argued that the average gas velocity should be proportional to the mean piston speed. During combustion and expansion he attempted to account directly velocities for

the gas induced by the change in density that results from combustion. Thus, he assumed that the characteristic gas speed to be;

$$w = \left[C_1 u_p + C_2 . \left(\frac{V_{disp}}{V_{cyl}} \right) . \left(\frac{P(\theta) - P_{motor}(\theta)}{P_{cyl}} \right) . T_{cyl} \right] \quad \text{[m/s]} \tag{3.34}$$

Where; $P(\theta)$ cylinder pressure [bar].

$P_{motor}(\theta)$ motoring pressure [bar].

C_1 and C_2 are model constant, which are specified as:

For the gas exchange period: C_1=6.18; C_2 =0

For the compression period: C_1 =2.28; C_2=0

For the combustion and expansion period: C_1=6.18; C_2=3.24e-3

The instantaneous radiant heat flux is expressed as:

$$\frac{dQ_{Radiation}}{dt} = \varepsilon . \delta . A . \left(T_g^4 - T_w^4 \right) \tag{3.35}$$

Due to the difficulties of calculation of shape factor and shortage of time, the heat transfer area in equation(3.60) is the same as for convection.

For the radiation term J.B. Heywood [2] assume that the emissivity of gases are equal to the emissivty of carbon dioxide and water vapor only. The emission of these two gases are calculated as follows;

$$\varepsilon_{co_2} = 0.711 \cdot (p_{co_2} \cdot L_r)^{1/3} / (T_g / 100)^{1/2} \tag{3.36}$$

$$\varepsilon_{H_2O} = 0.707 \cdot (p_{H_2O} \cdot L_r)^{1/3} / (T_g / 100)^{1/2} \tag{3.37}$$

$$\varepsilon = \varepsilon_{CO_2} + \varepsilon_{H_2O} - \varepsilon_{CO_2} . \varepsilon_{H_2O} \tag{3.38}$$

$$L_r = 0.9 \cdot \frac{4 \cdot V}{A} \tag{3.39}$$

Where; L_r is the radiation bath length [m].

3.7 The Power Cycle

3.7.1 Compression Model

The following assumption have been made during the calculation of compression stroke:

1. The mixing between fresh charge and residual gases is perfect.
2. No chemical reaction occurs during compression.

The calculation procedure starts with the trapped mass of fuel, air and residuals, and ends after delay period process, when the mixture is ignited by the spark plug.

The pressure and temperature in this process are then calculated using step by step method to solve the first law of thermodynamics equation and the equation of state.

The first law of thermodynamic for an open system is;

$$\frac{dQ_{ht}}{dt} = \frac{dE}{dt} + \frac{dW}{dt} \qquad \text{[kJ/sec]} \tag{3.40}$$

Where; dQ_{ht} Heat transfer to the cylinder wall [kJ], and it's computed from heat transfer model section (3.6).

dE Change of internal energy in the system [kJ], and its computed from internal energy section (3.5.1).

dW Work transfer from the system [kJ].

$$dW = P.\frac{dV}{dt} \tag{3.41}$$

And from definition of internal energy and specific heat;

$$\frac{dE}{dt} = N\ .CV\ (T).\frac{dT}{dt} \tag{3.42}$$

A combination of equations (3.40), (3.41), and (3.42) after rearrangement gives;

$$\frac{dQ_{ht}}{dt} = N.C_V(T).\frac{dT}{dt} + P\frac{dW}{dt} \tag{3.43}$$

By differentiating the state equation $(P.V = N.R_{mol}.T)$ with respect to the time, the following equation is obtained to calculate the change in temperature during the time step;

$$\frac{dT}{dt} = T \cdot \left[\frac{1}{P} \cdot \frac{dP}{dt} + \frac{1}{V} \cdot \frac{dV}{dt} \right] \tag{3.44}$$

By combination equation (3.43) with (3.44) the following equation is obtained to calculate the change in pressure during the time step;

$$\frac{dP}{dt} = \left[-\left(1 + \frac{R_{mol}}{C_V(T)} \right) . P . \frac{dV}{dt} + \frac{R_{mol}}{C_V(T)} \cdot \frac{dQ_{ht}}{dt} \right] / V \tag{3.45}$$

Equations (3.44) and (3.45) are solved by Runge-Kutta method to calculate the cylinder temperature and pressure respectively during each time step.

$$Y_{i+1} = Y_i + \frac{\Delta t}{6} [k_1 + 2k_2 + 2k_3 + k_4] \tag{3.46}$$

$$\frac{dY}{dt} = f(Y,t)$$

$$k_1 = f(Y_i, t)$$

$$k_2 = f(Y_i + \frac{k_1}{2}, t_i + \frac{\Delta t}{2})$$

$$k_3 = f(Y_i + \frac{k_2}{2}, t_i + \frac{\Delta t}{2})$$

$$k_4 = f(Y_i + k_3, t_i + \Delta t)$$

Where Y is any variable of equations as before.

3.7.2 Combustion Model

Flame geometry analysis is coupled with heat transfer and mass burning rate analysis to obtain a substantial additional insight into the behavior of spark ignition engine flame and the position of the front of the turbulent flame front.

The enflamed zone under normal flame conditions, is close to circle; only in the presence of very high swirl. Thus, the surface which defines the leading edge of the turbulent flame is a portion of the surface of a sphere. The flame is initiated at the spark plug, the volume within the chamber

behind this flame front is defined as the enflamed volume (V_f), and the spherical surface area of radius (r_f) is defined as flame front area (A_f). Appendix (D) show the geometric interactions of the combustion chamber.

3.7.2.1 Ignition Model

In the present work, the ignition model used the same approach as Zhichao[18], the ignition kernel is assumed to be spherical during the initial ignition process. When the kernel grows, the particles move outwards radially from the spark plug electrodes. The ignition particle's speed, i.e., the kernel growth rate, is influenced by the flow turbulence and air-fuel mixture stoichiometry.

A thermodynamic system of an ignition kernel is used to analyze the flame kernel growth rate. The following assumptions are made in the calculations:

1. The calculation starts at 1μs after the breakdown period. The ignition kernel is assumed to be spherical. Its radius is assumed to be 0.5mm at this time.
2. The ignition kernel flame is very thin and separates the burned and unburned gas.
3. The ignition kernel surface is located just in front of the flame, and thus, there is no heat transfer between the kernel and unburned gas.
4. The pressure is uniform inside the kernel and outside the kernel.
5. The temperature inside the kernel is uniform.

The ignition kernel mass-burning rate $M_k^{\bullet}$, which is also the increase in the flame kernel mass, is written as;

$$M_k^{\bullet} = \frac{dM_k}{dt} = \rho_u . A_K . S_T \qquad (3.47)$$

Where; ρ_u unburned gas density [kg/m³].

A_K flame kernel surface area [m²].

S_T turbulent speed [m/s].

In addition, using $M_k = \rho_k . V_k$, the mass-burning rate can be rewritten as;

$$\frac{dM_k}{dt} = \frac{d(\rho_k . V_k)}{dt} = \rho_k . \frac{dV_k}{dt} + V_k . \frac{d\rho_k}{dt} = \rho_u . A_k . S_T \quad (3.48)$$

Where; ρ_k gas density [kg/m³].

V_k kernel volume [m³].

Utilizing the ideal gas law($P = \rho . R . T$);

$$\frac{1}{\rho_k} . \frac{d\rho_k}{dt} = \frac{1}{P} . \frac{dP}{dt} - \frac{1}{T_k} . \frac{dT_k}{dt} \quad (3.49)$$

The following equation is obtained;

$$\frac{dV_k}{dt} = \frac{\rho_u}{\rho_k} . A_k . S_T + V_k (\frac{1}{T_k} . \frac{dT_k}{dt} - \frac{1}{P} . \frac{dP}{dt}) \quad (3.50)$$

Normalizing the volume increase to the flame kernel surface area A_k, the change in flame kernel radius can be obtained as;

$$\frac{dr_k}{dt} = \frac{\rho_u}{\rho_k} . S_T + \frac{V_k}{A_k} (\frac{1}{T_k} . \frac{dT_k}{dt} - \frac{1}{P} . \frac{dP}{dt}) \quad (3.51)$$

Zhichao[18], assumes that during the ignition process, the pressure increase due to the combustion is negligible, and the temperature inside the kernel is spatially uniform and equal to the adiabatic flame temperature of the fuel-air mixture.

With these two assumptions, the kernel growth rate is simplified as;

$$\frac{dr_k}{dt} = \frac{\rho_u}{\rho_k} . S_T \quad (3.52)$$

This flame kernel growth is initially laminar like, at least at low to mid-speed engine operating conditions[3].

3.7.2.2 Flame Propagation Model

In spark ignition engines, the premixed flame, where the chemical reactions take place, is relatively thin. This thin flame separates the unburned and burnt gas. In quasi-dimensional model, Figure(3.1) the cylinder charge is assumed to be composed of ideal gases, frozen in the un burnt gas region and in chemical equilibrium, (except for NO emission), in the burnt gas region. The first law of thermodynamic, equation of state and conservation of mass and volume are applied to the burnt and un burnt regions. The pressure is assumed to be uniform throughout the cylinder charge and a system of first order ordinary differential equations are obtained for the pressure, mass, volume, temperature of the burnt and un burnt gases, heat transfer from burnt and un burnt zones.

This model attempt to predict the burning rate as a function of turbulent flame speed (S_T) and instantaneous flame area (A_f). This approach allows the calculated burn rates to respond to cylinder geometry and flows.

The mass burning rate is predicted by the following formula [3];

$$\frac{dM_b}{dt} = A_f \cdot \rho u \cdot S_T \tag{3.53}$$

Where;

M_b mass of burnt gases [kg].

t time [sec].

But $M_b = \rho_b . V_b$ (3.54)

The mass-burning rate can be rewritten as;

$$\frac{dM_b}{dt} = \frac{d(\rho_b . V_b)}{dt} = \rho_b . \frac{dV_b}{dt} + V_b . \frac{d\rho_b}{dt} = \rho_u . A_f . S_T \tag{3.55}$$

Where; ρ_b burnt gas density [kg/m³].

V_b enflamed volume [m³].

Utilizing the ideal gas law($P = \rho . R . T$);

$$\frac{1}{\rho_b} . \frac{d\rho_b}{dt} = \frac{1}{P} . \frac{dP}{dt} - \frac{1}{T_b} . \frac{dT_b}{dt} \tag{3.56}$$

The following equation is obtained;

$$\frac{dV_b}{dt} = \frac{\rho_u}{\rho_b}.A_f.S_T + V_b\left(\frac{1}{T_b}.\frac{dT_b}{dt} - \frac{1}{P}.\frac{dP}{dt}\right) \quad (3.57)$$

Normalizing the volume increase to the flame front area, the change in flame radius can be obtained as;

$$\frac{dr_f}{dt} = \frac{\rho_u}{\rho_b}.S_T + \frac{V_b}{A_f}\left(\frac{1}{T_b}.\frac{dT_b}{dt} - \frac{1}{P}.\frac{dP}{dt}\right) \quad (3.58)$$

The first law of thermodynamic for an open system is:

$$\frac{dQ_{ht}}{dt} = \frac{dE}{dt} + \frac{dW}{dt} \quad \text{[kJ/sec]} \quad (3.59)$$

Where; dQ_{ht} total heat transfer rate to the cylinder wall [kJ].

dE change of internal energy in the system [kJ].

dW work transfer from the system [kJ].

$$\frac{dQ_{ht}}{dt} = \frac{dQ_b}{dt} + \frac{dQ_u}{dt} \quad (3.60)$$

$$\frac{dQ_b}{dt} = A_b.h_{cb}.(T_b - T_w) + A_b.\sigma.\varepsilon_g(T_b - T_w) \quad (3.61)$$

$$\frac{dQ_u}{dt} = A_u.h_{cu}.(T_u - T_w) \quad (3.62)$$

The total internal energy of cylinder contents is;

$$\frac{dE}{dt} = \frac{dE_b}{dt} + \frac{dE_u}{dt} \quad (3.63)$$

$$\frac{dE_b}{dt} = N_b.\frac{de_b(T_b)}{dt} + e_b.\frac{dN_b}{dt} \quad (3.64)$$

$$\frac{dE_u}{dt} = N_u.\frac{de_u(T_u)}{dt} + e_u.\frac{dN_u}{dt} \quad (3.65)$$

And from definition of specific heat at constant volume;

$$C_V(T) = \frac{de(T)}{dT} \quad (3.66)$$

Now;

$$\frac{dM_b}{dt} = -\frac{dM_u}{dt} \quad (3.67)$$

$$Mw_b.\frac{dN_b}{dt} = -Mw_u\frac{dN_u}{dt} \quad (3.68)$$

Where ; Mw_u molecular weight of un burnt mixture [kg/Kmol].

Mw_b molecular weight of burnt mixture [kg/Kmol].

Thus equation (3.63) becomes after rearrangement;

$$\frac{dE}{dt}=\left(e_b(T_b)-e_u(T_u).\frac{Mw_b}{Mw_u}\right)\frac{dN_b}{dt}+N_b.C_{Vb}(T_b).\frac{dT_b}{dt}+N_u.C_{Vu}(T_u).\frac{dT_u}{dt} \quad (3.69)$$

The work transfer from the system is;

$$\frac{dW}{dt}=P.\frac{dV}{dt} \quad (3.70)$$

$$\frac{dV}{dt}=\frac{dV_u}{dt}+\frac{dV_b}{dt} \quad (3.71)$$

The differentiation of the equation of state with respect to time gives;

$$\frac{dV_u}{dt}=\frac{R_{mol}.N_u}{P}.\frac{dT_u}{dt}+\frac{R_{mol}.T_u}{P}.\frac{dN_u}{dt}-\frac{V_u}{P}.\frac{dP}{dt} \quad (3.72)$$

$$\frac{dV_b}{dt}=\frac{R_{mol}.N_b}{P}.\frac{dT_b}{dt}+\frac{R_{mol}.T_b}{P}.\frac{dN_b}{dt}-\frac{V_b}{P}.\frac{dP}{dt} \quad (3.73)$$

$$\frac{dV}{dt}=(\frac{V_b}{N_b}-\frac{V_u}{N_u}.\frac{Mw_b}{Mw_u})\frac{dN_b}{dt}+\frac{R_{mol}.N_u}{P}.\frac{dT_u}{dt}+\frac{R_{mol}.N_b}{P}.\frac{dT_b}{dt}-\frac{V}{P}.\frac{dP}{dt} \quad (3.74)$$

Applying the first law of thermodynamic for unburned zone;

$$\frac{dQ_u}{dt}=\frac{dE_u}{dt}+P\frac{dV_u}{dt} \quad (3.75)$$

The combination of equations (3.65), (3.72), and (3.75) gives;

$$\frac{dT_u}{dt}=\frac{1}{N_u.C_{Pu}(T_u)}.\frac{dQ_u}{dt}+\frac{V_u}{N_u.C_{Pu}(T_u)}.\frac{dP}{dt} \quad (3.76)$$

A combination of equations (3.72), and (3.76) after rearrangement gives;

$$\frac{dT_b}{dt}=\frac{P}{N_bR_{mol}}\left[\frac{dV}{dt}-\left(\frac{R_{mol}.T_b}{P}-\frac{R_{mol}.T_u}{P}.\frac{Mw_b}{Mw_u}\right)\frac{dN_b}{dt}-\frac{V_u.R_{mol}}{P.C_{Pu}}.\frac{dP}{dt}-\frac{R_{mol}}{P.C_{Pu}}.\frac{dQ_u}{dt}+\frac{V}{P}.\frac{dP}{dt}\right] \quad (3.77)$$

Finally a combination of equations (3.67), (3.67), and (3.77) after rearrangement gives;

$$\frac{dP}{dt} = \frac{-\left[P\frac{dV}{dt}\left(1+\frac{C_{Vb}}{R_{mol}}\right)+\left(\frac{C_{Vu}}{CP_u}-\frac{C_{Vb}}{CP_u}\right)\frac{dQ_u}{dt}+\left[e_b - e_u\frac{Mw_b}{Mw_u}-C_{Vb}\left(T_b - T_u\frac{Mw_b}{Mw_u}\right)\right]\frac{dN_b}{dt}-\frac{dQ_{ht}}{dt}\right]}{\left[\frac{C_{Vu}(T_u)}{C_{Pu}(T_u)}.V_u - \frac{C_{Vb}(T_b)}{C_{Pu}(T_u)}.V_u + \frac{C_{Vb}(T_b)}{R_{mol}}.V\right]} \quad (3.78)$$

Equations (3.76), (3.77), and (3.78) are solved by Runge-Kutta method to calculate the unburned zone temperature, the burned zone temperature, and the cylinder pressure respectively during each time step.

3.7.3 Expansion Model

Once combustion process is complete the cylinder is considered as a single zone with a uniform temperature and pressure.

The number of moles for each species is calculated during each time step. The calculation stop at exhaust valve opening. This completes the power cycle.

The first law of thermodynamics for an open system is;

$$\frac{dQ_{ht}}{dt} = \frac{dE}{dt} + \frac{dW}{dt} \quad (3.79)$$

Where ; dQ_{ht} heat transfer rate to the cylinder wall [kJ], and it is computed from heat transfer section (3.6).

dE change of internal energy in the system [kJ], and it is calculated from internal energy model section (3.5.1).

dW work transfer from the system [kJ].

The work done is;

$$\frac{dW}{dt} = P.\frac{dV}{dt} \quad (3.80)$$

And from the definition of internal energy and specific heat;

$$\frac{dE}{dt} = N.C_V(T).\frac{dT}{dt} \quad (3.81)$$

A combination of equations (3.79), (3.80) and (3.81) after rearrange-ment gives;

$$\frac{dQ_{ht}}{dt} = N.C_V(T).\frac{dT}{dt} + P\frac{dV}{dt} \tag{3.82}$$

By differentiating the state equation, ($P.V = N.R_{mol}.T$) with respect to time and after rearrangement, the following equation is obtained to calculate the change in temperature during the time step;

$$\frac{dT}{dt} = T.\left[\frac{1}{P}.\frac{dP}{dt} + \frac{1}{V}\frac{dV}{dt}\right] \tag{3.83}$$

Combining equations (3.82), and (3.83) gives following equation which is to calculate the change in pressure during the time step;

$$\frac{dP}{dt} = \left[-\left(1 + \frac{R_{mol}}{C_V(T)}\right).P.\frac{dV}{dt} + \frac{R_{mol}}{C_V(T)}.\frac{dQ_{ht}}{dt}\right] \tag{3.84}$$

Equations (3.83), and (3.84) are solved by Runge-Kutta method to calculate the cylinder temperature and pressure respectively during each time step.

3.8 Flame Speed Model

The laminar flame speed is defined as the velocity, relative and normal to the flame front, with which the unburned gas moves into the front and is converted into products under laminar flow conditions.

The laminar flame speed increase monotonically with temperature, decreases monotonically with pressure, and peaks for equivalence ratios slightly rich of stoichiometric. The most commonly used relationships for laminar flame speed are those derived from spherical combustion bomb measurements by Metgalchi and Keck [6];

$$S_L = S_{L\circ}.(\frac{T_u}{T_\circ})^{\mu}.(\frac{P}{P_\circ})^{\beta} \tag{3.85}$$

Where; S_L laminar flame speed [m/s].

$S_{L\circ}$ laminar flame speed at reference condition[m/s].

T_u unburned gas temperature [K].

P pressure inside the cylinder [atm].

$T_\circ$ and $P_\circ$ temperature and pressure at reference condition.

The temperature and pressure exponents μ and β are independent of fuel types within the estimated experiments and can be represented by the expression;

$$\mu = 2.18 - 0.8(\Phi - 1) \tag{3.86}$$

And

$$\beta = -0.16 + 0.22(\Phi - 1) \tag{3.87}$$

The reference laminar flame speed $S_{L\circ}$ are a weak function of fuel type and can be fit by a second-order polynomial of the form;

$$S_{L\circ} = \beta_m + \beta_2(\Phi - \Phi_m)^2 \tag{3.88}$$

β_m, β_2 *and* Φ_m are constants for a given fuel, and their values are given in table (3.1) for several types for fuel [6].

Fuels	Φ_m	$\beta_m [cm/s]$	$\beta_2 [cm/s]$
Methanol	1.11	36.92	-140.51
Propane	1.08	34.44	-138.05
Isooctane	1.13	26.32	-84.72
RMFD-303	1.13	27.58	-78.34

Table (3.1): Constant values for $S_{L\circ}$

An important factor in the laminar flame speed correlation is the burned gas fraction in the unburned mixture(the residual gas).The effect is accounted for using the following formula;

$$S_{L)ResidualEff.} = S_L(1 - 2.06\,XR^{0.77}) \qquad [m/s] \tag{3.89}$$

Where; XR is the mole fraction of residual gas.

In a combustion chamber there are two phenomena that increase the laminar flame speed, namely the turbulence produced due to rapid expansion of the burnt gas, and the turbulence of the combustion chamber . Therefore the turbulent flame speed is described as [2];

$$S_T = S_L . ff . \{ \frac{(\rho_u / \rho_b)}{[(\rho_u / \rho_b) - 1] X_b + 1}) \} \quad (3.90)$$

$$X_b = [1 + (\rho_u / \rho_b).(\frac{1}{y_b} - 1)]^{-1} \quad (3.91)$$

$$y_b = V_b / V \quad (3.92)$$

Where; $\frac{\rho_u}{\rho_b}$ ratio of unburned to burned gas density .

V_b burned volume.

ff turbelization factor which is taken proportional to the engine speed RPM [30];

$$ff = 1 + 0.0018.RPM \quad (3.93)$$

For typical engine operating condition, the ratio of the unburned gas density to the burned gas density is about 4 as shown in Heywood [2].

3.9 Products of combustion

There are two methods to determine the composition of combustion products internal combustion engines [22].

The first one is a complete chemical equilibrium, and the second is a combination of chemical rate equations for some slower reactions, (CO and NO), with partial equilibrium for faster reactions. Both methods are used in this work as shown in the next section.

3.9.1 Equilibrium Thermodynamic Reactants

The calculation starts from the equation of combustion of the Hydrocarbon fuel and Air which is represented by;

$$\in .CnHm + \frac{\in}{\Phi}(n + m/4)\left[O_2 + \frac{78}{21}N_2 + \frac{1}{21}Ar\right] \rightarrow X_{H_2O}H_2O + X_{H_2}H_2 +$$

$$X_{OH}OH + X_H H + X_{N_2}N_2 + X_{NO}NO + X_N N + X_{CO_2}CO_2 + X_{CO}CO$$
$$+ X_{O_2}O_2 + X_O O + X_{Ar}Ar \qquad (3.94)$$

The species (H_2O, H_2 , OH, H , N_2, NO, N, CO_2 , CO, CO_2, O_2 , O , Ar). are considered to be present in the product in the cylinder and in the exhaust gases.

The composition is calculated in terms of molar fraction of these species denoted by X:

The equation assumes that one mole of the total products is generated from $\in$ moles of fuel plus $\frac{1}{\Phi}$ times the stoichiometric quantity of air. The equilibrium distribution of these species can be fully described by the following seven reactions [20];

$$(1)\ \frac{1}{2}H_2 \leftrightarrow H \qquad (3.95)$$

$$(2)\ \frac{1}{2}O_2 \leftrightarrow O \qquad (3.96)$$

$$(3)\frac{1}{2}N_2 \leftrightarrow N \quad (3.97)$$

$$(4)H_2O \leftrightarrow 2H_2 + O_2 \quad (3.98)$$

$$(5)H_2O \leftrightarrow OH + \frac{1}{2}H_2 \quad (3.99)$$

$$(6)CO_2 + H_2 \leftrightarrow H_2O + CO \quad (3.100)$$

$$(7)H_2O + \frac{1}{2}N_2 \leftrightarrow H_2 + NO \quad (3.101)$$

The equilibrium constants for these reactions are ;

$$(1)K_{P1} = \frac{X_H}{\sqrt{X_{H_2}}}.\sqrt{P} \quad (3.102)$$

$$(2)K_{P2} = \frac{X_O}{\sqrt{X_{O_2}}}.\sqrt{P} \quad (3.103)$$

$$(3)K_{P3} = \frac{X_N}{\sqrt{X_{N_2}}}.\sqrt{P} \quad (3.104)$$

$$(4)K_{P4} = \frac{X_{O_2}}{b^2}.\sqrt{P} \quad (3.105)$$

$$(5)K_{P5} = \frac{X_{OH}}{b.\sqrt{X_{H_2}}}.\sqrt{P} \quad (3.106)$$

$$(6)K_{P6} = \frac{b.X_{CO}}{X_{CO_2}} \quad (3.107)$$

$$(7)K_{P7} = \frac{X_{NO}}{b.\sqrt{X_{N_2}}}.\sqrt{P} \quad (3.108)$$

Where $b = \frac{X_{H_2O}}{X_{H_2}}$ (3.109)

The equilibrium constants K_P for these reactions are calculated by the method described in section (3.5.2).

There are 13 unknowns in equation (3.94), namely 12 mole fractions X_i and the total number of moles of fuel $\in$. seven equations are available (3.104 – 3.108), therefore, six more equations are needed for the solution .

One of these is;

$$\sum_{i=1}^{i=12} X_i = 1 \tag{3.110}$$

The reminder are the atomic balance for Argon, carbon, Hydrogen, Oxygen, and Nitrogen .

Let the number of atoms of Ar, C, H, O , and N corresponding to 1 mole of fuel by VE, WE, XE, LE , and ZE respectively, and noting that ($\in$) moles of fuel corresponds to 1 mole of products.

Therefore the atomic balance can be made as follows;

$$\text{Argon}: \text{XAr} = \in .\text{VE} \tag{3.111}$$

$$Carbon: X_{CO} + X_{CO2} = \in .WE \tag{3.112}$$

$$Hydrogen: 2X_{H2O} + 2X_{H2} + X_{OH} + X_H = \in .XE \tag{3.113}$$

$$Oxygen: X_{H2O} + X_{OH} + X_{NO} + 2X_{CO2} + X_{CO} + 2XO_2 + XO = \in .\text{LE} \tag{3.114}$$

$$Nitrogen: 2XN_2 + XNO + XN = \in .ZE \tag{3.115}$$

The values of VE, WE, XE, YE and ZE are known from fuel-air reaction equation (3.94).

The following relationships are obtained:

$$LE = \frac{1}{\Phi}\left(2n + \frac{m}{2}\right) \tag{3.116}$$

$$WE = n \tag{3.117}$$

$$XE = m \tag{3.118}$$

$$ZE = LE.\frac{78}{21} \tag{3.119}$$

$$VE = \frac{1}{2}.LE.\frac{1}{21} \tag{3.120}$$

Values of $\in$ and b are calculated as follows [31].

The first estimate of the parameters ($\in$) and (b) is made by using the following expressions, where Φ is the equivalence ratio, P is the pressure in atmospheres and T is the temperature in Kelvin.

For $\Phi < 1.0$;

$$\in = \frac{1.3}{\left[0.25XE + 2.363(2.WE + 0.5XE)/\Phi\right].\exp(0.13.T/1000)} \quad (3.121)$$

And for $\Phi \geq 1.0$,

$$\in = \frac{1.3}{\left[WE + 0.5XE + 1.863(2.WE + 0.5XE)/\Phi\right].\exp(0.13.T/1000)} \quad (3.122)$$

For temperature T≤ 3000 K

$$b = \exp(-9.0 - 0.5Log(P) + 30000/T) \quad (3.123)$$

And for temperature T > 3000 K

$$b = \exp(10.3 - (3.1 - 0.17Log(P)) + T/1000) \quad (3.124)$$

Adjust b for the following case :

$$BX = 2.0 - 9.0Log(\Phi) \quad (3.125)$$

If BX > 3.5;

$$BE = \exp(\exp(3.5) + 0.25Log(P)) \quad (3.126)$$

If BX ≤ 3.5;

$$BE = \exp(\exp(2.0 - 9.0Log(\Phi) + 0.25Log(P)) \quad (3.127)$$

If b > BE, then use;

$$b = BE \quad (3.128)$$

To evaluate the order 12 mole fractions , the following procedure is used. Using equation (3.102), (3.106), (3.109), and (3.113) the mole fraction of hydrogen is obtained;

$$X_{H_2} = \left[\frac{-\left(\frac{K_{P5}}{\sqrt{P}}.b + \frac{K_{P1}}{\sqrt{P}}\right) + \sqrt{\left(\frac{K_{P5}}{\sqrt{P}}.b + \frac{K_{P1}}{\sqrt{P}}\right)^2 + 4(2.b + 2).\in.XE}}{4(b+1)}\right]^2 \quad (3.129)$$

From equation (3.109) the mole fraction of water vapor is obtained;

$$X_{H_2O} = b.X_{H_2} \quad (3.130)$$

And from equation (3.106) the mole fraction of hydroxyl is obtained;

$$X_{OH} = \frac{K_{P5}.b.\sqrt{X_{H_2}}}{\sqrt{P}} \quad (3.131)$$

From equation (3.102) the mole fraction of atomic hydrogen is obtained;

$$X_H = \frac{K_{P1}\sqrt{X_{H_2}}}{\sqrt{P}} \tag{3.132}$$

By using equations (3.107) and (3.112) the mole fraction of carbon dioxide is obtained;

$$X_{CO_2} = \frac{\in .WE}{\left[\frac{K_{P6}}{b} + 1\right]} \tag{3.133}$$

From equations (3.112) the mole fraction of carbon monoxide is obtained;

$$X_{CO} = \in .WE - X_{CO_2} \tag{3.134}$$

Using equation (3.104), (3.108) and (3.115) the mole fraction of nitrogen is obtained;

$$X_{N_2} = \left[\frac{-\left(\frac{K_{P7}}{\sqrt{P}}.b + \frac{K_{P3}}{\sqrt{P}}\right) + \sqrt{\left(\frac{K_{P7}}{\sqrt{P}}.b + \frac{K_{P3}}{\sqrt{P}}\right)^2 + 8.\in .ZE}}{4}\right]^2 \tag{3.135}$$

From equation (3.104) the mole fraction of atomic nitrogen is obtained;

$$X_N = \frac{K_{P3}.\sqrt{X_{N_2}}}{\sqrt{P}} \tag{3.136}$$

And from equation (3.108) the mole fraction of nitric oxide is obtained;

$$X_{NO} = \frac{K_{P7}.b.\sqrt{X_{N_2}}}{\sqrt{P}} \tag{3.137}$$

And from equation (3.105) the mole fraction of oxygen is obtained;

$$X_{O_2} = \frac{K_{P4}.b^2}{P} \tag{3.138}$$

From equation (3.103) the mole fraction of atomic oxygen is obtained;

$$X_O = \frac{K_{P2}.\sqrt{X_{O_2}}}{\sqrt{P}} \tag{3.139}$$

Finally from equation (3.111) the mole fraction of argon is obtained;

$$X_{Ar} = \in .VE \tag{3.140}$$

These values are now tested in equations (3.110), and (3.114), neither of which has so far been used. If they do not balance within a stipulated accuracy the calculations are repeated with new value of $\in$ adjusted by an iterative technique.

Effect of Rate Kinetics on the Concentration of CO & NO

Carbon monoxide and nitric oxides are produced in the bulk of the reacting gases and involve high reaction temperatures. CARBON MONOXIDE is one result of incomplete combustion of hydrocarbon fuel. Under fuel rich conditions ($\Phi > 1$), concentration increase rapidly with increasing equivalence ration.

The principal CO oxidation reaction in hydrocarbon-air flame is [2];

$$CO + OH \leftrightarrow CO_2 + H \tag{3.141}$$

Heywood [2], showed that the rate constant for this reactions is;

$$K_f = 6.76 * 10^{10} \exp\left(\frac{T}{1102}\right) \qquad [cm^3 / g.mol] \tag{3.142}$$

Thus;

$$\frac{1}{Ven}.\frac{d([CO].Ven)}{dt} = K_f[CO].[OH] - K_b[CO_2][H] \tag{3.143}$$

Where V_{en} is the enflamed volume using;

$$\alpha_e = \frac{[CO]}{[CO]_e} \tag{3.144}$$

$$\delta_e = \frac{[CO_2]}{[CO_2]_e} \tag{3.145}$$

$$\beta_e = \frac{[OH]}{[OH]_e} \tag{3.146}$$

$$\beta_e = \frac{[OH]}{[OH]_e} \tag{3.147}$$

$$\sigma_e = \frac{[H]}{[H]_e} \tag{3.148}$$

Therefore;

$$\frac{1}{Ven}.\frac{d([CO].Ven)}{dt} = (\alpha_e.\beta_e - \delta_e.\sigma_e)R_f \tag{3.149}$$

Where; R_f one – way equilibrium rate.

After many experiments, the formation of CO inside the cylinder is assumed to be at equilibrium condition up to the park value. After that, the concentration of CO is assumed to lie between the peak equilibrium and the current equilibrium. This is because, at low temperature during the expansion process, the actual chemical reaction rates for the formation of CO lag behind the equilibrium value are leading to a higher value than obtained at the equilibrium.

Since the actual value of CO lies between the peak and exhaust equilibrium values, a multiplication factor called "COFAC" is introduced to obtain a more realistic value at the exhaust. Gupta [25] used the following relation to calculate the concentration of CO;

$$X_{CO} = X_{COeq} + COFAC.(X_{CO\max} - X_{COeq}) \tag{3.150}$$

Where; X_{CO} corrected concentration of CO.

X_{COeq} concentration of CO at equilibrium.

X_{max} maximum value of CO concentration at equilibrium condition.

$COEAC$ scale factor for CO formation.

The value of COFAC is adjusted with experimental results its about 0.6 as shown in Gupta [25].

The formation of NITRIC OXIDE [NO_X], in an engine combustion chamber is a non-equilibrium process. In the present study, the kinetic model for NO_X formation is based on the theory developed by Lavoie et. al. [33]. In this model, only the processes occurring in the burned gas behind

the reaction zone are considered, and it is assumed that the rate of the energy producing reactions in a flame are sufficiently fast so that the burned gases are close to thermodynamic equilibrium. Therefore, equilibrium concentrations may be assumed for all the species involved except for the No. Lavoie et. al. [33] have shown that on the time scale of interest, only the following three kinetic reactions are important (The extended Zeldovich mechanism).

$$N + NO \leftrightarrow N_2 + O \quad K_{1f} = 3.1*10^{10} \exp\left(\frac{-160}{T}\right) \quad [m^3 / Kmol.S] \qquad (3.151)$$

$$N + O_2 \leftrightarrow NO + O \quad K_{2f} = 6.4*10^6 * T * \exp\left(\frac{-3125}{T}\right) \quad [m^3 / Kmol.S] \qquad (3.152)$$

$$N + OH \leftrightarrow NO + H \quad K_{3f} = 4.2*10^{10} \quad [m^3 / Kmol.S] \qquad (3.153)$$

Where; K_{if} denotes the forward rate constant for the ith reaction.

Let K_{ib} the backward rate constant for the ith reaction and R_i the "One-way" equilibrium rate for the ith reaction then;

$$\alpha_{NO} = \frac{[NO]}{[NO]_e} \qquad (3.154)$$

$$\beta_N = \frac{[N]}{[N]_e} \qquad (3.155)$$

From equation (3.151) the net rate is;

$$-K_{1f}[N][NO]_e + K_1 b[N_2][O] = -\alpha_{NO}.\beta_N[N]_e.[NO]_e K_{1f} + K_1 b[N_2][O]_e \qquad (3.156)$$

But

$$K_1 f[N]_e[NO]_e = K_1 b[N_2]_e[O]_e = R_1 \qquad (3.157)$$

So that the net rate becomes:

$$K_1 f[N]\ [NO]_e + K_1 b[N_2][O]\ = -\alpha_{NO}\beta_N.R_1 + R_1 \qquad (3.158)$$

Using the similar term for equations (3.152), and (3.153), involving NO, then;

$$\frac{1}{Ven}.\frac{d([NO].Ven)}{dt} = -\alpha_{NO}(\beta_N R_1 + R_2 + R_3) + R_1 + \beta_N(R_2 + R_3) \qquad (3.159)$$

Also using equations (3.151), (3.152), and (3.153) the following relationship is obtained;

$$\frac{1}{Ven}.\frac{d([N].Ven)}{dt} = -\beta_{NO}(\alpha_{NO}R_1 + R_2 + R_3) + R_1 + \alpha_{NO}(R_2 + R_3) \quad (3.160)$$

Lavoie [33] found that a finite time is required for the reactions to reach their equilibrium values; this is called Relaxation time, the relaxation times are several orders of magnitude for the formation of atomic Nitrogen than those of NO, and hence it can be assumed that [N] values are at steady state, which means that the right hand sides of equation (3.160) can be set to equal zero, therefore;

$$\beta_N = \frac{R_1 + \alpha_{NO}(R_2 + R_3)}{\alpha_{NO}R_1 + R_2 + R_3} \quad (3.161)$$

Substituting for β_N in equation (3.159), gives;

$$\frac{1}{Ven}.\frac{d([NO].Ven)}{dt} = 2(1-\alpha_{NO}^2)\left[\frac{R_1}{(1+\alpha_{NO}(R_1/(R_2+R_3)))}\right] \quad (3.162)$$

Which is the final rate equation for [NO].

CHAPTER 4

COMPUTER PROGRAM

4.1 Introduction

In this chapter, an iterative Quick-Basic computer programs is developed to calculate pressure, temperature , flame speed, NOx and CO concentrations. These calculations are based on the theoretical analysis presented in chapter three.

4.2 Input Data

The input data required for running the programs are as follows: -

-Number of cylinders

-Cylinder bore.

-Cylinder stroke.

-Compression ratio.

-Connecting rod length.

-Crank radius.

-Reference temperature (298.15 K).

-Reference pressure (1.01325 bar).

-Air-fuel ratio.

-Engine speed.

-Crank angle steps.

-Angle of advance.

-Cylinder wall temperature.

-Fuel identification:

- Polynomial coefficient of properties of fuel.
- Percentage carbon content in fuel.
- Percentage hydrogen content in fuel.
- Fuel heating value.
- Fuel molecular weight.

4.3 Programs Output

- Pressure versus crank angle.

-Temperature contours.

-Flame speed contours.

-NOx and CO concentrations.

4.4 Main Program

This part of the programme controls the reading of the input data, the call of the different subroutines to perform the calculations and the writing and or plotting of the output from the programme.

As mentioned earlier this programme is based on the Quasi-Dimensional model developed in Chapter 3. It used the first law of thermodynamics, equation of state and conservation of mass and volume to obtain a system of first-order ordinary differential equations which is sloved for each time step to predict the cylinder pressure and temperture and all cycle characteristics. The procedure of calculations during each times as follows;

1- Read all constant (Rmol, TA).

2- Read the polynomial coefficients of thermodynamic properties of all species considered (H_2O, H_2, OH, H, N_2, NO, N, CO_2, CO, O_2, Ar, C_nH_m).

3- Read the physico–chemical properties of Iso-octane fuel (n, m, LHV,

Mw).

4- Select engine geometry parameters (B, L, ℓ).

5- Select engine operating parameters (Φ , CR, Tw, RPM).

6- Calculate the cylinder total mass, residual gas, pressure and temperature at trapped conditions.

7- Calculate the number of moles of each species in the cylinder charge at trapped conditions using SUB(1)

($N_{H_2}, N_{CO_2}, N_{H_2O}, N_{N_2}, N_{O_2}, N_{CO}$).

Compression Stage

8. Calculate the internal energy and specific heats of the cylinder charge ($E(T), CV(T), CP(T)$).

9. Calculate the cylinder volume and the volume increment during the time step ($V(t), dV/dt$).

10. Calculate the cylinder pressure $P(t)$, and temperature $T(t)$ by using the second order Runge-Kutta method to solve the ordinary differential equations of pressure dP/dt and temperature dT/dt.

11. Calculate the work down and its summation ($\sum P(t).dV(t)$).

12. Check if the spark starts ($\theta = \theta_S$) then estimate the delay period (Dp).

13. Check if the crank angle degree is less than that of ignition, then increase the crank angle by its increment and repeat steps (8-13).

Combustion Stage

A- Ignition Model Development

14. Calculate the flame front speed.
15. Calculate the flame kernel radius, flame kernel area, flame kernel volume.
16. Calculate the rate of flame kernel growth (dM_k/dt).

B- Second stage:

17. Calculate the internal energy, specific heats, and molecular weight of burnt and unburnt zone.
18. Calculate the cylinder volume and the volume increment during the time step ($V(t), dV/dt$).
19. Calculate the flame front speed, turbulent flame front factor (ff, S_L , S_T).
20. Calculate the flame front area, enflamed volume and contact area of the flame with cylinder wall using SUB(3).
21. Calculate the rate of mass burning (dMb/dt).
22. Calculate the heat transfer rate by convection and radiation from unburnt and burnt zones.
23. Calculate the flame front radius r(t), cylinder pressure P(t), unburnt gas temperature $T_u(t)$ and burnt gas temperature $T_b(t)$, by using the second order Runge-Kutta method to solve the ordinary differential equations of pressure dP/dt and temperatures.
24. Calculate the mole fraction of product gas species (Equilibrium thermodynamic) using SUB (2);
    ($XH_2O, XH_2, XOH, XH, XN_2, XNO, XN, XCO_2, XCO, XO_2, XNO, XAr$).
25. Check to see if the combustion is over, then the expansion stage is start.
26. If the combustion stage isn't over (the burnt volume is less than the

total volume), then increase the crank angle by it increment and repeat steps (17-25).

Expansion Stage

27. Calculate the internal energy and specific heats of the cylinder contents ($E(T),CV(T),CP(T)$).
28. Calculate the cylinder volume and the volume increment during the time step ($V(t),dV/dt$).
29. Calculate the cylinder pressure $P(t)$, and temperature $T(t)$ by using the second order Runge-Kutta method to solve the ordinary differential equations of pressure dP/dt and temperature dT/dt.
30. Check to see if the exhaust valve opens. In this case, the expansion stage is over.
31. If the exhaust valve is still closed, then increase the crank angle by its increment and repeat steps (28-31).
32. Calculate the kinetic rate concentration of nitric oxide (X_{NO_x}) using SUB (4).
33. Select the plot option to plot the result graphically and/or select the save option to save the result as a data file.
34. Repeat steps 29 or end the programme.

The output of the programme are cylinder pressure, burnt zone temperature, flame speed, kinetic rate concentration of nitric oxide and carbon monoxide.

The flow chart of the main program is shown in Figure (4.1).

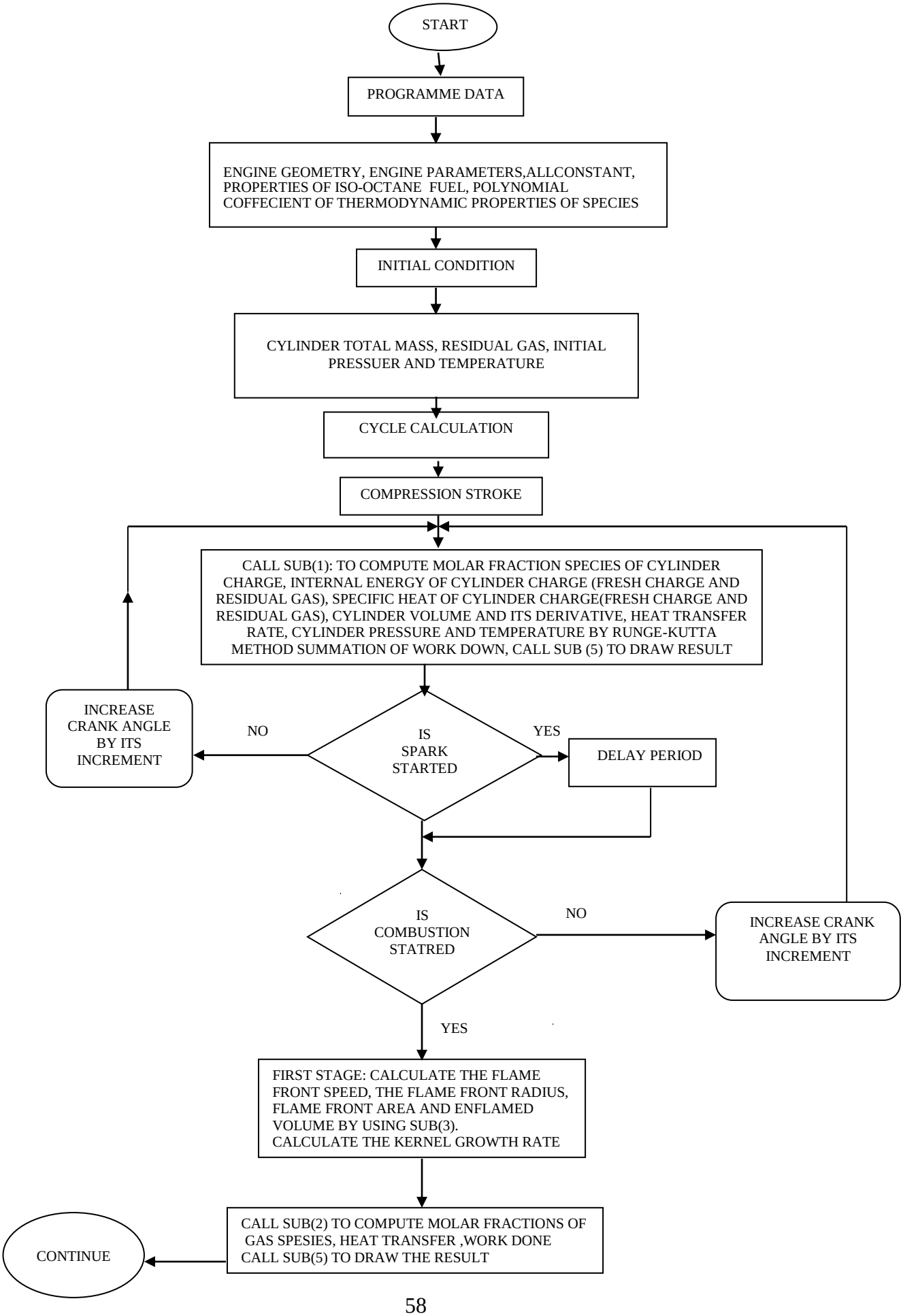
START
PROGRAMME DATA
ENGINE GEOMETRY, ENGINE PARAMETERS,ALLCONSTANT, PROPERTIES OF ISO-OCTANE FUEL, POLYNOMIAL COFFECIENT OF THERMODYNAMIC PROPERTIES OF SPECIES
INITIAL CONDITION
CYLINDER TOTAL MASS, RESIDUAL GAS, INITIAL PRESSUER AND TEMPERATURE
CYCLE CALCULATION
COMPRESSION STROKE
CALL SUB(1): TO COMPUTE MOLAR FRACTION SPECIES OF CYLINDER CHARGE, INTERNAL ENERGY OF CYLINDER CHARGE (FRESH CHARGE AND RESIDUAL GAS), SPECIFIC HEAT OF CYLINDER CHARGE(FRESH CHARGE AND RESIDUAL GAS), CYLINDER VOLUME AND ITS DERIVATIVE, HEAT TRANSFER RATE, CYLINDER PRESSURE AND TEMPERATURE BY RUNGE-KUTTA METHOD SUMMATION OF WORK DOWN, CALL SUB (5) TO DRAW RESULT
IS SPARK STARTED
NO
YES
INCREASE CRANK ANGLE BY ITS INCREMENT
DELAY PERIOD
IS COMBUSTION STATRED
NO
INCREASE CRANK ANGLE BY ITS INCREMENT
YES
FIRST STAGE: CALCULATE THE FLAME FRONT SPEED, THE FLAME FRONT RADIUS, FLAME FRONT AREA AND ENFLAMED VOLUME BY USING SUB(3). CALCULATE THE KERNEL GROWTH RATE
CALL SUB(2) TO COMPUTE MOLAR FRACTIONS OF GAS SPESIES, HEAT TRANSFER ,WORK DONE CALL SUB(5) TO DRAW THE RESULT
CONTINUE

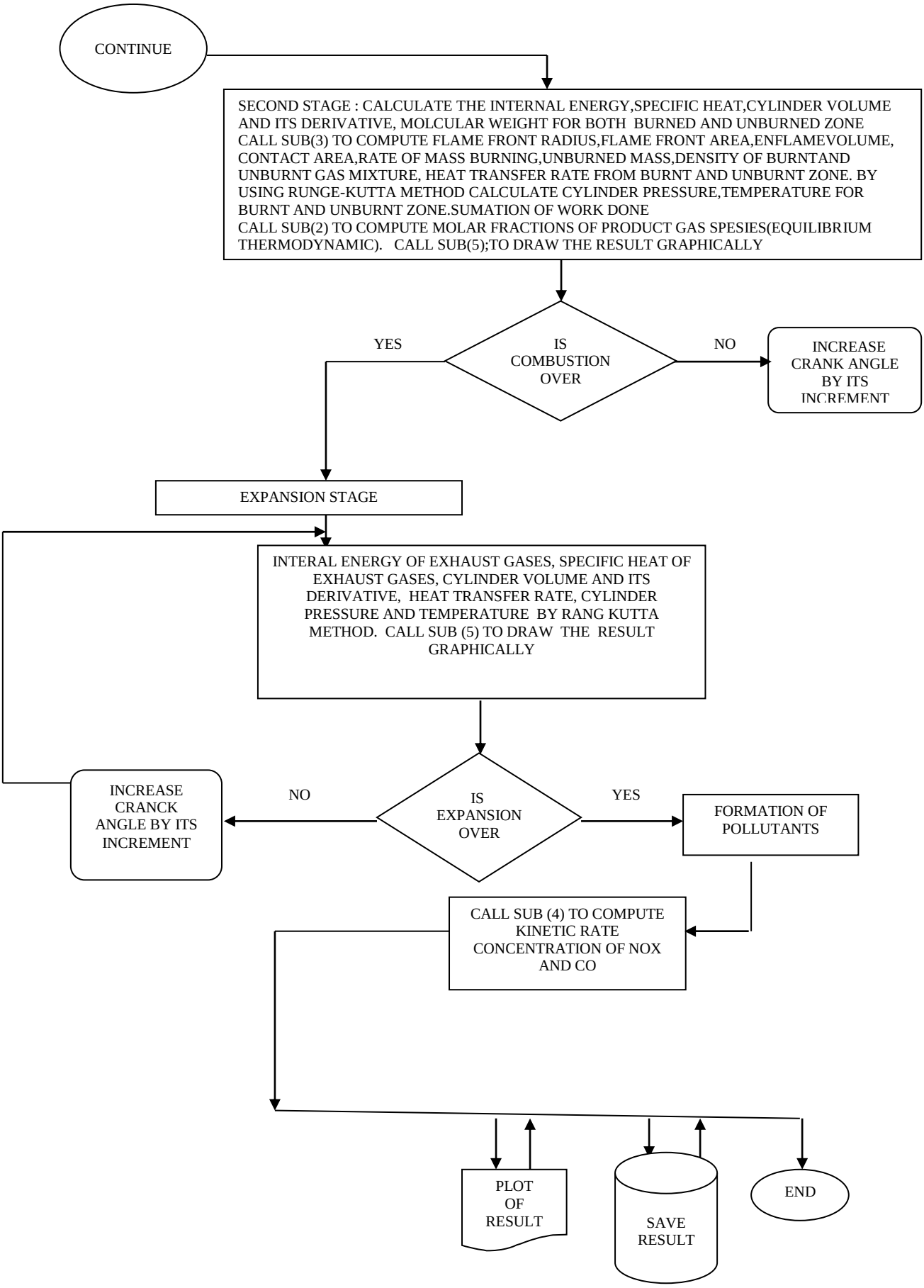

Figure (4.1) Procedure flowcharts of the main Program

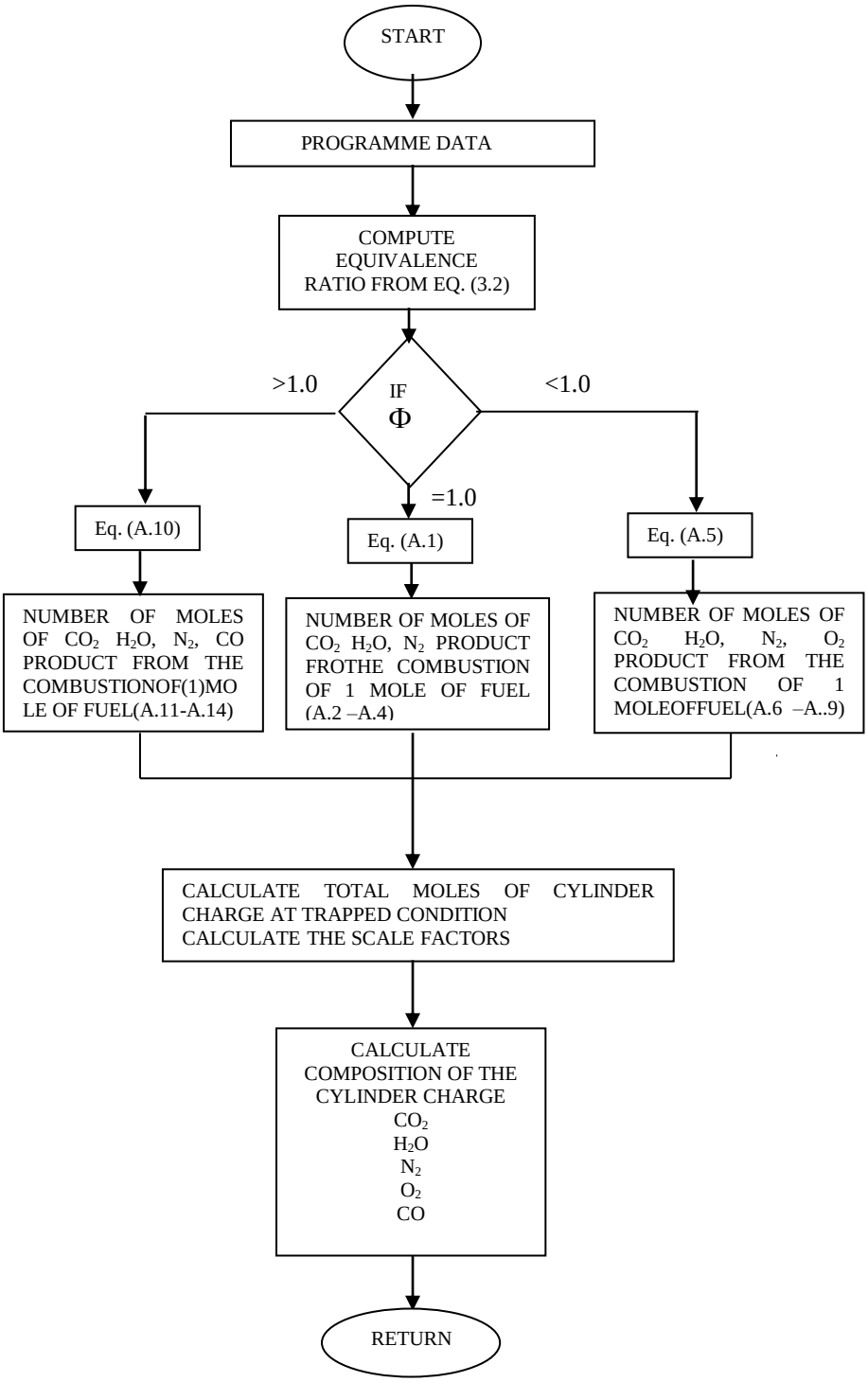

Figure(4.2) Procedure flowchart of the subroutine SUB(1)

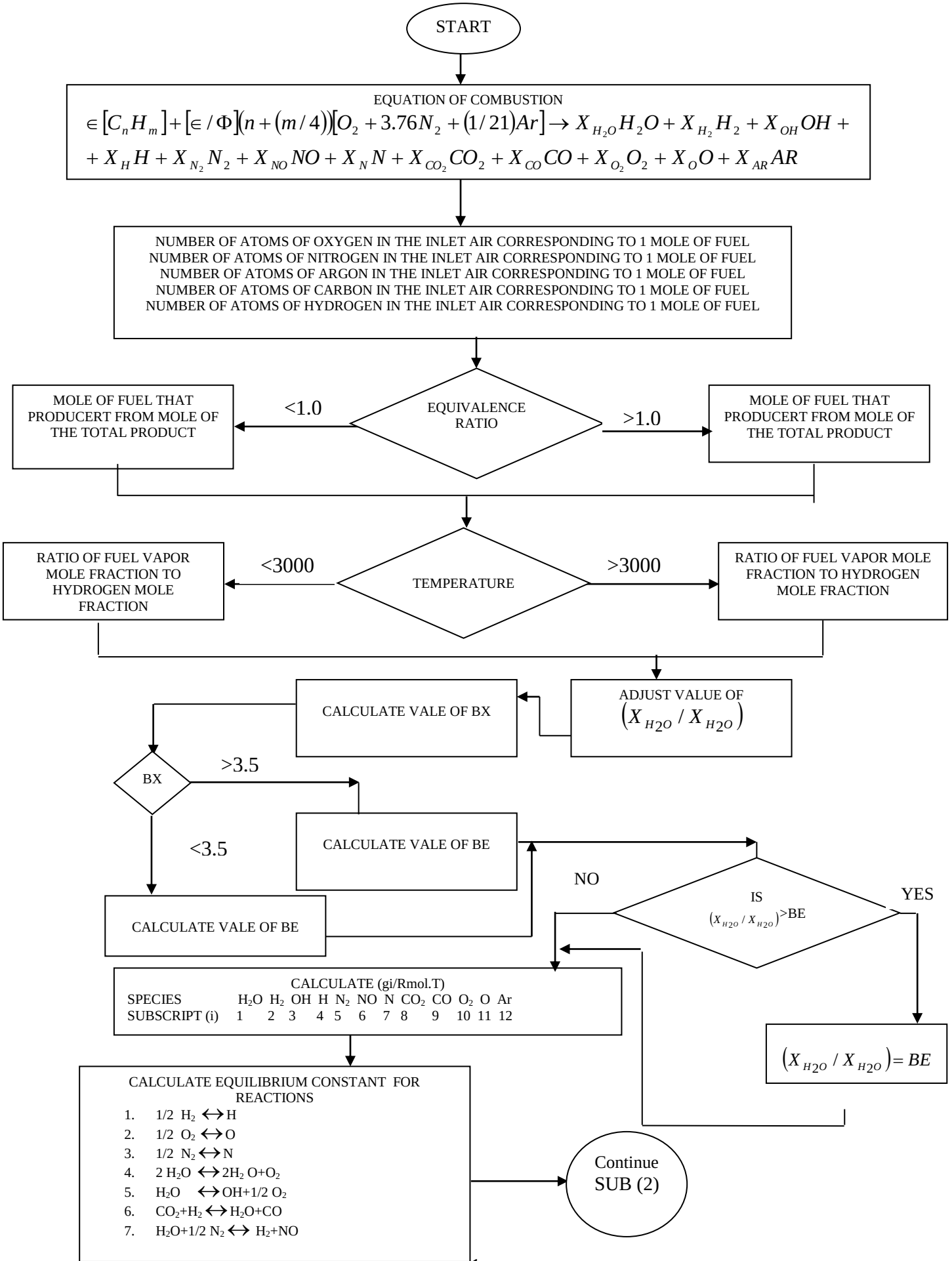
START
EQUATION OF COMBUSTION
$\in [C_n H_m] + [\in / \Phi](n + (m/4))[O_2 + 3.76N_2 + (1/21)Ar] \rightarrow X_{H_2O} H_2O + X_{H_2} H_2 + X_{OH} OH +$
$+ X_H H + X_{N_2} N_2 + X_{NO} NO + X_N N + X_{CO_2} CO_2 + X_{CO} CO + X_{O_2} O_2 + X_O O + X_{AR} AR$
NUMBER OF ATOMS OF OXYGEN IN THE INLET AIR CORRESPONDING TO 1 MOLE OF FUEL
NUMBER OF ATOMS OF NITROGEN IN THE INLET AIR CORRESPONDING TO 1 MOLE OF FUEL
NUMBER OF ATOMS OF ARGON IN THE INLET AIR CORRESPONDING TO 1 MOLE OF FUEL
NUMBER OF ATOMS OF CARBON IN THE INLET AIR CORRESPONDING TO 1 MOLE OF FUEL
NUMBER OF ATOMS OF HYDROGEN IN THE INLET AIR CORRESPONDING TO 1 MOLE OF FUEL
MOLE OF FUEL THAT PRODUCERT FROM MOLE OF THE TOTAL PRODUCT
<1.0
EQUIVALENCE RATIO
>1.0
MOLE OF FUEL THAT PRODUCERT FROM MOLE OF THE TOTAL PRODUCT
RATIO OF FUEL VAPOR MOLE FRACTION TO HYDROGEN MOLE FRACTION
<3000
TEMPERATURE
>3000
RATIO OF FUEL VAPOR MOLE FRACTION TO HYDROGEN MOLE FRACTION
ADJUST VALUE OF (X_{H2O} / X_{H2O})
CALCULATE VALE OF BX
BX
>3.5
<3.5
CALCULATE VALE OF BE
CALCULATE VALE OF BE
NO
IS (X_{H2O} / X_{H2O})>BE
YES
$(X_{H2O} / X_{H2O}) = BE$
CALCULATE (gi/Rmol.T)
SPECIES H2O H2 OH H N2 NO N CO2 CO O2 O Ar
SUBSCRIPT (i) 1 2 3 4 5 6 7 8 9 10 11 12
CALCULATE EQUILIBRIUM CONSTANT FOR REACTIONS
1. 1/2 H2 ↔ H
2. 1/2 O2 ↔ O
3. 1/2 N2 ↔ N
4. 2 H2O ↔ 2H2 O+O2
5. H2O ↔ OH+1/2 O2
6. CO2+H2 ↔ H2O+CO
7. H2O+1/2 N2 ↔ H2+NO
Continue SUB (2)

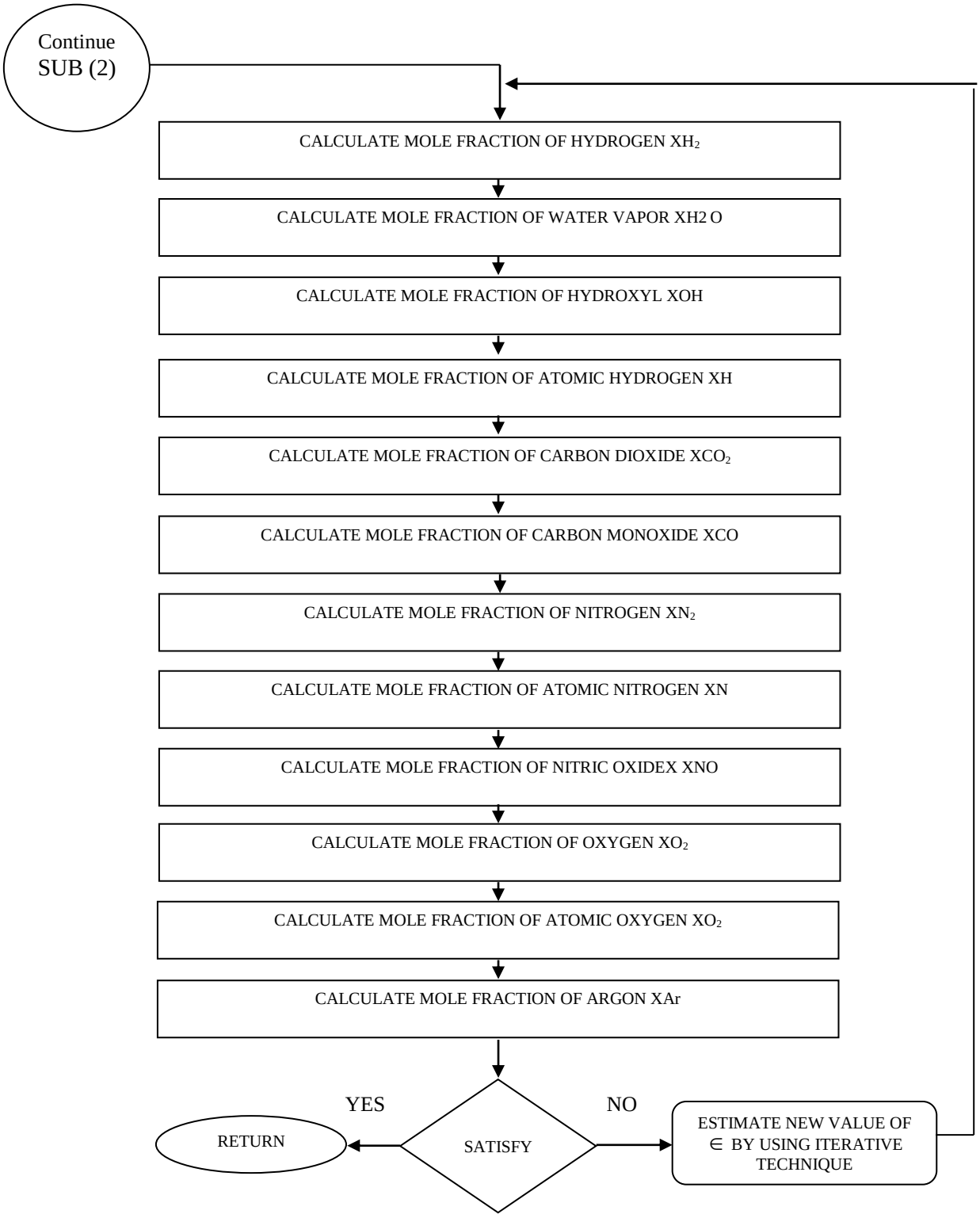

Note: Bracket number refers to that equation used.
Figure(4.3): Procedure flowchart of the subroutine SUB(2)

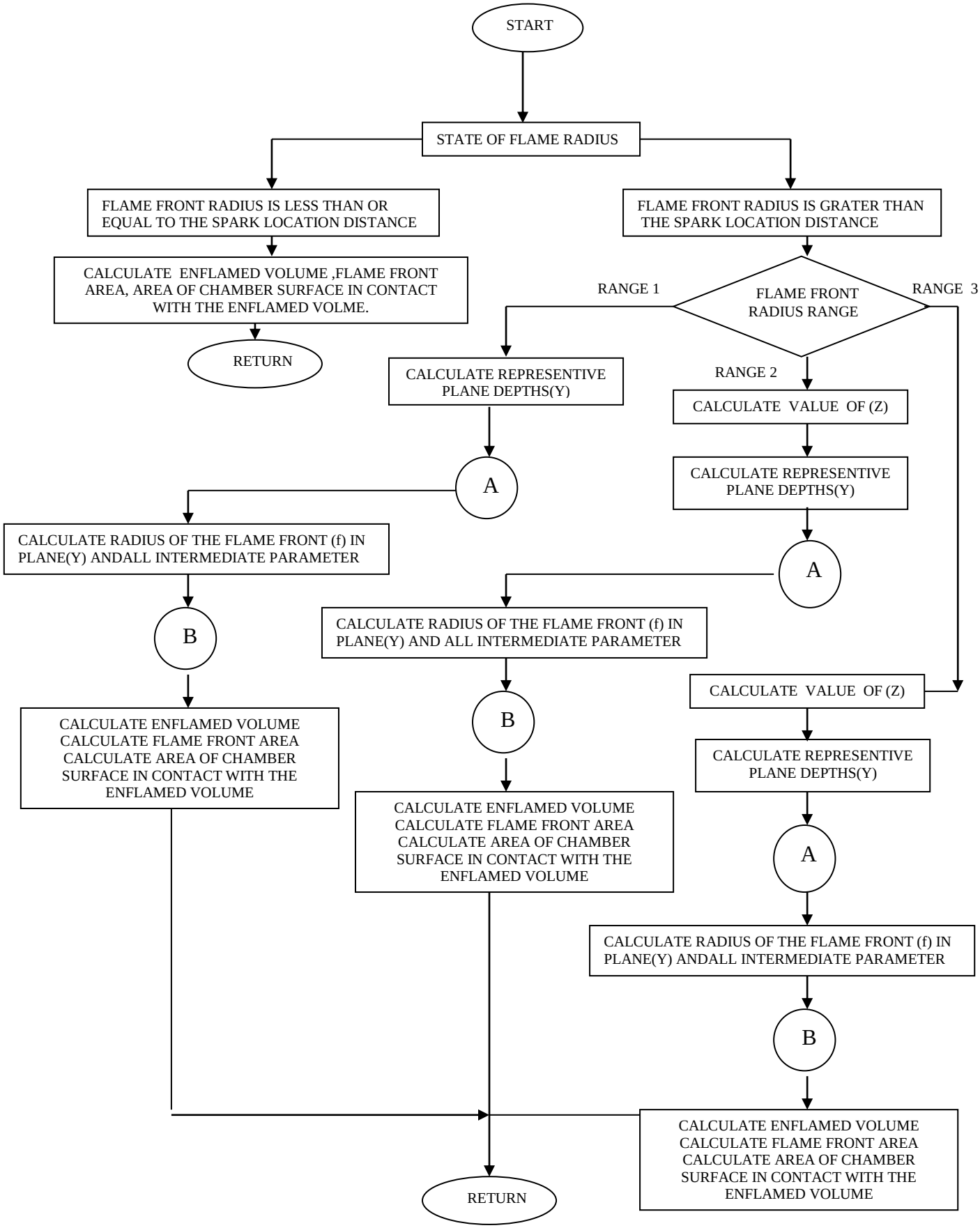

Figure(4.4): Procedure flowchart of SUB(3)

Procedure (A)----(B) are detailed in this figure;

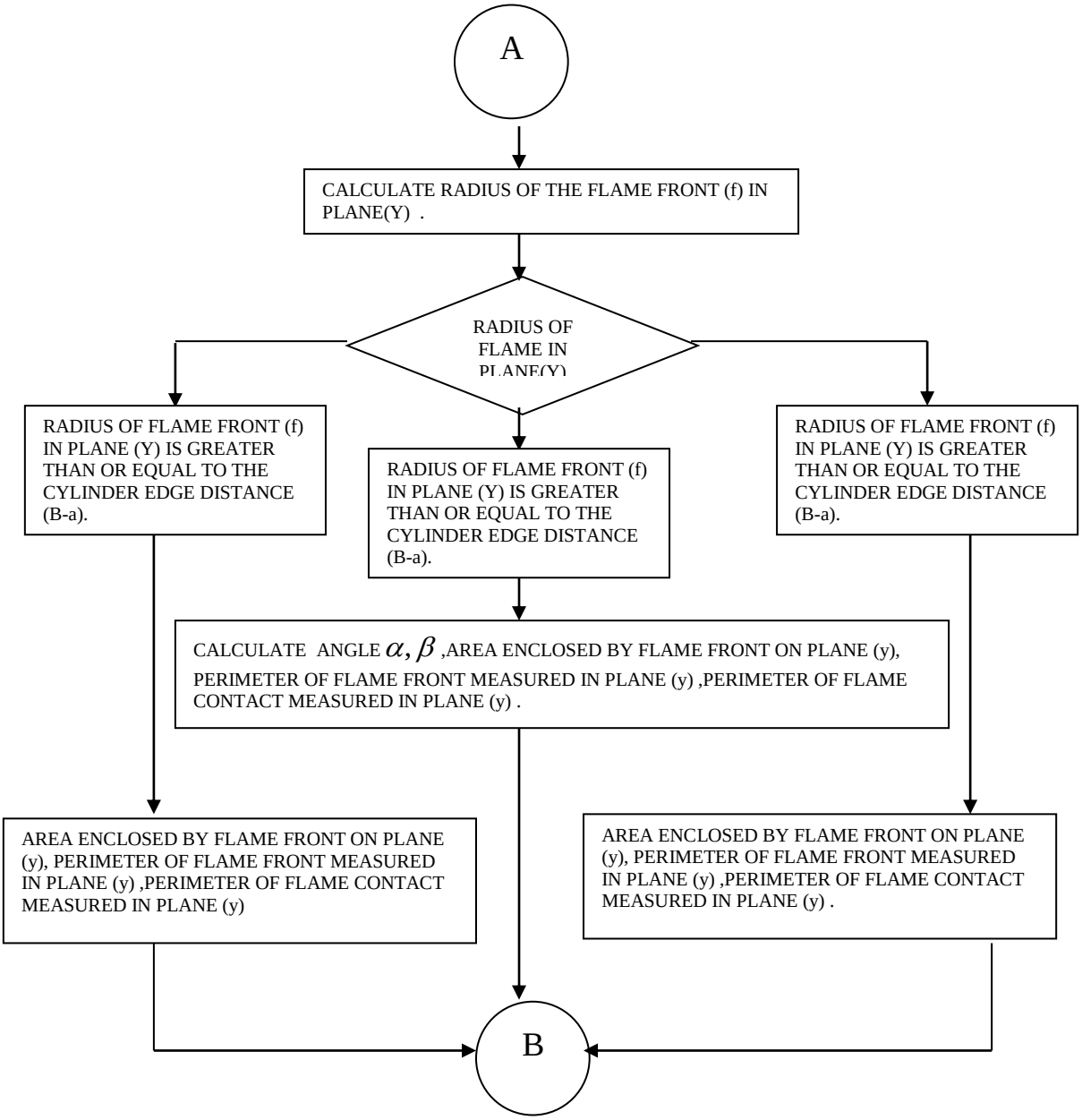

Figure (4.5): Procedure flow chart of the procedure (A)-----(B) of the SUB(3).
Note: Bracketed number refer to that of the procedure (A)-----(B) of the SUB(3).

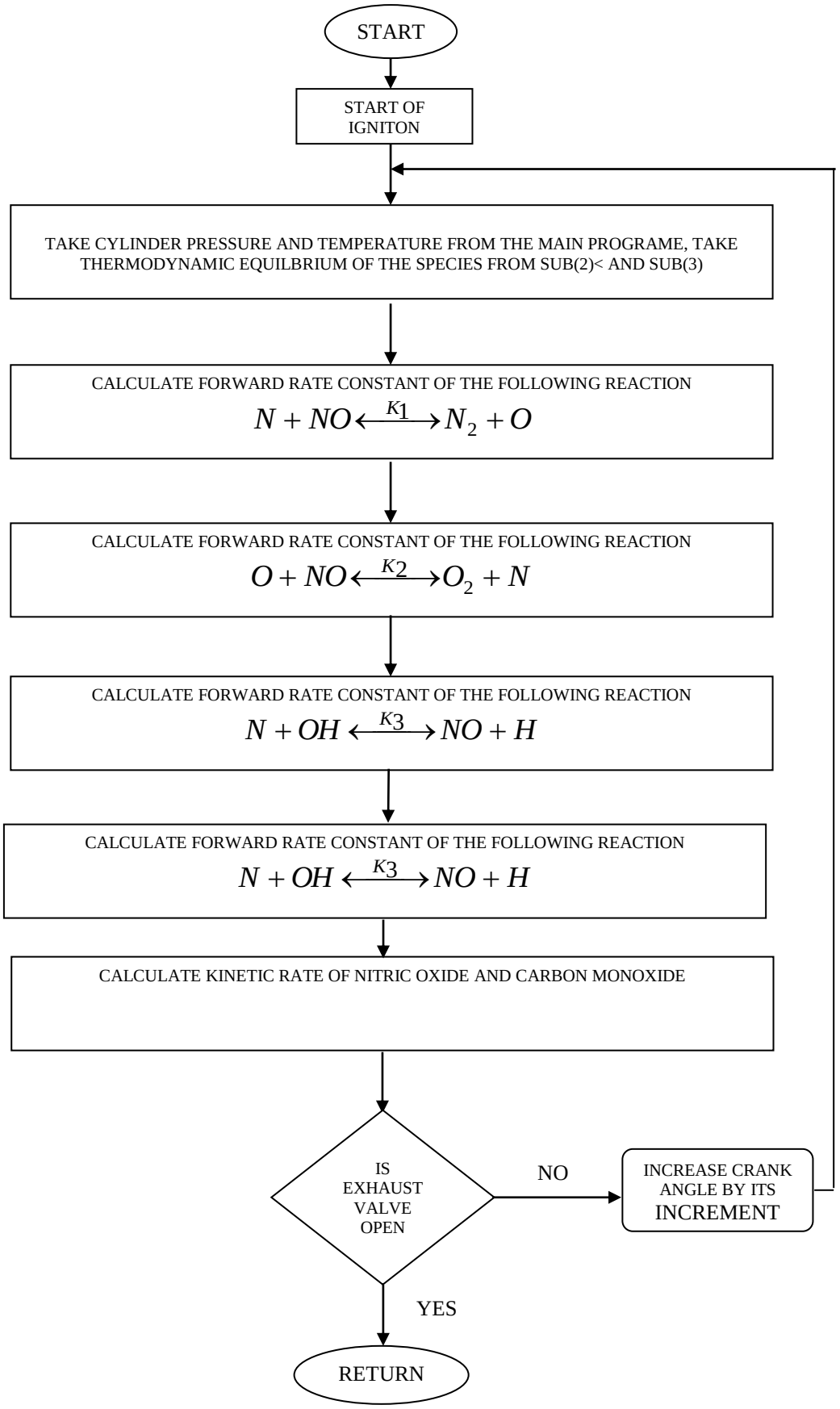

Figure(4.6): Procedure flowchart of the subroutine SUB(4)

CHAPTER 5

RESULTS AND DISCUSSION

5.1: Introduction

In this chapter the effect of engine variables on predicted cylinder pressure, temperature contours, flame speed contours, NOx and CO emissions are presented and discussed.

The results are compared with the available theoretical and experimental results of other researchers [15, 18], and show a good agreement as will be seen in the following sections.

Figures (5.1a to 5.10a) show the variation of the cylinder pressure with crank angle. In general the behavior for these figures is the same except the difference in the value and timing of peak pressure which depend on the engine variable.

Figures (5.1b to 5.10b) show how the flame grows roughly spherically and steadily from the time of the spark discharge. The burned gas temperature and the associated pressure rise due to combustion significantly as the flame front has traveled through the combustion chamber. The maximum temperature and pressure occurs close to the time that the flame makes contact with the cylinder wall.

Figures (5.1c to 5.10c) show the flame speed contours. The flame speed decrease as the flame radius increase, this is because the increase in the cylinder pressure and the effect of cylinder walls.

Figures (5.1d to 5.10d) show the variation of NOx and CO concentrations with crank angle. The NOx and CO concentrations increase sharply with time and then freeze due to temperature drop where the reactance cannot proceed.

The value of the maximum pressure, temperature, flame speed, NOx and CO emissions are affected by the engine variable.

2.2 Effect of Engine Variables on the Pressure, Temperature Contours, Flame Speed Contours, NOx and CO emissions

5.2.1 The Effect of Compression Ratio

As the compression ratio increases, the maximum temperature and maximum pressure increase. This is due to the increase in mixture temperature at the time of the spark and the reduction in residual gas fraction.

Figures (5.1a to 5.3a) show the effect of the increase of the compression ratio on the predicted pressure. As the compression ratio increases by 12.5%, the maximum pressure increases by about 8.5%.

Figures (5.1b to 5.3b) show the effect of the compression ratio on the burnt temperature contours. As the compression ratio increases by 12.5%, the maximum temperature increases by about 0.18%.

Figures (5.1c to 5.1c) show the effect of the compression ratio on the flame speed contours. As the compression ratio slightly increases the flame speed slightly increases too.

Figures (5.1d to 5.11d) show the effect of the compression ratio on NOx and CO concentrations. As the compression ratio increases, the NOx and CO concentrations increase, due to temperature increase.

5.2.2 The Effect of Equivalence Ratio

Figures (5.4a , 5.5a) and (5.4b , 5.5b) show the effect of the equivalence ratio on the predicted pressure and burnt temperature contours respectively. The burnt temperature is low at the leaner mixture Figure (5.4). Maximum burned gas temperature occurs at Φ =1.1; however, at this equivalence ratio oxygen concentration are low. As the mixture is enriched, burned gas temperature fall.

Figure (5.4c) shows the effect of equivalence ratio on flame speed contours. As the mixture is leaned (Φ =0.9), the flame speed decreases. This is because at lean mixtures less thermal energy liberated which increases the ignition delay and slows the flame propagation. Furthermore, the incomplete combustion due to oxygen deficiency at rich mixtures has the same effect over the flame speed as shown in Figure (5.5c). The maximum flame speed occurs when the mixture strength is slightly rich.

Figure (5.4d) shows the effect of the equivalence ratio on NOx and CO concentrations. As the mixture is leaned (Φ =0.9) both NOx and CO decreases as the maximum temperature decreases.
In lean mixtures NO concentrations freeze early in the expansion process.

As the mixture gets richer (Φ >1.1), there is no enough oxygen so the NOx decreases and CO increases as shown in Figure (5.5d).

Figures (5.11) to (5.16) show the variation of flame speed with equivalence ratio. The flame speed peaks at slightly richer than stoichiometric, and then decreases for richer and leaner mixture. Flame speed is higher at a full load than a part load. The maximum flame speed decreases, by increasing the inlet temperature, due to the decrease in the fuel mass per unit displaced volume). The maximum flame speed at residual mass fraction 0% is higher than at residual mass fraction 5% and 10%, due to decreasing the charge mass which leads to less fuel mass.

5.2.3 The Effect of Spark Timing

Combustion starts before the end of the compression stroke, continues through the early part of expansion stroke, and ends after the point in the cycle at which the peak pressure occurs.
Spark timing significantly affects the pressure, temperature, flame speed, NOx and CO emission levels.

Figures (5.6a) and (5.7a) show the effect of retarding the spark timing on the cylinder pressure. Retarding the spark timing decreases the peak cylinder pressure because more of the fuel burns after TDC.

Figure(5.6b) and Figure(5.7b) show the effect of retarding the spark timing on the temperature contours (the other parameters are set to be constant). It is seen that the maximum temperature decreases as the spark timing is retarded.

Retarding spark timing from 30º reduces the combustion temperature which gives low rate of heat loss, but the heat losses will last over a longer length of time and the overall energy loss will be greater. Late ignition timing extends the combustion process longer in the expansion stroke, resulting in higher exhaust temperature and hotter exhaust valves and spots.

Figures(5.6d) and (5.7d) show that if the combustion process retards, NOx and CO formation occur later, and concentrations are lower since peak temperature is lower.

5.2.4 The Effect of Spark Plug Location

The rate of combustion should be such that the combustion duration is minimum with high rate of pressure rise.

Relocating the spark plug from the center to the side is far more effective in increasing burn duration. Hence, the decrease is in the pressure and the temperature (both burned and unburned) and also the NOx and CO concentrations. This is because of the increased percentage heat loss as shown in figures.

Figures (5.9) and (5.10) show that as the spark is shifted from the center (i.e. (a/B) =0.5), to the peripheral position (i.e (a/B) =0.4, 0.3), the peak pressure and temperature decrease because the increased percentage in heat loss since the flame makes contact earlier with cylinder walls. The combustion duration is also increased.

Figure (5.9c) and (5.10c) show the effect of the spark plug location on the flame speed. The figures show that as the spark is shifted from the center (i.e. (a/B) = 0.5), to the peripheral position (i.e. (a/B) = 0.4, 0.3), the flame speed decrease. This is because of the increase in the fraction

residual gases. This creates a favorable condition for the increasing of ignition lag and decrease in the flame speed.

Figure (5.9d) and (5.10d) show the effect of the spark plug location on the NOx and CO emissions. The figures show that as the spark is shifted from the center (i.e. (a/B) = 0.5), to the peripheral position (i.e. (a/B) = 0.4, 0.3), the NOx and CO emissions are lower. This is because there is more time for the combustion to complete, hence the concentration of CO is reduced. Further, the peak burned temperature is low and therefore the formation of NO is reduced. From the emission point of view, the location ((a/B) = 0.3) is most favorable.

5.3 Model Verification

Figure (5.17) and (5.18) show a comparison between present model and the models predicted by Zhicho [18] and Holger [15] models respectively. It can be seen that the agreement between these results is fairly encouraging, and the trends of shape changes are also quite as anticipated. In Figure (5.17) and (5.18) the predicted cylinder pressure, and NOx concentration respectively are compared with those in Zhicho [18] and Holger [15] models. It can be seen that the present model represents an intermediate step between those theoretical models, this indicate that there is reasonable agreements between this work and these models and imply that present work is regarded as a potentially use full tool for predicting the burnt temperature, flame speed, and CO concentration.

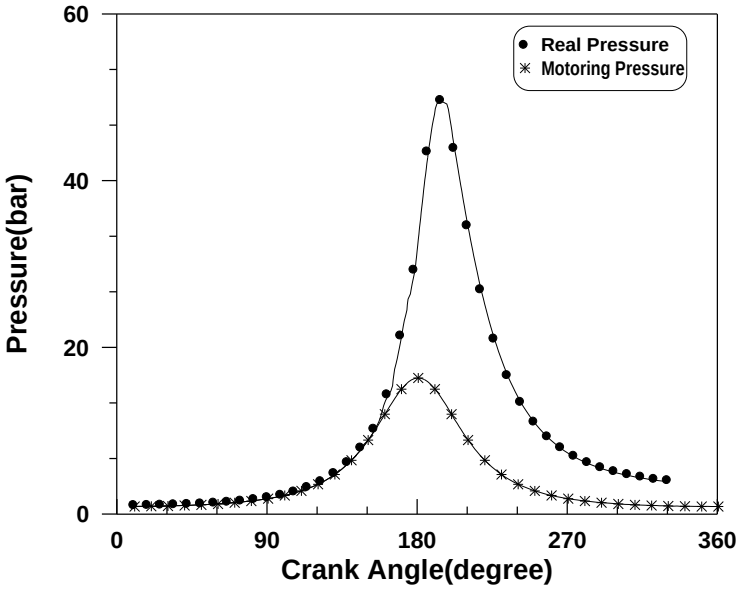

Figure(5.1a): Variation of cylinder pressure with crank angle.

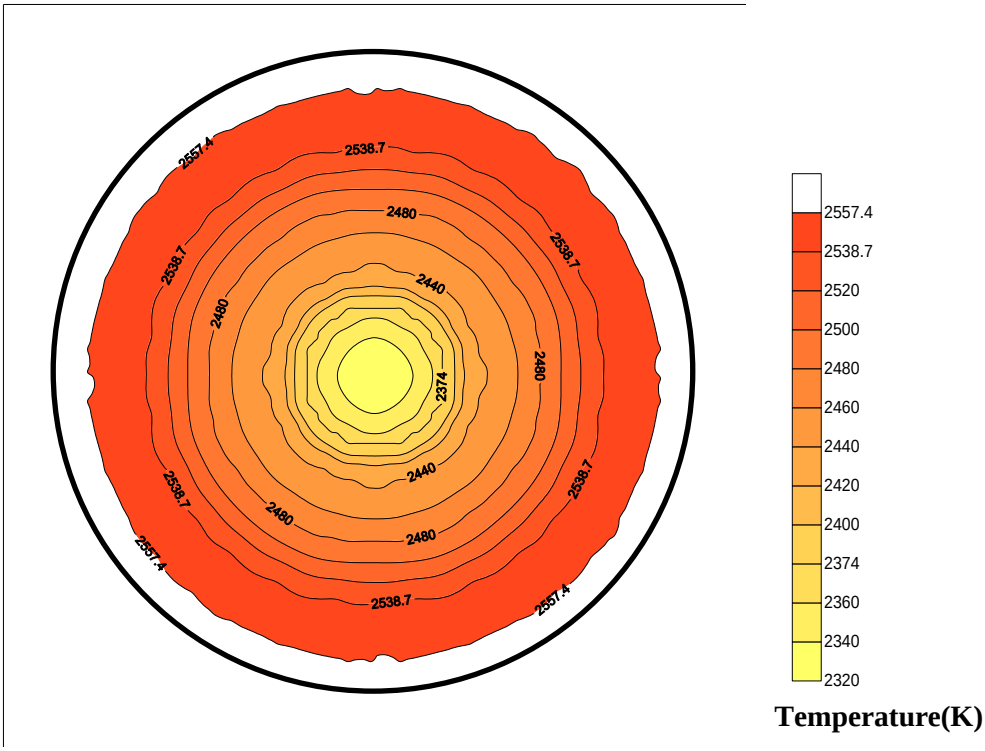

Figure(5.1b): Temperature contours
Equivalence ratio:1.0, Compression ratio: 7.5, Engine speed: 1500
Spark timing: 30 BTDC, Spark Plug Location: (a/B) = 0.5.

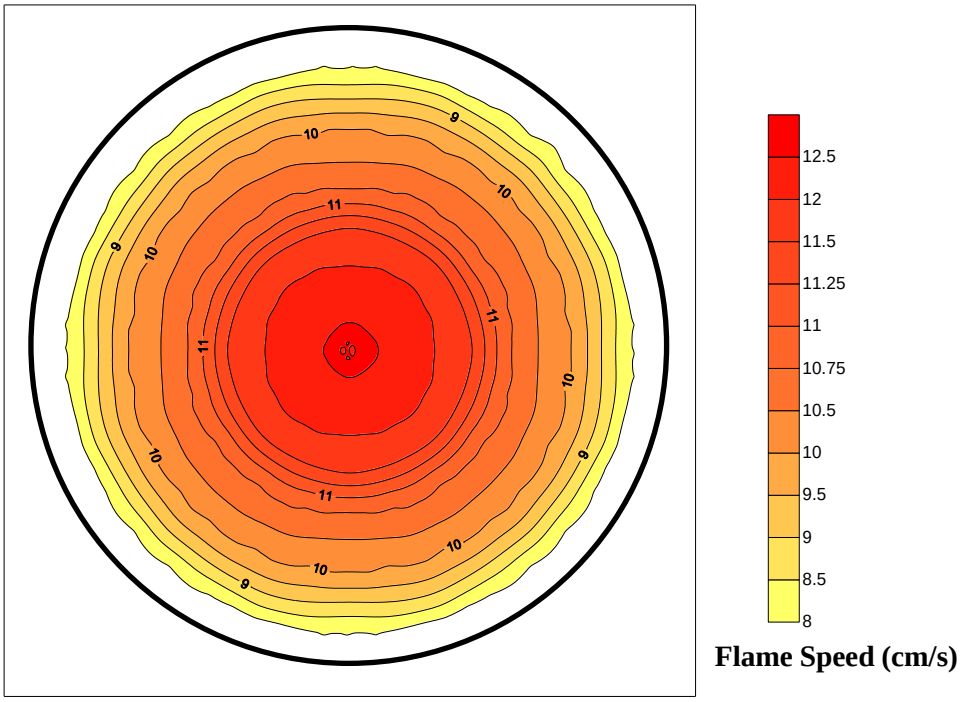

Figure (5.1c): Flame speed contours

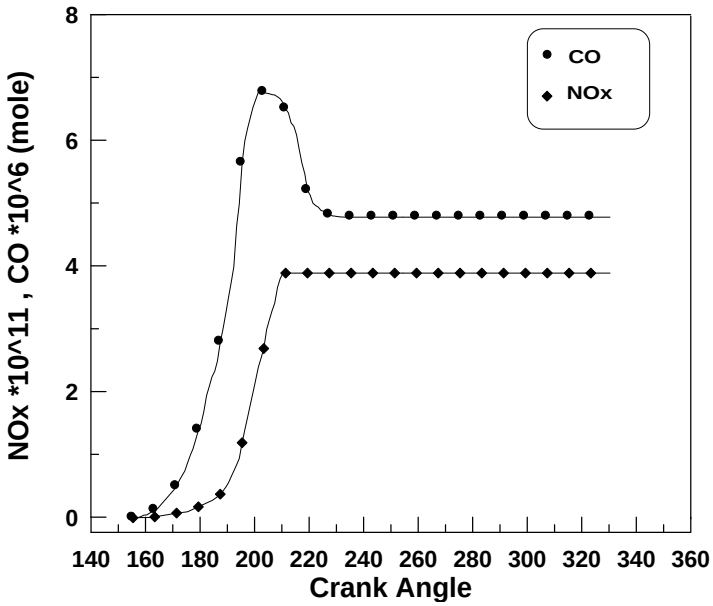

Figure(5.1d): Variation of concentration of NOx and CO with crank angle

Equivalence ratio:1.0, Compression ratio: 7.5, Engine speed: 1500
Spark timing: 30 BTDC, Spark Plug Location: (a/B) = 0.5.

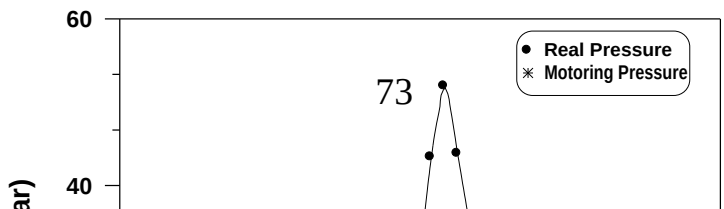

Figure(5.2a): Variation of cylinder pressure with crank angle.

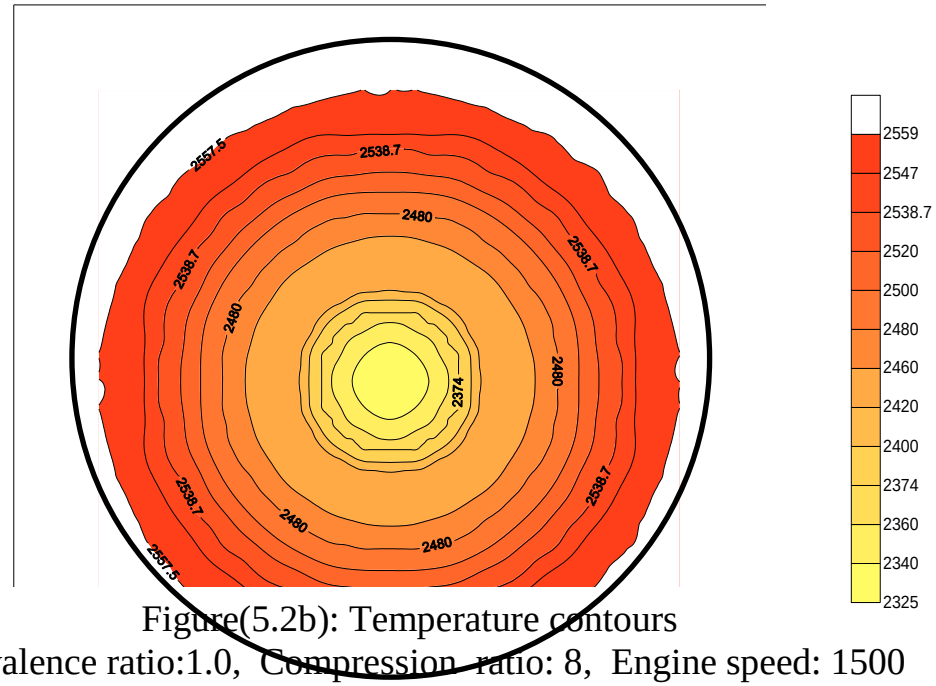

Figure(5.2b): Temperature contours
Equivalence ratio:1.0, Compression ratio: 8, Engine speed: 1500
Spark timing : 30 BTDC, Spark Plug Location: (a/B) = 0.5.

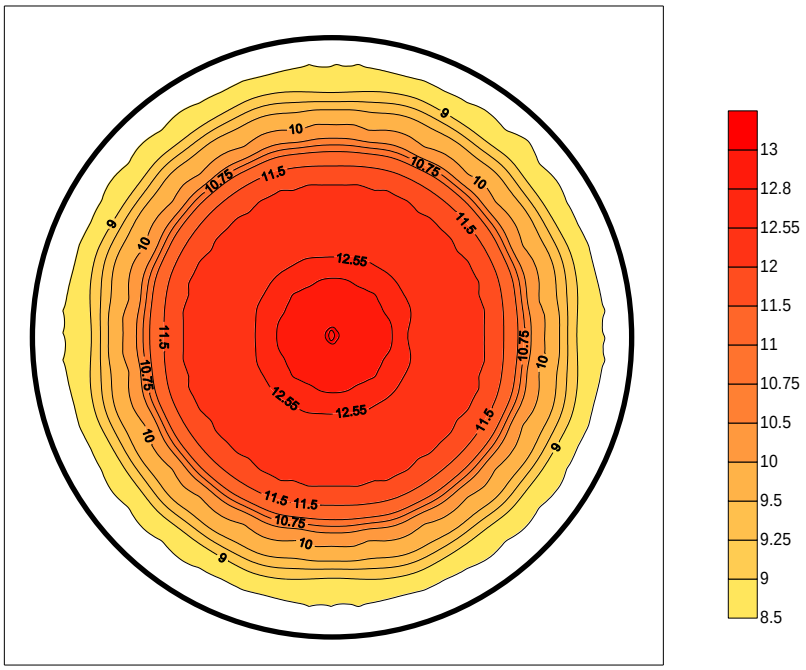

Figure(5.2c): Flame speed contours

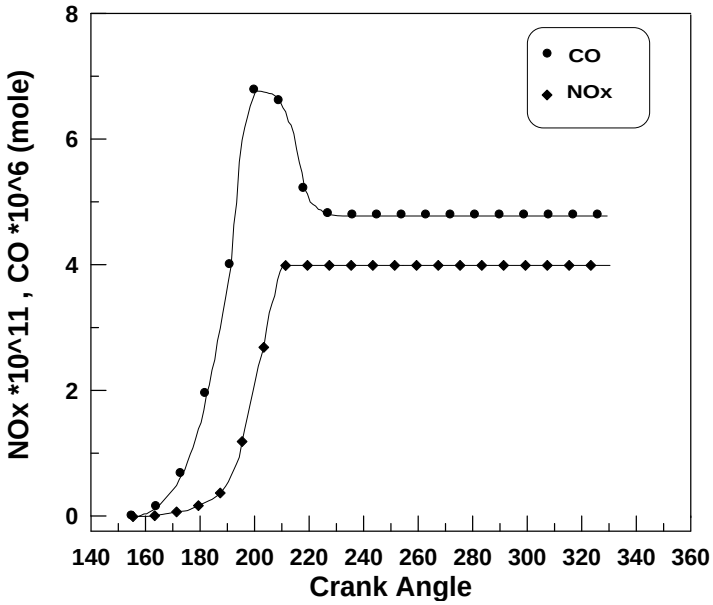

Figure(5.2d):Variation of concentration of NOx and CO with crank angle.

Equivalence ratio:1.0, Compression ratio: 8, Engine speed: 1500
Spark timing: 30 BTDC, Spark Plug Location: (a/B) = 0.5.

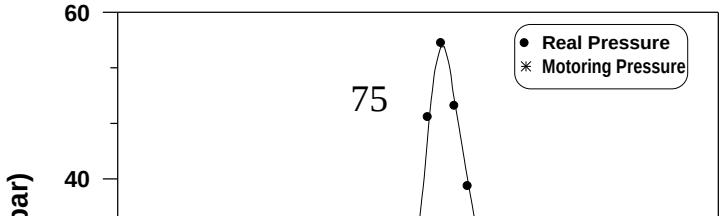

Figure(5.3a): Variation of cylinder pressure with crank angle

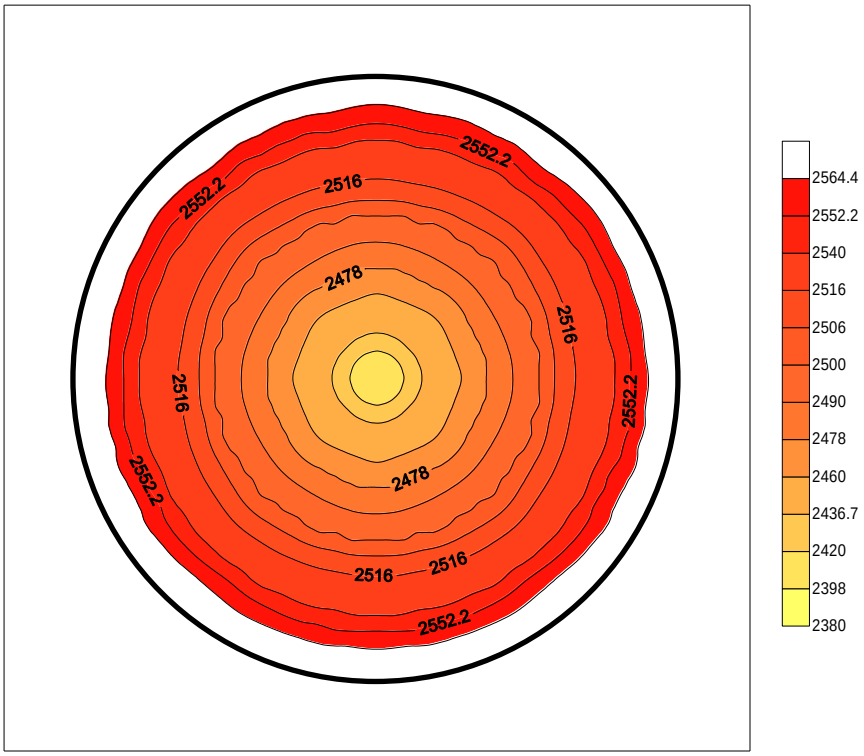

Figure(5.3b): Temperature contours
Equivalence ratio:1.0, Compression ratio: 9, Engine speed: 1500
Spark timing: 30 BTDC, Spark Plug Location: (a/B) = 0.5.

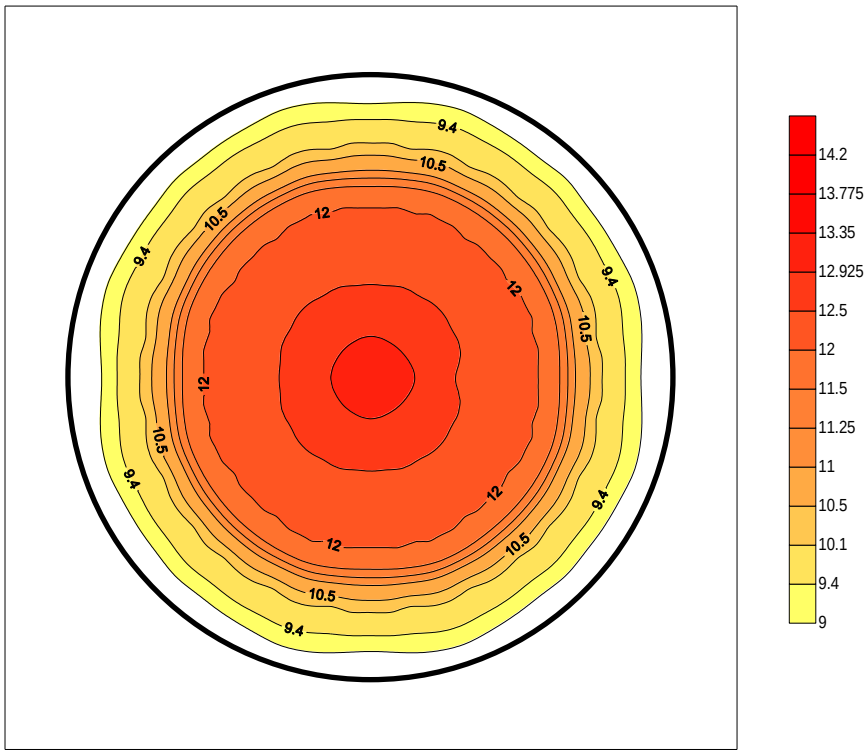

Figure(5.3c): Flame speed contours

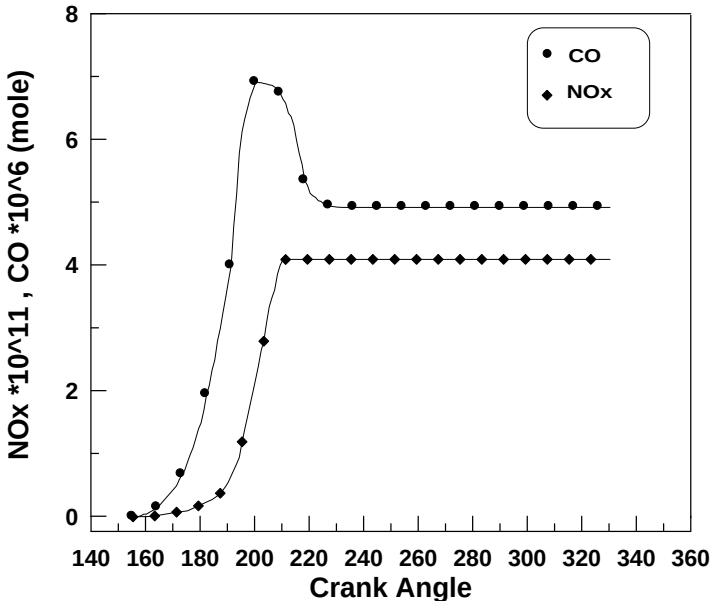

Figure(5.3d):Variation of concentration of NOx and CO with crank angle.

Equivalence ratio:1.0 , Compression ratio: 9 , Engine speed: 1500 Spark timing : 30 BTDC, Spark Plug Location: (a/B) = 0.5.

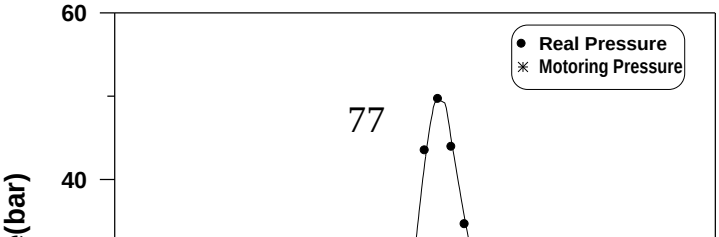

Figure(5.4a): Variation of cylinder pressure with crank angle.

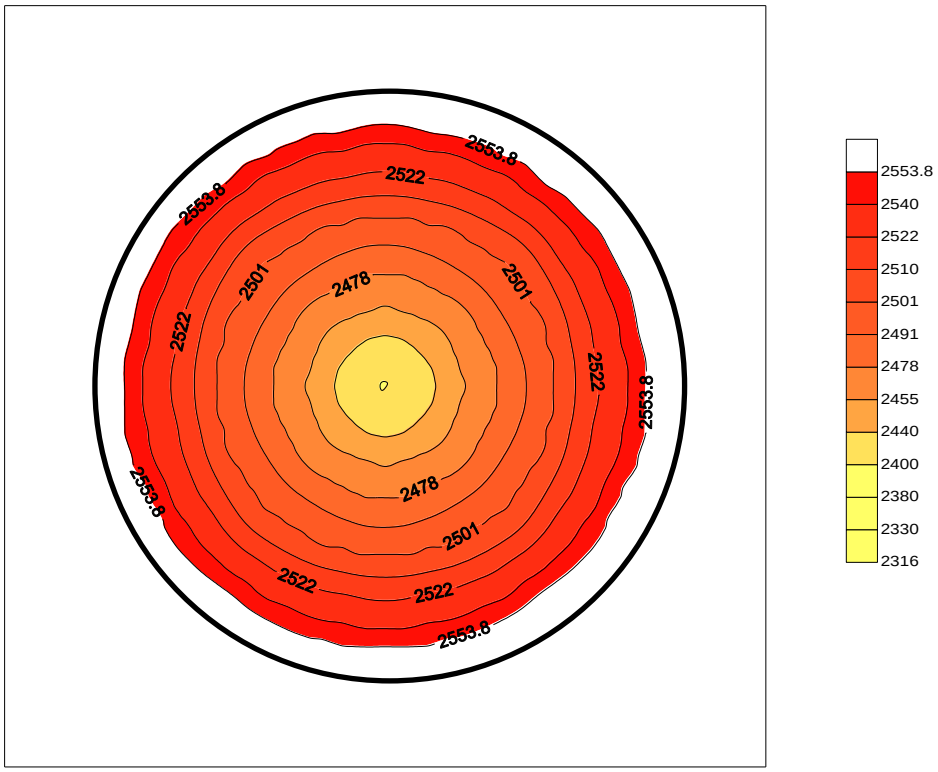

Figure(5.4b): Temperature contours
Equivalence ratio:0.9 , Compression ratio: 7.5, Engine speed: 1500
Spark timing : 30 BTDC, Spark Plug Location: (a/B) = 0.5.

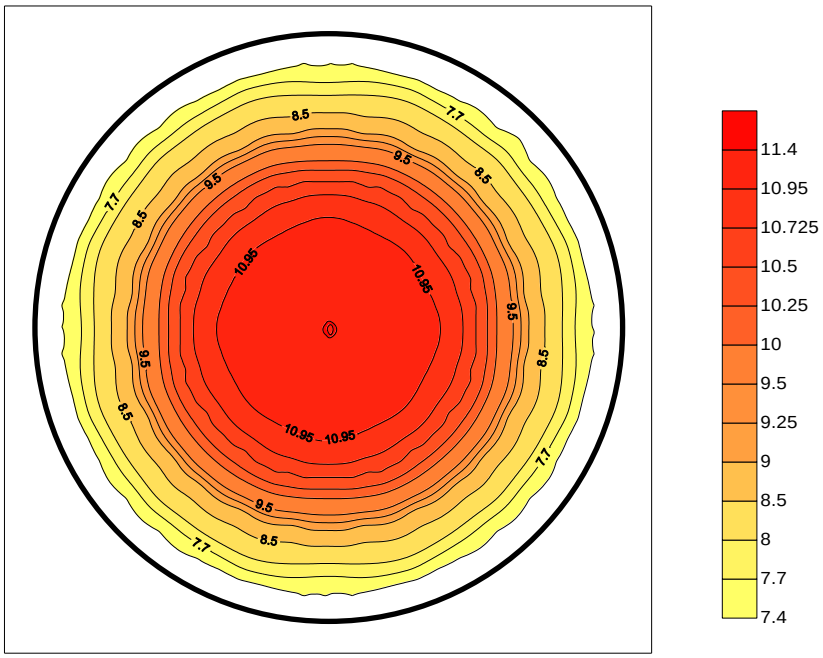

Figure(5.4c): Flame speed contours

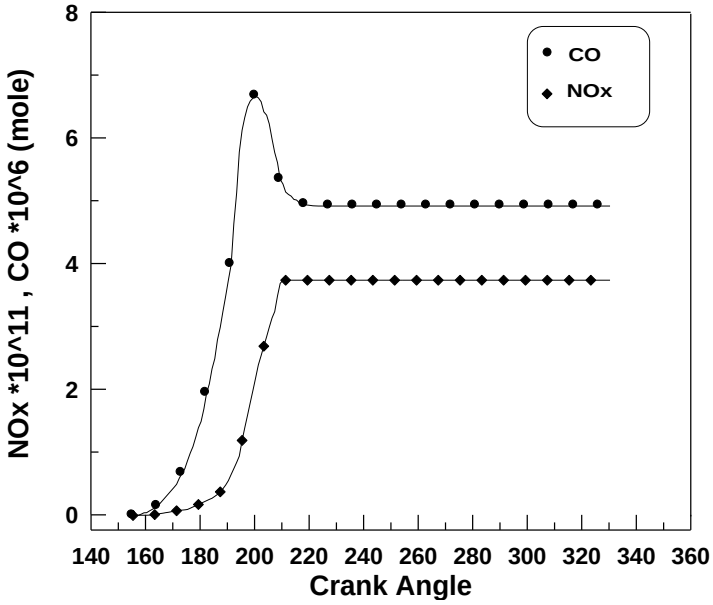

Figure(5.4d):Variation of concentration of NOx and CO with crank angle.

Equivalence ratio:0.9 , Compression ratio: 7.5 , Engine speed: 1500
Spark timing : 30 BTDC, Spark Plug Location: (a/B) = 0.5.

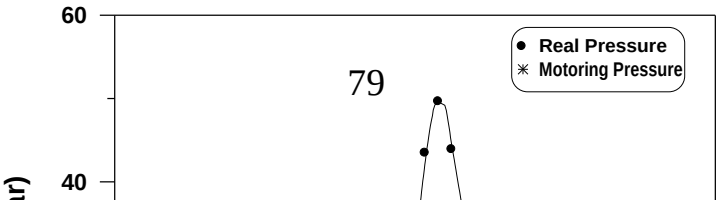

Figure(5.5a): Variation of cylinder pressure with crank angle

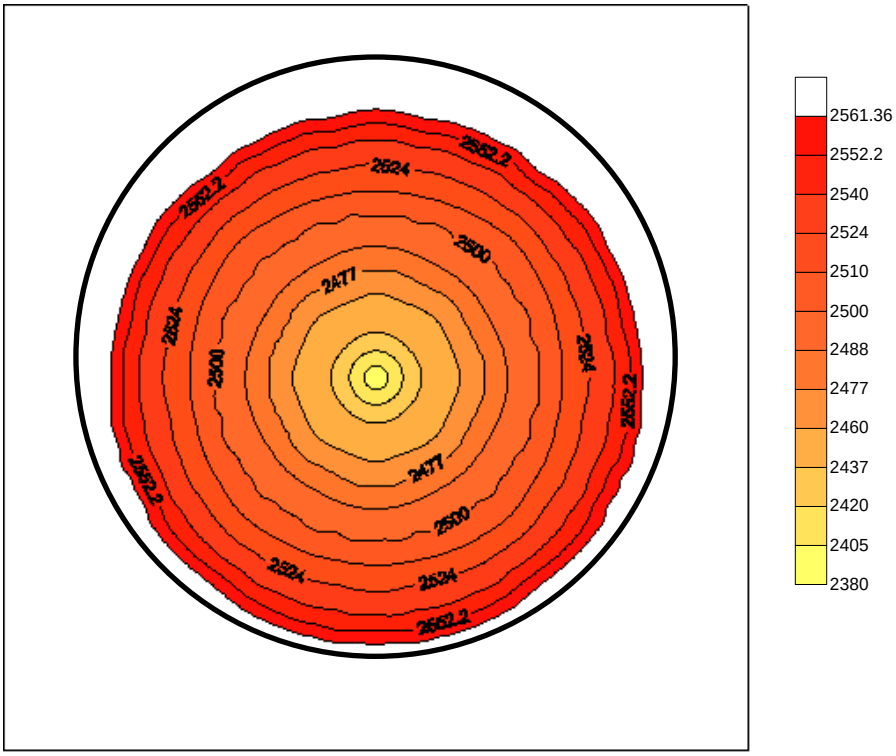

Figure(5.5b): Temperature contours
Equivalence ratio:1.1, Compression ratio: 7.5, Engine speed: 1500
Spark timing : 30 BTDC, Spark Plug Location: (a/B) = 0.5.

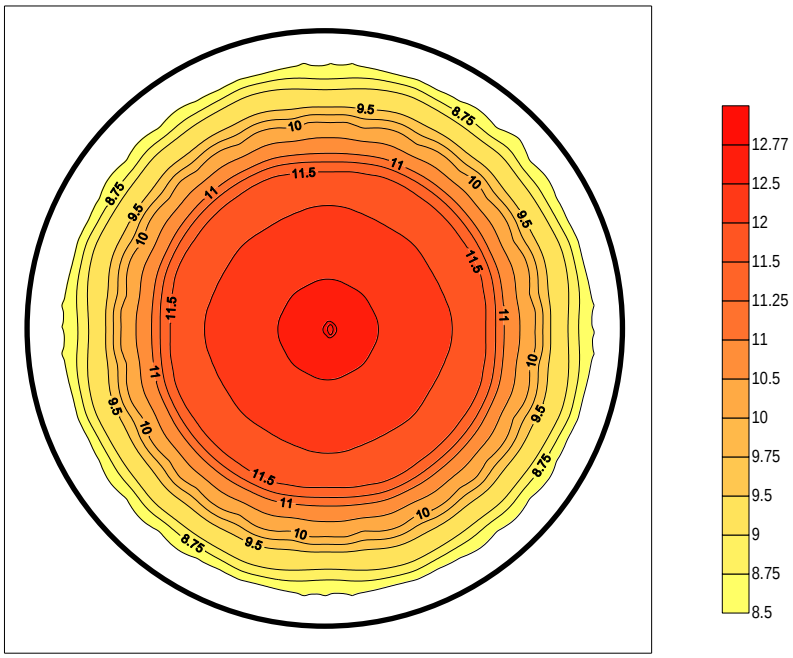

Figure(5.5c): Flame speed contours

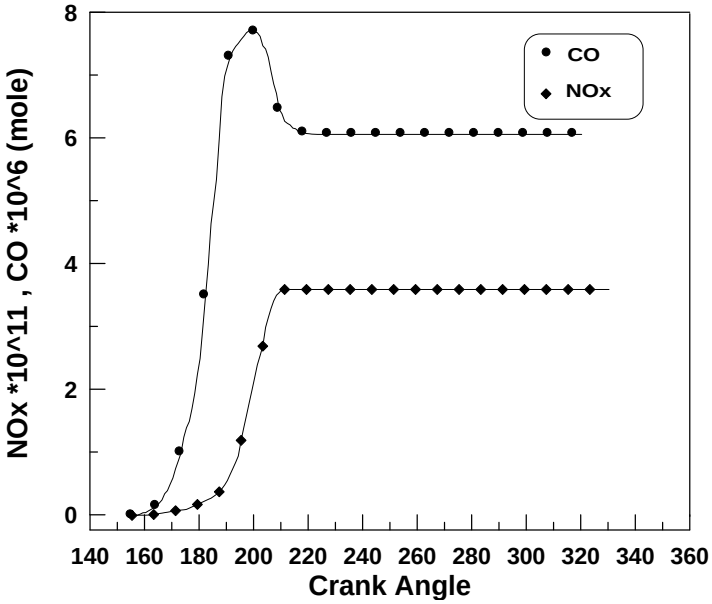

Figure(5.5d): Variation of concentration of NOx and CO with crank angle.

Equivalence ratio:1.1, Compression ratio: 7.5, Engine speed: 1500 Spark timing : 30 BTDC, Spark Plug Location: (a/B) = 0.5.

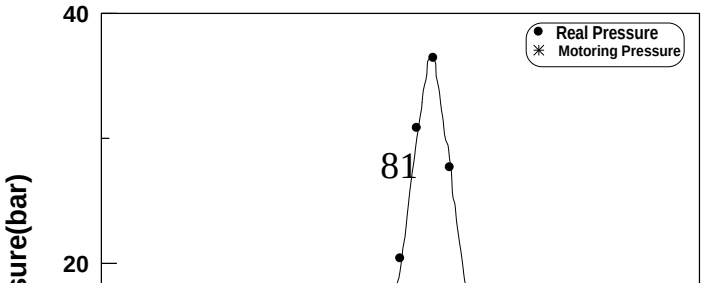

Figure(5.6a): Variation of cylinder pressure with crank angle.

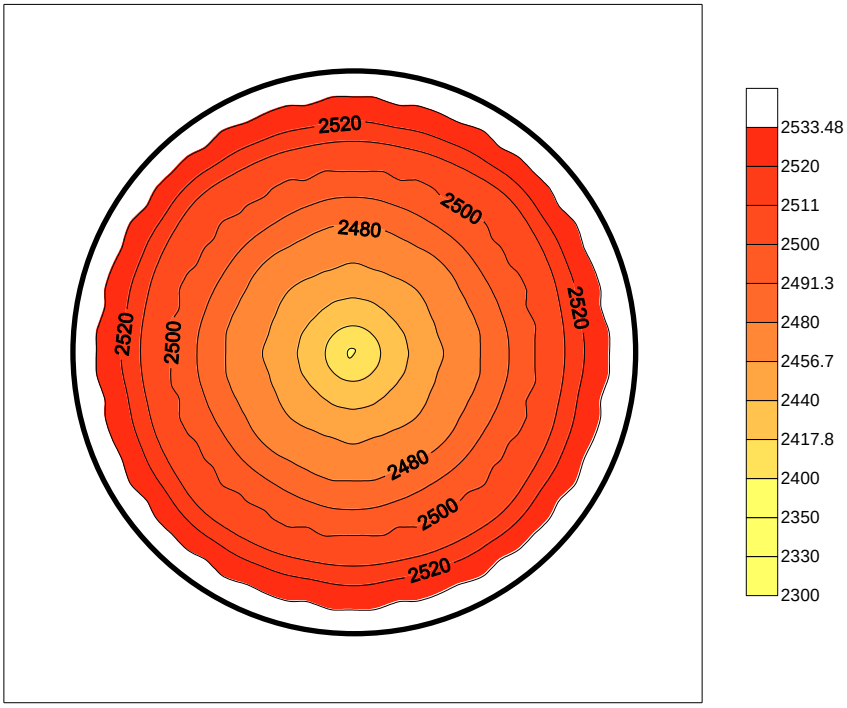

Figure(5.6b): Temperature contours
Equivalence ratio:1, Compression ratio: 7.5, Engine speed: 1500
Spark timing : 20 BTDC, Spark Plug Location: (a/B) = 0.5.

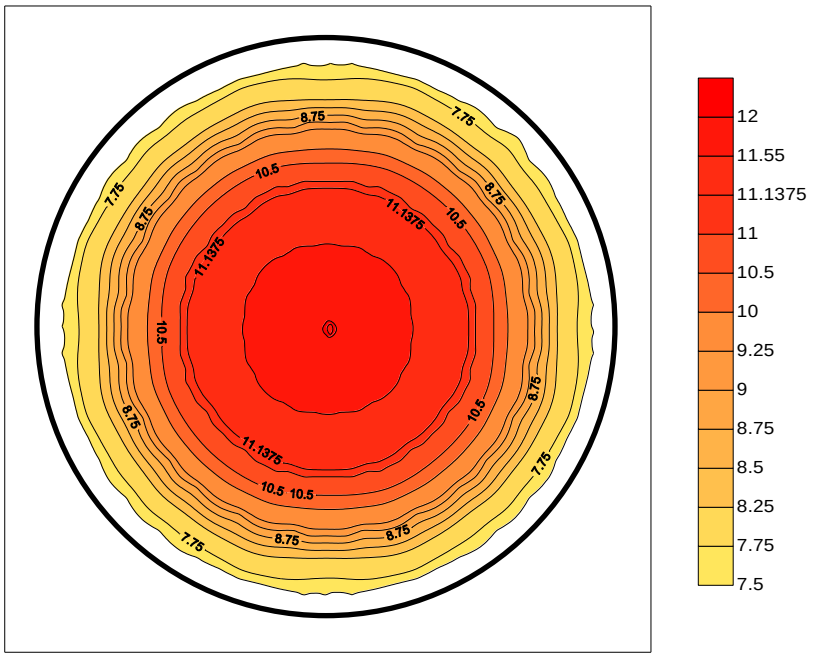

Figure(5.6c): Flame speed contours

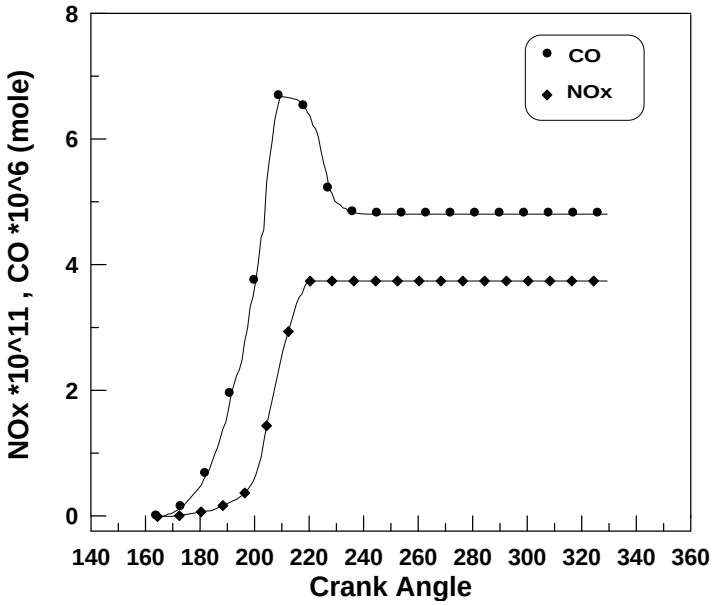

Figure(5.6d): Variation of concentration of NOx and CO with crank angle.

Equivalence ratio:1.0, Compression ratio: 7.5, Engine speed: 1500
Spark timing : 20 BTDC, Spark Plug Location: (a/B) = 0.5.

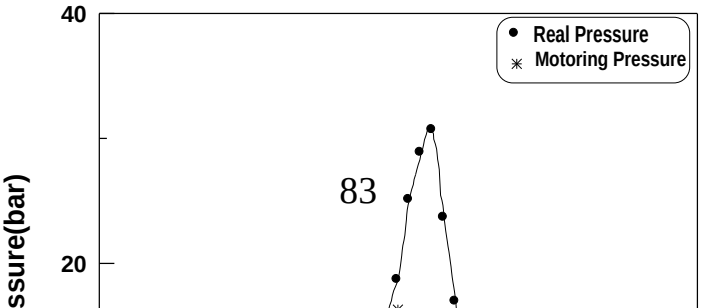

Figure(5.7a): Variation of cylinder pressure with crank angle.

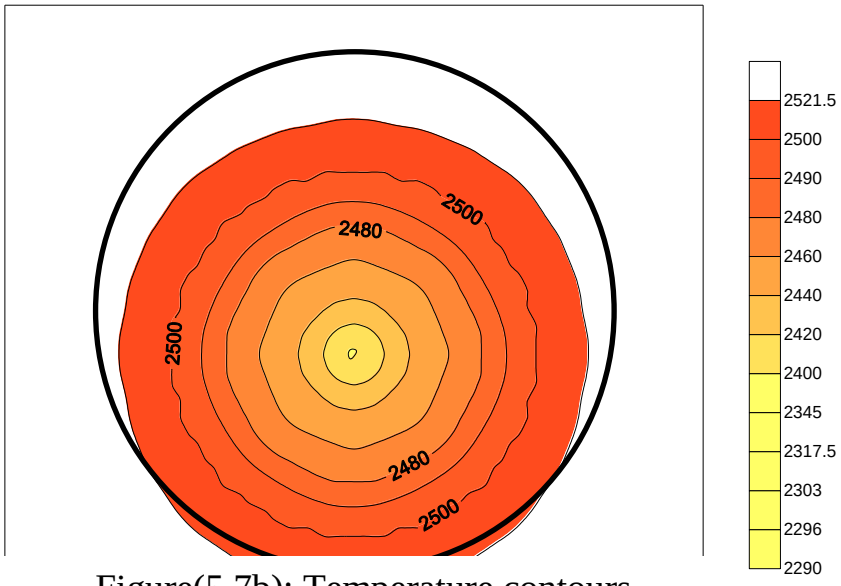

Figure(5.7b): Temperature contours
Equivalence ratio:1, Compression ratio: 7.5, Engine speed: 1500
Spark timing: 15 BTDC, Spark Plug Location: (a/B) = 0.5.

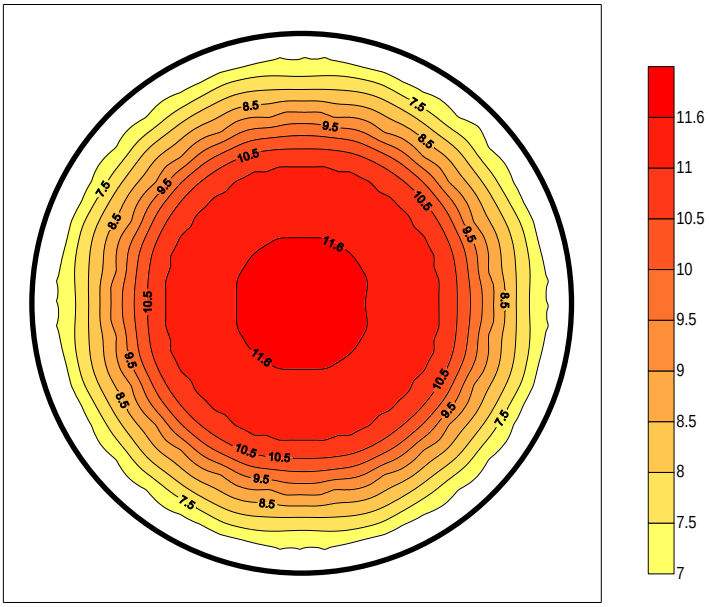

Figure(5.7c): Flame speed contours

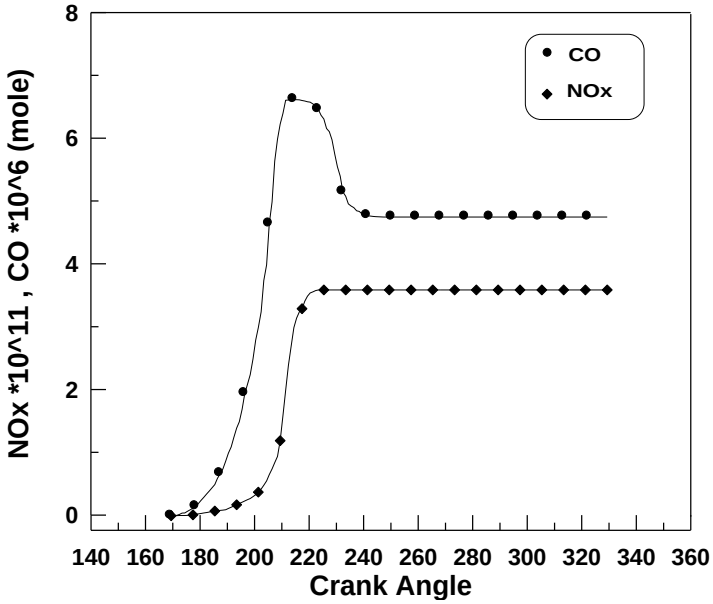

Figure(5.7d): Variation of concentration of NOx and CO with crank angle.

Equivalence ratio:1.0, Compression ratio: 7.5, Engine speed: 1500
Spark timing: 15 BTDC, Spark Plug Location: (a/B) = 0.5.

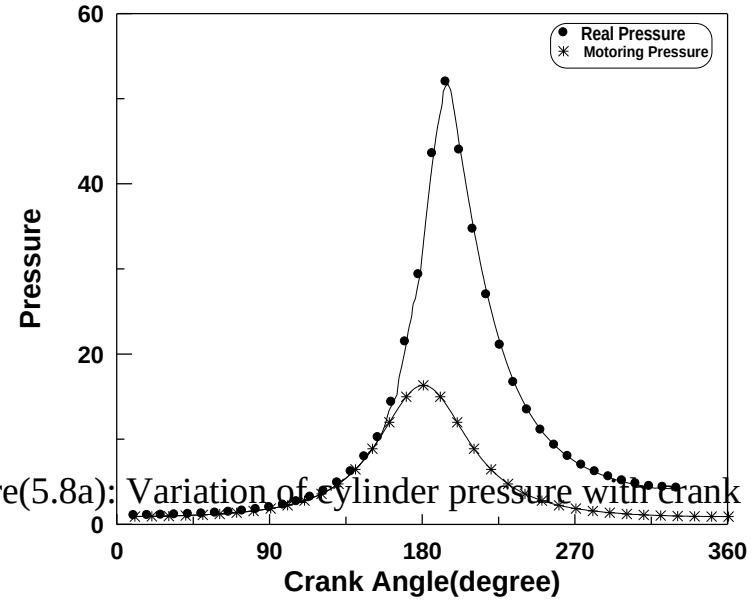

Figure(5.8a): Variation of cylinder pressure with crank angle.

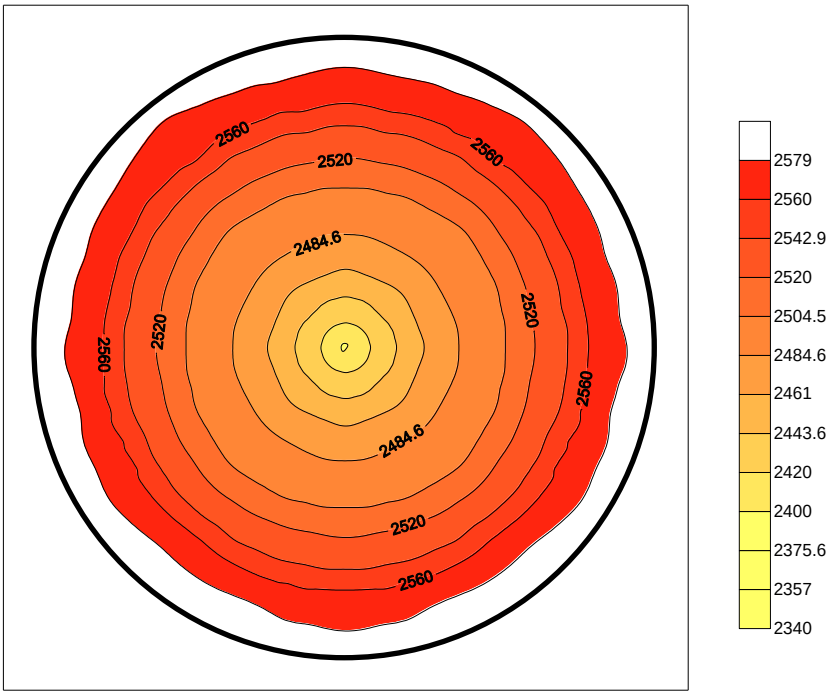

Figure(5.8b): Temperature contours
Equivalence ratio:1, Compression ratio: 8, Engine speed: 2500
Spark timing: 30 BTDC, Spark Plug Location: (a/B) = 0.5.

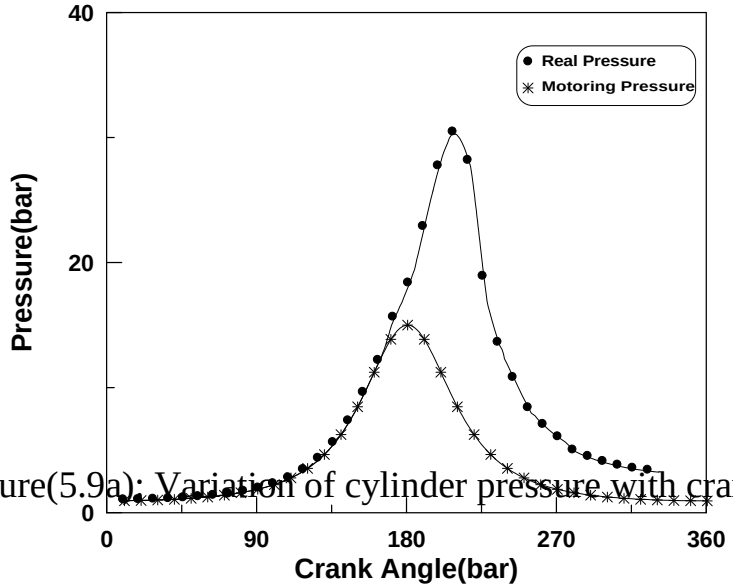

Figure(5.9a): Variation of cylinder pressure with crank angle

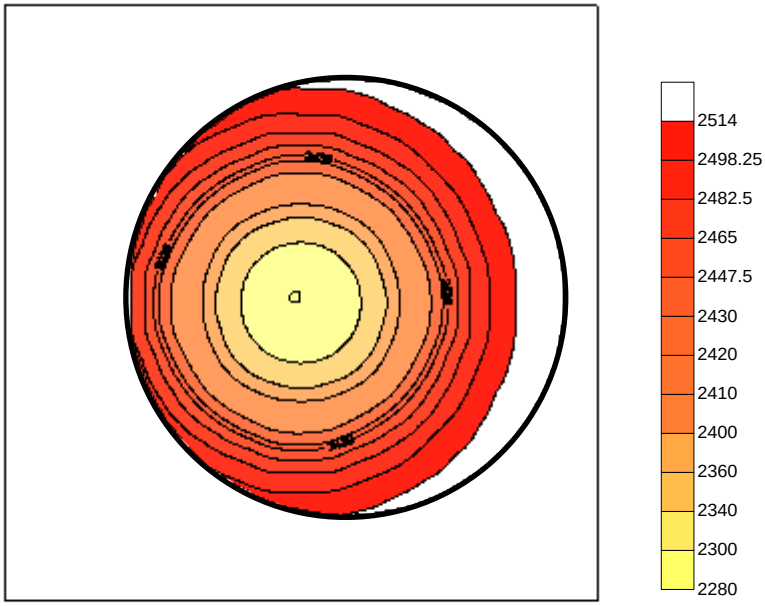

Figure(5.9b): Temperature contours.
Equivalence ratio:1.0, Compression ratio: 7.5, Engine speed: 1500
Spark timing: 20 BTDC, Spark Plug Location: (a/B) = 0.4.

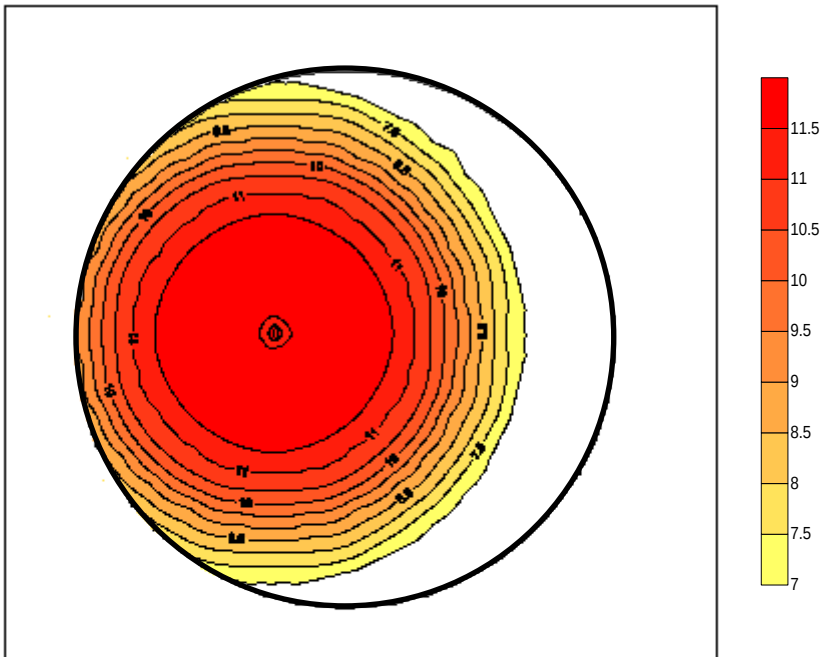

Figure(5.9c): Flame speed contours

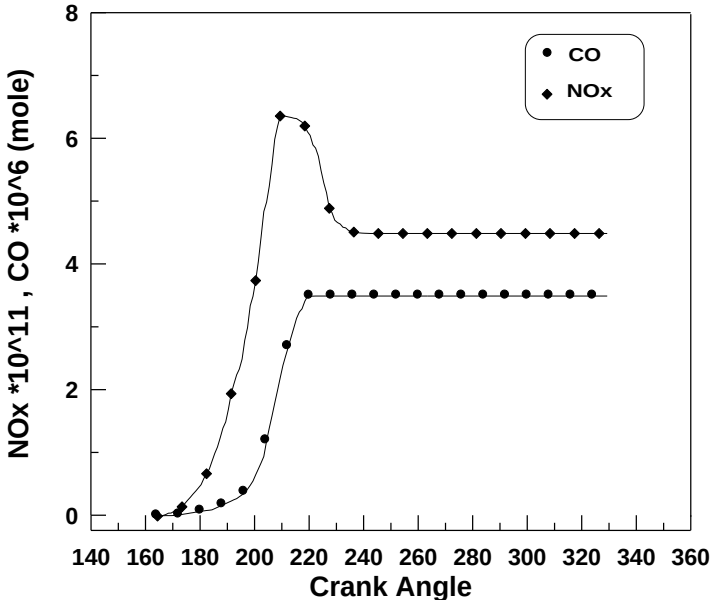

Figure(5.9d):Variation of concentration of NOx and CO with crank angle.
Equivalence ratio:1.0, Compression ratio: 7.5, Engine speed: 1500
Spark timing: 20 BTDC, Spark Plug Location: (a/B) = 0.4.

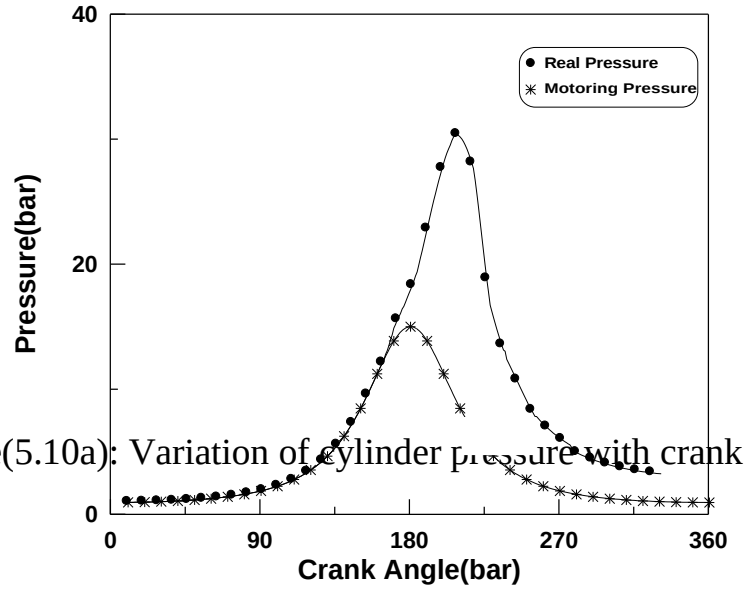

Figure(5.10a): Variation of cylinder pressure with crank angle

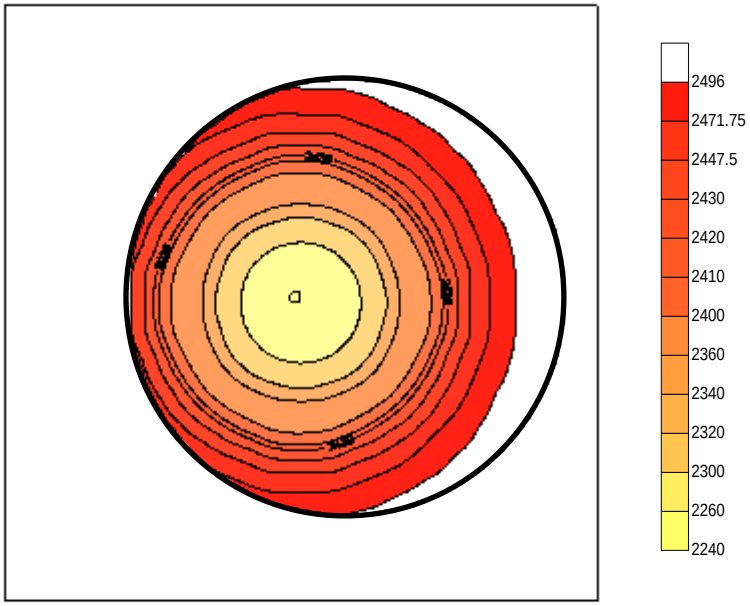

Figure(5.10b): Temperature contours
Equivalence ratio:1, Compression ratio: 7.5, Engine speed: 1500
Spark timing: 20 BTDC, Spark Plug Location: (a/B) = 0.3

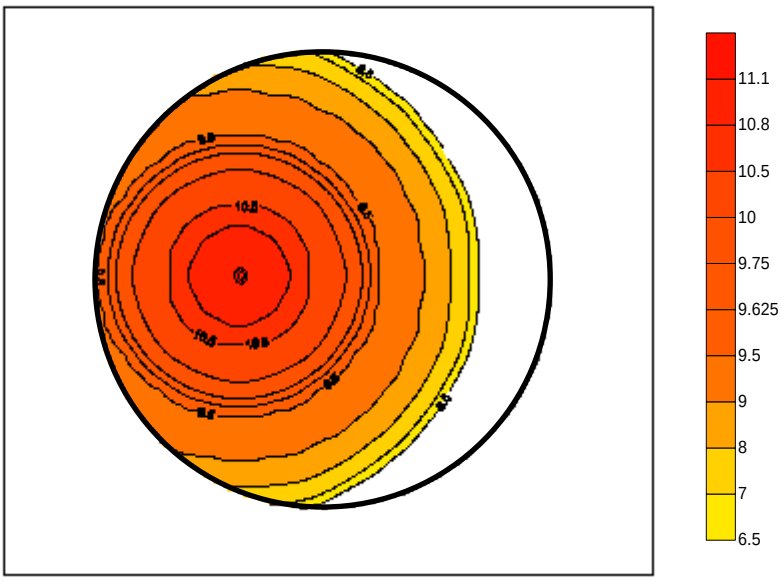

Figure(5.10c): Flame speed contours

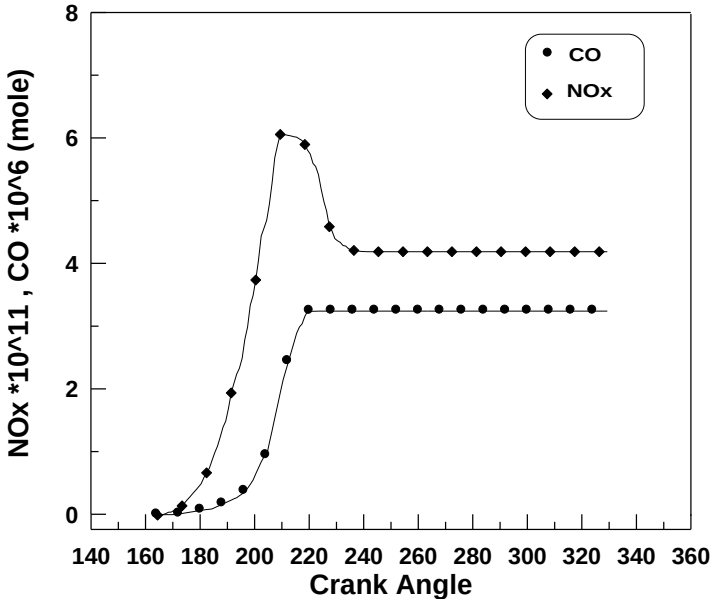

Figure(5.10d): Variation of concentration of NOx and CO with crank angle
Equivalence ratio:1.0, Compression ratio: 7.5, Engine speed: 1500
Spark timing: 20 BTDC, Spark Plug Location: (a/B) = 0.3

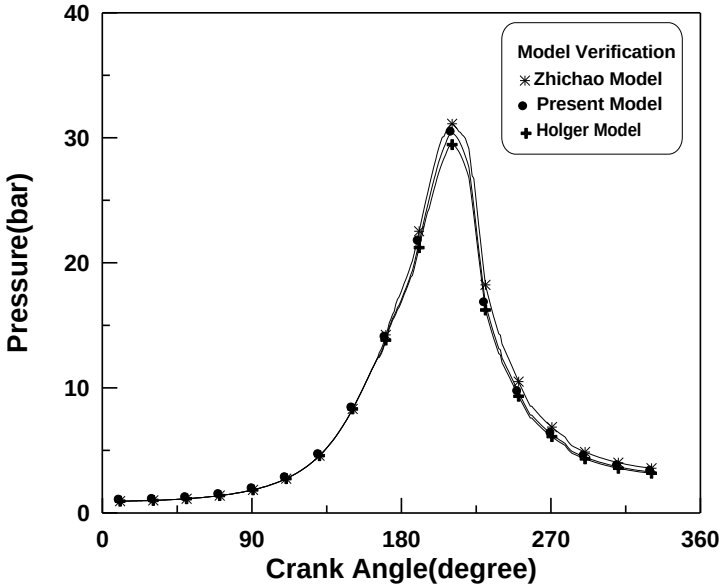

Figure(5.17): A comparison between predicted cylinder pressure and other theoretical models

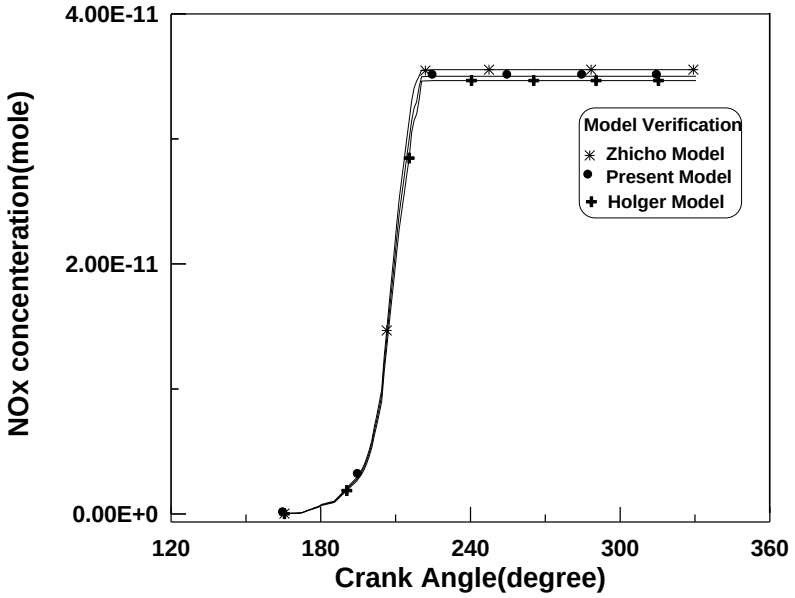

Figure(5.18): A comparison between NOx concentration and other theoretical models

CHAPTER 6

CONCLUSIONS AND SUGGESTION

6.1 Conclusions

The present level of modeling is capable of predicting the cylinder pressure, temperature contours, Flame speed contours, NOx and CO emissions.

These results characterize that the value of maximum cylinder pressure and temperature, flame speed, NOx and CO emissions are affected by the engine variables.

The following conclusions can be drawn;

- When the compression ratio is increased by 12.5%, the flame speed increases by about 10.25%. The maximum pressure increases by about 8.5%, the maximum temperature increases by about 0.18% this causes that the NOx and CO emission increased.
- When the equivalence ratio is increased by 10%, the flame speed increases by about 5%, and flame speed reduces after Φ =1.2. Maximum burned gas temperature occurs at Φ =1.1. CO emission also increased. NOx emission is maximum at Φ =1 and then decreased.
- Spark timing affects the value and the location of the maximum pressure. It is found that the cylinder maximum pressure, temperature, NOx and CO emission decrease with the retarding the spark timing than 30º BTDC.

- The position of the spark plug has a strong effect on the pressure, temperature field, flame speed, NOx and CO concentrations. Shifting the spark plug from central position toward the wall reduces all studied parameters.

6.2 Suggestions for Future Work

1. ***Investigate the quenching phenomenon.***
2. ***Investigate knock phenomenon.***
3. ***Use numerical method to investigate the optimum combustion process.***
4. ***Modify the present work to study the effect of air swirl on the parameters studied.***
5. ***Study the effect of turbocharging on the parameters studied in the present work.***

ACKNOWLEDGMENT

(In The Name of Allah ,The Gracious and Merciful)

Praise be to ***"ALLAH"*** *and his prophet* ***"Mohammed"****. This research has been completed under their benediction.*

I would like to express my deep thanks and gratitude to my supervisors, ***Dr. Haroun A.K. Shahad & Dr. Tahssen AL-Hattab*** *for their great support, guidance, advice and assistance throughout the various stages of the present work.*

I am also indebted to the staff of Mechanical Engineering Department.

I record my sincere gratitude to my family and specially to my ***father****,* ***mother*** *and my* ***husband*** *for their assistance, encouragement and support during the period of preparing this work.*

Finally, I would also like to thank all my friends in Babylon University for their assistance during the entire period of this research.

Intesar Fadhil Hachim
2007

Nomenclature

The following symbols are used generally throughout the text. Others are defined as when used.

symbol	Description	unit
A	Total area of cylinder	m^2
C_P	Specific heat at constant pressure	kJ/kg.K
C_V	Specific heat at constant volume	kJ/kg.K
G	Gibbs free energy	kJ
g	Specific Gibbs free energy	kJ/kg
H	Total enthalpy	kJ
h	Specific enthalpy	kJ / kg
K_P	Equilibrium constant	
L	Stroke	m
ℓ	Connecting rod length	m
N	Total mole of mixture or products	Mole
Q	Total heat transfer	kJ/kg
n_i	NO. of moles of species i	Mole
P	Pressure	N/m^2
pr	Prandtl number	
Re	Reynolds number	
R_{mol}	Universal gas constant	kJ/Kmol .K
r	Crank radius	m
rps	Rotational speed of the crank shaft	Rev/s
T	Temperature	K
t	Time	s
U	Internal energy	kJ
u	Specific internal energy	kJ /kg
U_{ij}	Polynomial coefficient for species i	
V	Volume	m^3
W	Work	kJ
X_i	Mole fraction of species i	Mole of species i/total mole

Abbreviations	
AFR	Air to fuel ratio
CR	Compression ratio

Creek symbols		
Φ	Equivalence ratio	
ε	Total emissivity	
δ	Stefan-Boltzman constant	5.67E-8W/m².K^4
θ	Crank angle	degree
w	Local average gas velocity in the cylinder	m/s
μ	Dynamic viscosity	kg/m . s

Subscripts	
a	Air
b	Burned
c	Clearance
dic	Displacement
f	Flame
g	Gas
ht	Heat Transfer
i	Species
j	Loop from 1 to 5
m	Mechanical
o	At absolute zero
p	Products or Pressure
R	Reactants
st	Stoichiometric
T	Total
u	Unburned
v	Constant volume
w	Wall

References

[1] Henning, B., and Jochen, F., ***"Numerical Modeling of Flames"***, Combustion Instabilities", International Energy Agency, 2003.

[2] Johen, B. Heywood, ***"Internal Combustion Engine Fundamentals"***, 1988.

[3] Johen, B. Heywood, ***"Combustion and its Modeling in Spark-Ignition Engine"***, International SymposiumCOMODIA94(1994).

[4] Alkides, A. C., ***"Heat Transfer Characteristics of a Spark Ignition Engine"***, Journal of Heat Transfer, May 1980.

[5] Mohammed, M., ***"Laminar Burning Velocity of Propane-Air Mixtures at High Temperature and Pressure"***, Combustion and Flame, 38:143-154, 1980.

[6] Mohammed, M., and J.C. KECK, ***"Burning Velocities of Mixture of Air with Methanol, Isooctane and Indolene at High Pressure and Temperature"***, Combustion and Flame 48, PP.191-210, 1982.

[7] Stephen G. Poulos and John B.Heywood, ***"The Effect of Chamber Geometry on Spark-Ignition Engine Combustion"***, SAE, Paper No. 830334, 1983.

[8] Elia, C. Bedran and Gian, P. Beretta, ***"General Thermodynamic Analysis for Engine Combustion Modeling"***, SAE paper, 860459,1986.

[9] Naitoh, K., ***"Numerical Simulation of the Detailed Flow and Flame Propagation in a Homogeneous-Charge, Spark-Ignition Engine",*** International Symposium COMODIA90: PP. 75-80(1990).

[10] Ishii, K., and Niu, K., ***"Analysis of Ignition Mechanism of Combustible Mixtures by Short Duration Sparks"***, International Symposium COMODIA90: PP. (153-158)1990.

[11] Cannoly, F.T.,and Yagle, A. E.,***"Modeling and Identification of the Combustion Pressure Process in I.C.E"***, Experimental Results Journal of Engineering for Gas Turbines and Power, October, Vol.115/801, 1993.

[12] Yacoub, Y. M., and Bata, R. M. ***"Development and Validation of a Thermodynamic Model for an SI-Single Cylinder Engine"***, Journal of Engineering for Gas Turbines and Power, ASME, Vol.120/209, January 1998.

[13] Jaekeun, P., and Jaewon, H., ***"The Temperature Interpretation in Gasoline Engine Using Breakdown Voltage Characteristics"***, Seoul 2000 FISITA World Automotive Congress F2000A116. June12-15, Inha University, South Korea.

[14] Catania, A. E., and Misul,D., ***"A Refined Two-Zone Heat Release Model for Combustion Analysis in SI Engines"*** The Fifth International Symposium on Diagnostics and Modeling of Combustion in Internal Combustion Engines (COMODIA 2001), Nagoya, July 1-4,2001.

[15] Holger, P., and Ralph W., ***"Numerical Analyses of the Combustion Process in a Spark-Ignition Engine"***, International Symposium COMODIA90: PP. (153-158) 2001.

[16] Inyong, C., ***"Studies of Temperature Elevation due to the Pre-Flame Reaction in a Spark- Ignition Engine with CARS Temperature Measurements Using Fuels of Various Octane Numbers"***, International Symposium COMODIA90: PP. (75-80)2001.

[17] Razavi, M. R., ***"The Effect of Spark Plug Position on Spark Ignition Combustion"***, Faculty of Engineering, Ferdowsi University of Mashhad Iran (2002).

[18] Zhichao, T. ,and Rolf, D. Reitz, ***"Development of G-Equation Combustion Model for Direct Injection SI Engine Simulations"***, SAE, PP. 01-0722, 2003.

[19] Tatschl, R., and Bogensperger, M. ***"Flame Propagation and Knock Onset Analysis For Full Load SI-Engine Combustion "***, SAE Congress, Detroit, MI, April 10, 2005.

[20] Benson, R. S., W.J.D. Annand, and P.C. Baruah, ***"Simulation Model Including Intake and Exhaust System for a Single Cylinder Four Stroke Cycle Spark Ignition Engine"***, Int. J. Mech. SI Pergamon Press Vol. 17 PP.97-124, 1975.

[21] Mayo, J., ***"The Effect of Engine Design Parameters on Combustion Rate in Spark-Ignited Engine"***, SAE, Paper, 750355, 1975.

[22] Way, R.J.B, ***"Methods for Determination of Composition and Thermodynamic Properties of Combustion Products for Internal Combustion Engine Calculation"***, Proc.Inst, Mech. Engrs. Vol.190, 1977.

[23] Westbrook, C.K., and Pitz, W.J., ***"The Inevitability of Engine-Out NOx Emissions from Spark-Ignition and Diesel Engines"***, Twenty-Seventh Symposium (International) on Combustion. PP.397-283, The Combustion Institute, Pittsburgh, 1998.

[24] Ivan, A., and Antonio, B., ***"Models for the Predication of Performance and Emission a Spark Ignition Engine"***, SAE, Society of Automotive Engineers, 980779, 1998.

[25] Gupta, H.N., and Jehad, Y., ***"The Effect of Combustion Duration on the Performance and Emission Characteristics of Propane-Fueled 4-Stroke S.I. Engines"***, Emirates Journal for Engineering Research,8(1),1-14(2003).

[26] Willard W. Pulkrabek, University of Wisconsin-Platteville. ***"Engineering Fundamental of the Internal Combustion Engine"***, 1997.

[27] Richard Stone, (Translated by Dr. Haroun AL-Janabi 1989), ***"Introduction to Internal Combustion Engine"***.

[28] Woshni, G., ***"A Universally Applicable Equation for the Instantaneous Heat Transfer Coefficient in the Internal Combustion Engine "***, SAE, Paper No. 670931, 1967.

[29] Ferguson, C. R., ***"Internal Combustion Engine"***, Copyright by John Wiley and Sons, Inc. , 1986.

[30] Benson, R. S., ***"Advanced Engineering Thermodynamics"***, 1977.

[31] Benson, R. S., and Whitehouse, N. D., ***"Internal Combustion Engines"***, 1979.

[32] Annand, W. J. D., ***"Geometry of Spherical Flame Propagation in a Disk-Shaped Combustion Chamber"***, Journal of Mechanical Engineering Science, Vol.12, No.2, 1970.

[33] Lavoie, G.A. and J.B. Heywood, ***"Experimental and Theoretical Investigation of Nitric Oxide Formation in Internal Combustion Engine"***, Combustion Science Technology, Vol.1, pp. 313-326, 1970.

[34] SARAO, A. S., ***"Thermal Engineering"***, Textbook 1993.

[35] Charles Fayette Taylor, ***"The Internal Combustion Engine in Theory and Practice"***, volume I: Thermodynamics, fluid flow, performance, 1985.

[36] Charles Fayette Taylor, ***"The Internal Combustion Engine in Theory and Practice"***, volume II: Combustion, Fuels, Materials, Design, 1985.

[37] Edward F. Obert, ***"Internal Combustion Engines and Air Pollution"***, 1973.

[38] Ballaney, P.L., ***"Internal Combustion Engine in Theory and Practice"***, 1986.

[39] Peter, O. Witze, ***"The Effect of Spark Location on Combustion in a Variable-Swirl Engine"***, SAE, Paper No. 820044, 1982.

[40] Paulina, S. Kuo, ***"Cylinder Pressure in a Spark-Ignition Engine : A Computational Model"***, SAE, Society of Automotive Engineers, 960335, 1996.

[41] Benson, R. S. ***"Numerical Solution of One-Dimensional Non-Steady Flow with Supersonic and Subsonic Flows and Heat Transfer"***, Int. J. Mech. Sci. Pergamon Press.Vol, 14, PP.635-642. 1972.

[42] Stephen R. Torns. ***"An Introduction to Combustion Concepts and Applications"***, 1996.

[43] Technical report by U.S.DOE, "***Automotive Emission: An Overview"***, U.S.DOE, Office of Energy Efficiency and Renewable Energy, March, 2005. Web Site :< http:/www.eere.energy.gov>.

[44] Anders, T. P., "***The Use of Cylinder Pressure for Estimation of the In-Cylinder Air/Fuel Ratio of an Internal Combustion Engine"***, PhD, Thesis, Mechanical Engineering, Lund University, Sweden, 2000.

[45] Hacohen, Y., and Sher, E., ***"Measurements and Predictions of the Fuel Consumption and Emission of a Spark Ignition Engine Fuelled with Hydrogen Enriched Gasoline"***, Proc. Instn. Mech. Enggs. Vol.203, 1989.

APPENDIX A

The composition of the working fluid during intake and compression strokes

To analyze the state of working fluid at the trapped conditions, the following three cases, depending on the equivalence ratio, are considered [2];

At first the following symbol definition are noted;

n: Number of carbon atoms in hydrocarbon fuel.

m: Number of hydrogen atoms in hydrocarbon fuel.

X : Number of Kmoles of Oxygen for one Kmol of fuel and it is equal to;

$(\frac{1}{\Phi})\cdot(n+m/4)$

$E1$: Number of Kmoles of CO_2 from the combustion of 1 Kmol of fuel.

$E2$: Number of Kmoles of H_2O from the combustion of 1 Kmol of fuel.

$E3$: Number of Kmoles of N_2 in the product of 1 Kmol of fuel.

$E4$: Number of Kmoles of O_2 in the product of 1 Kmol of fuel.

$E5$: Number of Kmoles of CO from the combustion of 1 Kmol of fuel.

CASE A- Stoichiometric mixture, (Φ=1.0)

$$C_nH_m + XO_2 + 3.76\,XN_2 \rightarrow E1.CO_2 + E2.H_2O + E3.N_2 \qquad \text{(A.1)}$$

The atomic balance of C, O, N and H gives;

$$E1 = n \qquad \text{(A.2)}$$

$$E2 = m/2 \qquad \text{(A.3)}$$

$$E3 = 3.76\,X \qquad \text{(A.4)}$$

CASE B- Weak mixture, (Φ<1.0)

$$C_nH_m + XO_2 + 3.76\,XN_2 \rightarrow E1.CO_2 + E2.H_2O + E3.N_2 + E4.O_2 \qquad \text{(A.5)}$$

The atomic balance of C, O, N and H gives;

$$E1 = n \quad \text{(A.6)}$$

$$E2 = m/2 \quad \text{(A.7)}$$

$$E3 = 3.76X \quad \text{(A.8)}$$

$$E4 = X - n - m/4 \quad \text{(A.9)}$$

CASE C- Rich mixture, (Φ >1.0)

$$C_nH_m + XO_2 + 3.76XN_2 \rightarrow E1.CO_2 + E2.H_2O + E3.N_2 + E5.CO \quad \text{(A.10)}$$

The atomic balance of C, O, N and H gives;

$$E1 = 2X - m/2 - n \quad \text{(A.11)}$$

$$E2 = m/2 \quad \text{(A.12)}$$

$$E3 = 3.76X \quad \text{(A.13)}$$

$$E5 = 2n + m/2 - 2X \quad \text{(A.14)}$$

The total number of moles of residual gas, fuel, and air in the cylinder at trapped condition;

$$Nm = \frac{P_{cyl}.V_{cyl}}{R_{mol}.T_{cyl}} \quad \text{[Kmol]} \quad \text{(A.15)}$$

Where; P_{cyl} Cylinder pressure at trapped condition [kPa].

T_{cyl} Cylinder temperature at trapped condition [K].

V_{cyl} Cylinder volume [m^3].

R_{mol} Universal gas constant [kJ/Kmol.K].

For any of the previous cases, the composition of the charge at trapped conditions is calculated as follows;

$$N_{C_nH_m} = CM \quad \text{[Kmol]} \quad \text{(A.16)}$$

$$N_{CO_2} = E1.CD \quad \text{[Kmol]} \quad \text{(A.17)}$$

$$N_{H_2O} = E2.CD \quad \text{[Kmol]} \quad \text{(A.18)}$$

$$N_{N_2} = 3.79X + E3.CD \quad \text{[Kmol]} \quad \text{(A.19)}$$

$$N_{O_2} = X + E4.CD \quad \text{[Kmol]} \quad \text{(A.20)}$$

$$N_{CO} = E5.CD \quad \text{[Kmol]} \quad \text{(A.21)}$$

Where CM and CD are scale factors reducing the mole numbers to the proper size to fit in the engine.

$$CM = \frac{Nm - Nx}{Nmo} \quad \text{(A.22)}$$

$$CD = \frac{Nx}{N\,po} \quad \text{(A.23)}$$

Where ; Nmo Kilo moles of air plus fuel (vapor/gas) in a mixture containing 1 Kmol of fuel.

Npo Kilo moles of products formed from the combustion of Nmo.

Nm Kilo moles of fuel (vapor/gas) and air in the engine at trapped conditions.

Nx Kilo moles of residual exhaust from previous cycle in the engine.

Heywood [2], showed that the typical residual fractions in spark engines range from 5% - 20%.

APPENDIX B

ENGINE SPECIFICATION

Engine Type	(4-Stroke, Spark Engine)
Bore	800 mm
Stroke	1100 mm
Connected Rod Length	243 mm
Intake Valve Timing (Deg.Crank Angle)	Opens 16 BTDC
	Close 40 ABDC
Exhaust Valve Timing (Deg.Crank Angle)	Opens 42 BBDC
	Close 16 ATDC

APPENDIX C

POLYNOMIAL COAFFICIENT OF THERMODYNAMIC PROPERTIES OF SPECIES

U (i,j)

Temperature Range 500-3000 K

Reference Pressure P_o=1.01325 bar

i Species j	1	2	3	4	5	6	7
1 CO_2	3.0959	2.73114e-3	-7.8542e-4	8.66002e-11	0.0000000	6.5839600	-3.9364e8
2 H_2O	3.7429	5.65590e-4	4.952400e-8	-1.8180e-11	0.0000000	0.9651400	-2.3922e8
3 O_2	3.2530	6.52350e-4	-1.49524e-7	1.53897e-11	0.0000000	5.7124300	0.0000000
4 N_2	3.3443	2.94260e-4	1.953000e-9	-6.5747e-12	0.0000000	3.7586300	0.0000000
5 H_2	3.4332	-8.1810e-6	9.669900e-8	-1.4439e-11	0.0000000	-3.844700	0.0000000
6 NO	3.5017	2.99380e-4	-9.58800e-9	-4.9036e-12	0.0000000	5.1134600	8.99680e7
7 N	2.4990	2.87441e-6	-2.44816e-9	6.15151e-13	0.0000000	4.1850400	4.71650e8
8 OH	3.4502	3.67521e-4	-2.43560e-8	-3.0487e-12	0.0000000	4.7812300	3.94580e7
9 CO	3.3170	3.76970e-4	-3.22080e-8	-2.1945e-12	0.0000000	4.6328400	-1.1390e8
10 H	2.5000	0.0000000	0.0000000	0.0000000	0.0000000	-4.593100	2.16230e8
11 O	2.7640	-2.5142e-4	1.001870e-7	-1.3867e-11	0.0000000	3.7330900	2.74070e8
12 Ar	2.5000	0.0000000	0.00000000	0.00000000	0.0000000	0.0000000	0.0000000
13 C_8H_{18}	-0.719	4.6426e-2	-1.68385e-5	2.67009e-9	0.0000000	0.0000000	-4.9290e8

APPENDIX D

Geometric Interactions

If spark plug is located at the center of the combustion chamber four different cases as shown in Figure (D.1) can be distinguished as follows[17].

Case (a); $h \geq r_f \leq B/2$

Case (b); $h \prec r_f \leq B/2$

Case (c); $h \geq r_f \succ B/2$

Case (d); $h \prec r_f \succ B/2$

Where; h is the height of the combustion chamber.

The following equation is used for calculating the enflamed volume of burned region for the centered spark plug.

$$V_b = (\pi/8).B^3\{[1/3(2.r_f/B)^3].[\alpha_c^3 - \beta_c^3 - 3.(\alpha_c - \beta_c)] - (2.r_f/B).\alpha_c\} \quad \text{(D.1)}$$

The flame front area is calculated as follows;

$$A_f = (\pi/4).B^2[2(2.r_f/B)^2.(\alpha_c - \beta_c)] \quad \text{(D.2)}$$

The equation for calculating the heat transfer area of the burned region is given by;

$$A_b = \pi.r_f[2 + (B.\alpha_c/r_f) - (\alpha_c^2 - \beta_c^2)] \quad \text{(D.3)}$$

Where; α_c and β_c can be obtained from following equations in regard to the four cases;

If $r_f \leq B/2$

$$\alpha_c = 0 \quad \text{(D.4)}$$

If $r_f \succ B/2$

$$\alpha_c = \sqrt{[1-[((B/2)/r_f)^2]]} \quad \text{(D.5)}$$

If $r_f \leq h$

$$\beta_c = 1 \quad \text{(D.6)}$$

If $r_f \succ h$

$$\beta_c = h/r_f \quad \text{(D.7)}$$

The heat transfer area of the unburned region is therefore can be calculated;

$$A_u = A - A_b \quad \text{(D.8)}$$

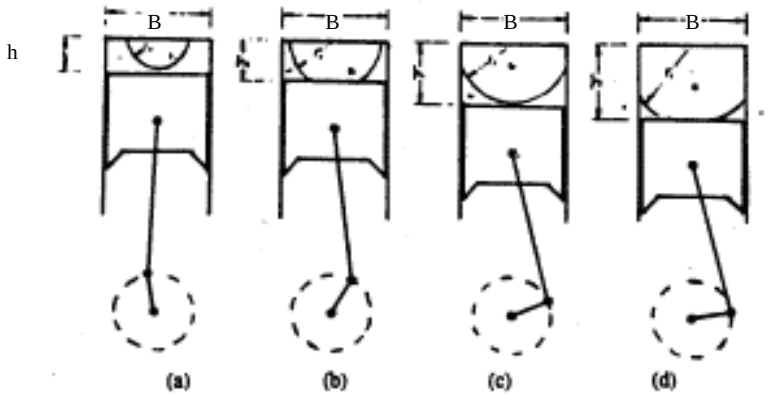

Figure (D.1): Four different cases of geometric interaction between spherical flame and the combustion chamber walls and piston top surface when the position of the spark plug is centered [17].

If the spark plug is not located at the center [32], as shown in Figure(D.2).

The possible cases can be distinguished due to different value of the spark plug location (a).

The equation for calculating the heat transfer area of the burned region is given by;

$$A_b = C1 + C2 + C3 \qquad [m^2] \qquad \text{(D.9)}$$

Where; $C1$ contact area on the upper flat surface of cylinder head $[m^2]$.

$C2$ contact area on the cylinder wall $[m^2]$.

$C3$ contact area on upper flat surface of the piston crown $[m^2]$.

$$A_u = A - A_b \qquad [m^2] \qquad \text{(D.10)}$$

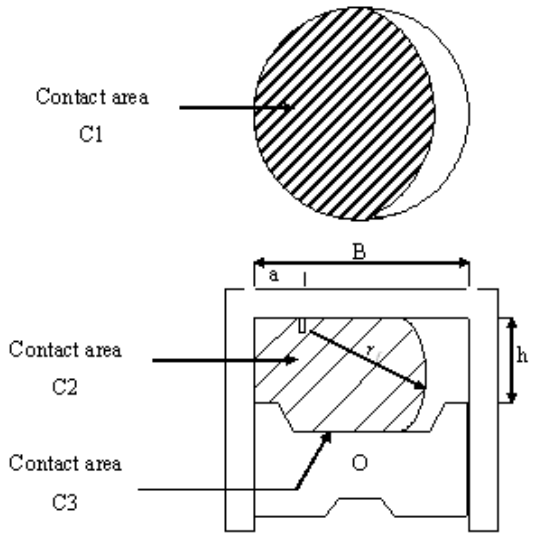

Figure (D.2): Basic geometry

Let $X_\circ$ be a variable such that $X_\circ = r_f$ if $r_f \le h$, other wise $X_\circ = h$.

The following cases are considered;

Case 1: $r_f \le a$

When flame front radius is less than or equal to the spark location distance a, as shown in Figure (D.3), all parameters are easily evaluated as follows;

$$V_b = BB.X_\circ(r_f^2 - \frac{X_\circ^2}{3}) \qquad [m^3] \qquad \text{(D.11)}$$

$$A_f = 2.\pi.r_f.X_\circ \qquad [m^2] \qquad \text{(D.12)}$$

$$C1 = \pi.r_f^2 \qquad [m^2] \qquad \text{(D.13)}$$

$$C2 = 0 \qquad [m^2] \qquad \text{(D.14)}$$

$$C3 = \pi(r_f^2 + X_\circ^2) \qquad [m^2] \qquad \text{(D.15)}$$

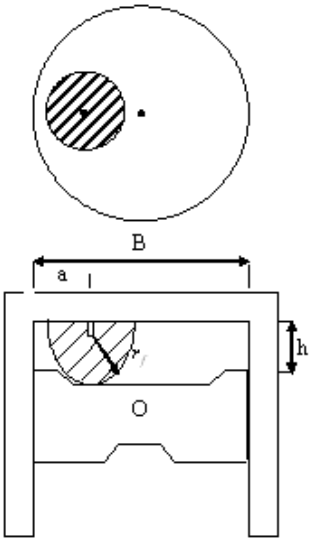

Figure (D.3): Front radius is less than or equal to the spark location

Case 2: r_f > a

When flame front radius is greater than spark location distance a, the calculation becomes more complex, and another parameter may be defined.

The intersection of the flame front and the curved chamber wall with a plane parallel to the flat face, at distance(y) from the upper surface is shown in Figure (D.4). Let BB represents the enclosed area, pp represents the "free" perimeter, and QQ represents the perimeter of wall contact. Let (f) is defined as a radius of intersection of flame front with plane (y) and is given by the following equation;

$$f = \sqrt{\left(r_f^2 + Y^2\right)} \qquad [m] \qquad \text{(D.16)}$$

To calculate the enclosed area BB, the "free" perimeter PP and the perimeter of wall contact QQ, the following three cases, depending on the value of (f), may be considered.

{ When f ≤ a }, Figure (D.4 - A);

$$BB = \pi . f^2 \qquad \text{(D.17)}$$

$$PP = 2.\pi.f \tag{D.18}$$

$$QQ = 0 \tag{D.19}$$

{When a < f < (B-a) }, Figure (D.4 - B);

The angles α and β which are defined in Figure (D.4 - B), are given by;

$$COS\alpha = \left[\frac{a}{B} - \left(\frac{a}{B}\right)^2 - \left(\frac{f}{B}\right)^2\right] \Big/ \left[\frac{(1-2a)f}{B}\right] \tag{D.20}$$

$$COS\beta = 1 + \left[\left(\frac{a}{B}\right)^2 - \left(\frac{f}{B}\right)^2\right] \Big/ \left[\frac{1}{2} - \frac{a}{B}\right] \tag{D.21}$$

Then

$$BB = \left[\pi - \alpha + \frac{1}{2}sin(2\alpha)\right] f^2 + [2\beta - sin(2\beta)]\left(\frac{B^2}{8}\right) \tag{D.22}$$

$$PP = 2.f.(\pi - \beta) \tag{D.23}$$

$$QQ = B.\beta \tag{D.24}$$

{When f ≥ (B-a) }, Figure (D.4 - C);

$$BB = \frac{\pi B^2}{4} \tag{D.25}$$

$$PP = 0 \tag{D.26}$$

$$QQ = \pi.a \tag{D.27}$$

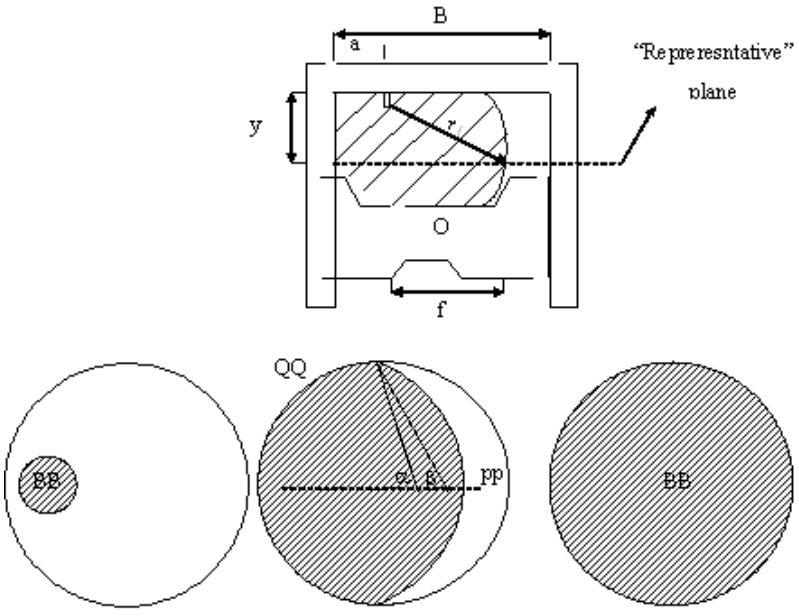

Figure (D.4): Flame front radius is greater than spark location distance

There are three ranges in case 2 (i.e r_f >a), Which are ;

(1) $\sqrt{(a^2+h^2)} \le r_f \le (B-a)$: Figure(D.5)

In this range the set of equations suggested by Annand [32] are used;

$$Y = 0.58X_\circ \qquad [m] \qquad \text{(D.28)}$$

$$V_b = BB.X_\circ \qquad [m^3] \qquad \text{(D.29)}$$

$$A_f = \frac{r_\circ.PP}{f}.X_\circ \qquad [m^2] \qquad \text{(D.30)}$$

$$C1 = BB \qquad [m^2] \qquad \text{(D.31)}$$

$$C2 = QQ.X_\circ \qquad [m^2] \qquad \text{(D.32)}$$

$$C3 = BB \qquad [m^2] \qquad \text{(D.33)}$$

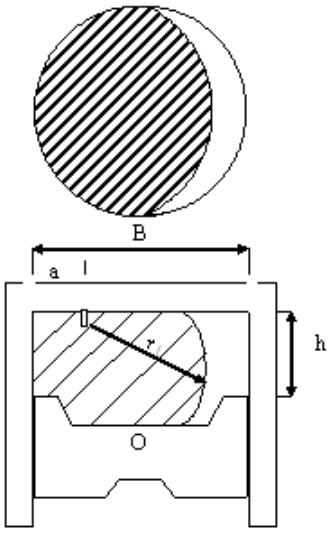

Figure (D.5): $\sqrt{(a^2+h^2)} \le r_f \le (B-a)$

(2) a < $r_f \le \sqrt{(a^2+h^2)}$:

In this range, it is necessary to divided the enflamed zone into two regions, above and below the intersection of the flame with the cylindrical wall, as indicated in Figure (D.6), and the following set of equations are used [32];

$$Z = \sqrt{\left(r_f^2 - a^2\right)} \qquad [m] \qquad \text{(D.34)}$$

$$Y = 0.58Z \qquad [m] \qquad \text{(D.35)}$$

$$V_b = BB.Z + \pi(X_\circ - Z).\left[r_f^2 - (X_\circ + X_\circ.Z + Z^2)/3\right] \qquad [m^3] \qquad \text{(D.36)}$$

$$A_f = \frac{r_f.PP.Z}{f} + 2\pi.r_f(X_\circ - Z) \qquad [m^2] \qquad \text{(D.37)}$$

$$C1 = BB \qquad [m^2] \qquad \text{(D.38)}$$

$$C2 = QQ.Z \qquad [m^2] \qquad \text{(D.39)}$$

$$C3 = 0 \qquad [m^2] \qquad \text{(D.40)}$$

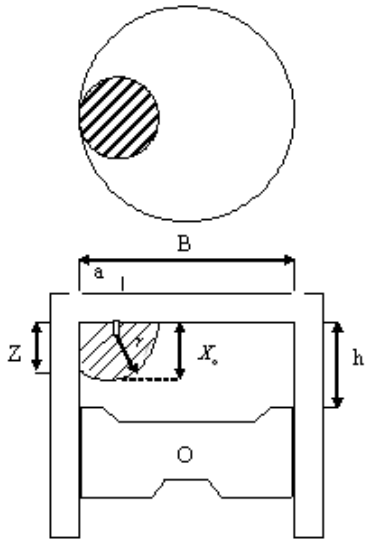

Figure (D.6): $a \prec r_f \prec \sqrt{(a^2 + h^2)}$

3) $r_f \succ (B - a)$:

In this range, the enflamed zone is divided as in Figure (D.7). If Z represents the depth at which the flame just touches the most remote point on the cylindrical wall, then the following set of equations are used [32];

$$Z = \sqrt{r_f^2 - (B - a)^2} \qquad [m] \qquad \text{(D.41)}$$

$$Y = Z + 0.5(X_\circ - Z) \qquad [m] \qquad \text{(D.42)}$$

$$V_b = \frac{\pi}{4} B^2.Z + BB(X_\circ - Z) \qquad [m^3] \qquad \text{(D.43)}$$

$$A_f = \frac{PP.r_f.(X_\circ - Z)}{f} \qquad [m^2] \qquad \text{(D.44)}$$

$$C1 = \frac{\pi B^2}{4} \qquad [m^2] \qquad \text{(D.45)}$$

$$C2 = \pi.BB.Z + QQ(X_\circ - Z) \qquad [m^2] \qquad \text{(D.46)}$$

$$C3 = BB \qquad [m^2] \qquad \text{(D.47)}$$

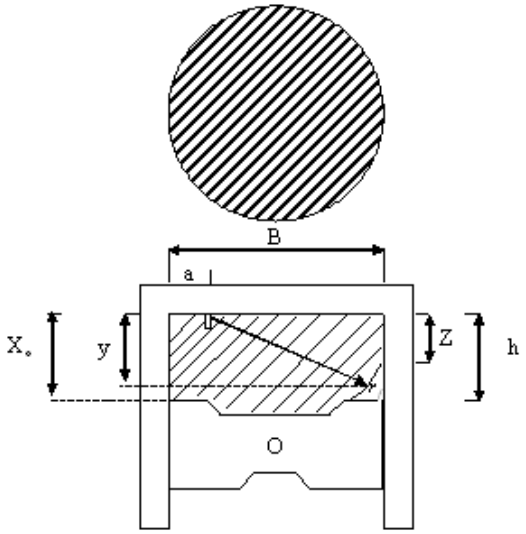

Figure (D.7): $r_f \succ (B-a)$

List of contents